VERTICAL SEISMIC PROFILING IN DEVIATED WELLS: A STUDY OF THE SIGNAL PROCESSING CONSIDERATIONS WHEN DETERMINING TRAVEL TIMES AND VELOCITY ANISOTROPY ESTIMATES FROM A VERTICAL INCIDENCE AND WALKAWAY SURVEY CONDUCTED IN A DEVIATED PRODUCTION WELL

DAVID S. McCALLUM

Vertical Seismic Profiling in Deviated Wells:

A Study of the Signal Processing Considerations When Determining Travel Times and Velocity Anisotropy Estimates from a Vertical Incidence and Walkaway Survey Conducted in a Deviated Production Well

by

© David S. McCallum, B. Sc. B. Ed.

A thesis submitted to the

School of Graduate Studies

in partial fulfillment of the

requirements for the degree of

Master of Science

Department of Earth Sciences,
Memorial University of Newfoundland

2008

St. John's Newfoundland

ABSTRACT

Travel times are essential for processing and velocity determination from VSP surveys. Even though many wells drilled today are deviated from vertical, there is very limited geophysical literature on the effects of well deviation on travel time measurements and processing issues when a VSP is conducted in a deviated well. An investigation of the processing considerations associated with acquiring precise travel times from a vertical incidence and walkaway survey conducted in a deviated well was carried out. Compensating for well deviation by rotating the vertical component in-line with the downgoing P-wave particle motion for each source-receiver pair of the vertical incident survey had a negligible effect on acquired travel times. Rotation of the vertical component in-line with the downgoing P-wave particle motion for each source-receiver pair of the walkaway survey proved to follow conventional practice and the deviation of the well was not an issue.

The issue of well deviation when acquiring travel times from VSP surveys conducted in deviated wells is a concern when characterizing a reservoir by determining aspects like anisotropic characteristics of a specific rock layer. Using the travel times acquired from both the vertical incidence and walkaway surveys, it is demonstrated, by producing a percent velocity anisotropy estimate of 17.1 % for a marine shale, that the travel time-inversion method is well suited for a deviated well setting. This estimate is appropriate when compared to published values and to an independent estimate of 17.9 % obtained by modifying the phase-slowness method using the same assumptions that govern the travel time-inversion method. Modifying the phase-slowness method also made it operationally less intense. In general, with the application of reasonable assumptions, velocity anisotropy measurements can be obtained within a deviated well without rigorous computational adjustments.

ACKNOWLEDGEMENTS

I would especially like to thank Dr. Charles Hurich for his guidance, patience and words of encouragement over the years. His philosophy pertaining to pedagogy and his ability to instill in his students the enthusiasm to always inquire should be commended.

I would like to thank a number of people for which without their help the completion of this thesis would not have been possible: Mrs. Sharon Deemer, Mr. Craig Ennis, Ms. Lori Ennis, Dr. John Hanchar, Dr. Joseph Hodych, Mr. Ayiaz Kaderali (Husky Energy Canada), Mr. Tony Kocurko, Mr. Ray Patzold, Dr. Hugh G. Miller, Mrs. Michelle Miskell, Mr. Bill Scott (Hibernia Management and Development Corporation), Dr. Michael A. Slawinski, Mr. Gerry Whelan (Schlumberger Canada), Dr. James Wright and Dr. Richard Wright.

I would also like to thank Landmark Geophysical Corporation and the Natural Sciences and Engineering Research Council of Canada (NSERC) for providing the funding and software needed to maintain a state of the art seismic processing lab.

Lastly, I would like to thank my parents, Mr. and Mrs. Freeborn, my little Leah and Megan and especially my wife Amanda. Without their guidance, encouragement, understanding and love, I would have never completed this journey.

TABLE OF CONTENTS

LIST OF TABLES

LIST OF FIGURES

SYMBOLS AND ABBREVIATIONS

ASI	Array Seismic Imager
AVO	Amplitude Variation With Offset
f-k	Frequency-wavenumber
GBS	Gravity-Based Structure
H1	X-Component of Geophone Package
H1(theta)	First Rotation of the X-Component Through the Angle Theta
H1(theta,phi)	Second Rotation of the X-Component Through the Angle Phi
H2	Y-Component of Geophone Package
H2(theta)	Rotation of the Y-Component Through the Angle Theta
KB	Kelly Bushing
MD	Measured Depth
P-wave	Compressional Elastic Wave
S-wave	Shear Elastic Wave
SH-wave	Horizontal Shear Wave
SRD	Standard Reference Datum
SV-wave	Vertical Shear Wave
TVD	True Vertical Depth
VSP	Vertical Seismic Profiling
Vx	Horizontal Ray Velocity
Vz	Vertical Ray Velocity
V1	Vertical Component of Geophone Package

V1(phi)	Rotation of the Vertical Component Through the Angle Phi
χ	Anisotropy Parameter
Φ	Percent Difference Between Vertical and Horizontal Ray Velocities

LIST OF APPENDICES

CHAPTER 1 Introduction

Vertical seismic profiling (VSP) is a seismic technique that has been used for a number of years in the hydrocarbon industry. The measurement involves recording the total upgoing and downgoing wavefields propagating through the subsurface by means of geophones clamped to the walls of a drilled well and a source situated at or near the surface.

An important use of VSP's is the acquisition of direct travel times from the source to the receiver. These travel times then can be used to calculate average velocities of the elastic wave from the source to the geophone located within the rock under investigation. Average velocity is easily calculated using:

$$\vec{V}_{Average} = \frac{\text{distance from source position to receiver position}}{\text{direct travel time from source position to receiver position}}.$$

These velocities can provide a better understanding of the rocks under investigation and can be integrated into an exploration and development program. For example, estimates of velocity anisotropy are increasingly being used to better image and characterize reservoirs. Travel times from VSP's are utilized to calculate the average and interval velocities needed to determine if a rock unit displays anisotropic properties. However, the reliability of these velocities depends on the reliability of travel times. Errors in velocity determinations that are used to help characterize a reservoir - by determining such aspects as anisotropic parameters and Vs/Vp - could significantly decrease the confidence in the calculated results.

What causes differences in travel times when the VSP data comes from the same source-to-receiver configuration? One possible cause investigated in this study, is processing VSP data to account for well deviation. Although many wells currently drilled are highly deviated away from vertical, there is limited documentation pertaining to the possible effects of well deviation on measured travel times and associated data processing issues. This study first introduces specific uses of VSP's and different VSP survey configurations. I then use a vertical incidence VSP to investigate whether or not travel times, acquired after processing VSP data to account for well deviation, display significant differences compared to travel times acquired when well deviation is not considered.

The possibility of additional processing issues when acquiring travel times results in a concern when trying to characterize a reservoir by determining aspects like anisotropic characteristics of a specific rock layer. The question must be asked - can anisotropy within a rock be measured using VSP data acquired from a deviated well without rigorous computational adjustments to account for well deviation? This study investigates this question by using travel times acquired from the vertical incidence and walkaway surveys to demonstrate that the travel time-inversion method (Slawinski et. al., 2003) is well suited for acquiring velocity anisotropy measurements in deviated wells.

Although travel time measurements are essential for processing and velocity determination from VSP surveys, there is very limited geophysical literature on the affects of well deviation on travel time measurements and processing issues in this type of setting. The literature on these topics consists primarily of short notes or extended

abstracts presented at annual geophysical meetings. Therefore, the objective of this thesis is to develop a systematic study of processing issues and their potential affect on deriving precise travel times from a three component vertical incidence and walkaway survey conducted in a deviated well. Furthermore, using these travel times I will show that with the application of reasonable assumptions, velocity anisotropy measurements can be obtained within a deviated well without rigorous computational adjustments.

1.1 A Brief History of Vertical Seismic Profiling

Seismology has been used to image and explore the Earth's subsurface and has been in existence for many years. Much of the emphasis of this technique for exploration has been placed on surface-positioned seismic energy sources and receivers. However, very little time passed after the inception of surface-positioned exploration seismology before scientists began to think about using boreholes as a location to either place seismic sources or geophones.

The first credited use of boreholes in seismology was in 1917 when R.A. Fessenden patented a method for detecting subsurface ore bodies by means of acoustic sources and receivers in water-filled boreholes (Hardage, 2000). M^{c}Collum and LaRue (1931) emphasized that existing wells were not used for collecting exploration seismic data. They proposed that local geological structure could be determined by measuring the travel times from surface positions to geophones located in existing boreholes. Even though the fundamentals of vertical seismic profiling were now in place, geophysicists mostly ignored the idea using seismology in the borehole, and persisted in continuing the emphasis on surface seismology. The only use geophysicists had in the 1930's for borehole seismology was measurement of seismic wave propagation velocities (Dix, 1939). This led to the development of the valuable velocity check-shot survey, which is still widely used today in the hydrocarbon industry.

The potential of vertical seismic profiling was not recognized until there were rigorous studies of not just the first arriving waves but also the character of the seismic wave propagation after the direct arrivals. These studies were implemented by Jolly

(1953), Riggs (1955), and Levin and Lynn (1958). They showed that wavelet attenuation and interaction between primary and multiple reflections could all be addressed. Even with these rigorous studies during the 1950's, geophysicists in the Western Hemisphere continued to use boreholes only for velocity measurements and not for rigorous vertical seismic profiling (Hardage, 2000).

Throughout the 1950's, 1960's and into the 1970's the interest in vertical seismic profiling was minimal in Western countries. However, this was not the situation in the former Soviet Union. Soviet geophysicists intensely developed vertical seismic profiling applications. Gal'perin (1974) provides a comprehensive look at applications of vertical seismic profiling (VSP) and signal processing considerations and techniques.

By the late 1970's and into the early 1980's geophysicists in the Western Hemisphere began to take a serious look at the potential applications of vertical seismic profiling. Hardage (1985) prepared an excellent comprehensive summary of the utility of this seismic profiling technique by outlining the basic guidelines needed for the acquisition, signal processing and interpretation of VSP data.

The utility of recording three component data in the borehole and the benefit of the VSP technique for providing additional seismic interpretational insight was discussed by DiSiena et al. (1981) and Toksöz and Stewart (1984). They discussed signal processing methods that allowed for the extraction of information from the total propagating wavefield in a three component coordinate system.

Today, the emphasis of VSP experiments is integration with surface seismic profiling to reduce the financial and economic risks associated with developing oil and

gas fields. VSP data is used to optimize surface seismic planning, guide the signal processing of surface seismic data, assist in reservoir characterization and even help guide the drilling of boreholes.

1.2 Basic Seismic Wavefields Obtained From VSP's

When first examining any VSP seismic trace gather, it becomes apparent that this technique of seismic acquisition represents the subsurface differently then the surface seismic trace gather (**Figure 1.2.1**). There are two different wavefields recorded during a VSP survey. These wavefields are characterized by upgoing and downgoing waves. The recorded time of downgoing waves on the VSP trace gather increases. This corresponds to the time an event is recorded on specific geophones that increase with depth. However, for upgoing waves the opposite is true. The time recorded of an event on a specific geophone decreases with depth. Once there is a reflection of a downward propagating wave it will propagate upward and therefore will be recorded by successive geophones whose position in the borehole decreases with depth. When the receiver is located at the reflector depth, the upgoing wave is coincident with that of the direct downgoing wave. In the context of actual field-recorded data, the downgoing waves are often about 30 decibels (dB) stronger in amplitude than the upgoing waves and these upgoing events are not as easily identified as the downgoing events (Cassell, 1984).

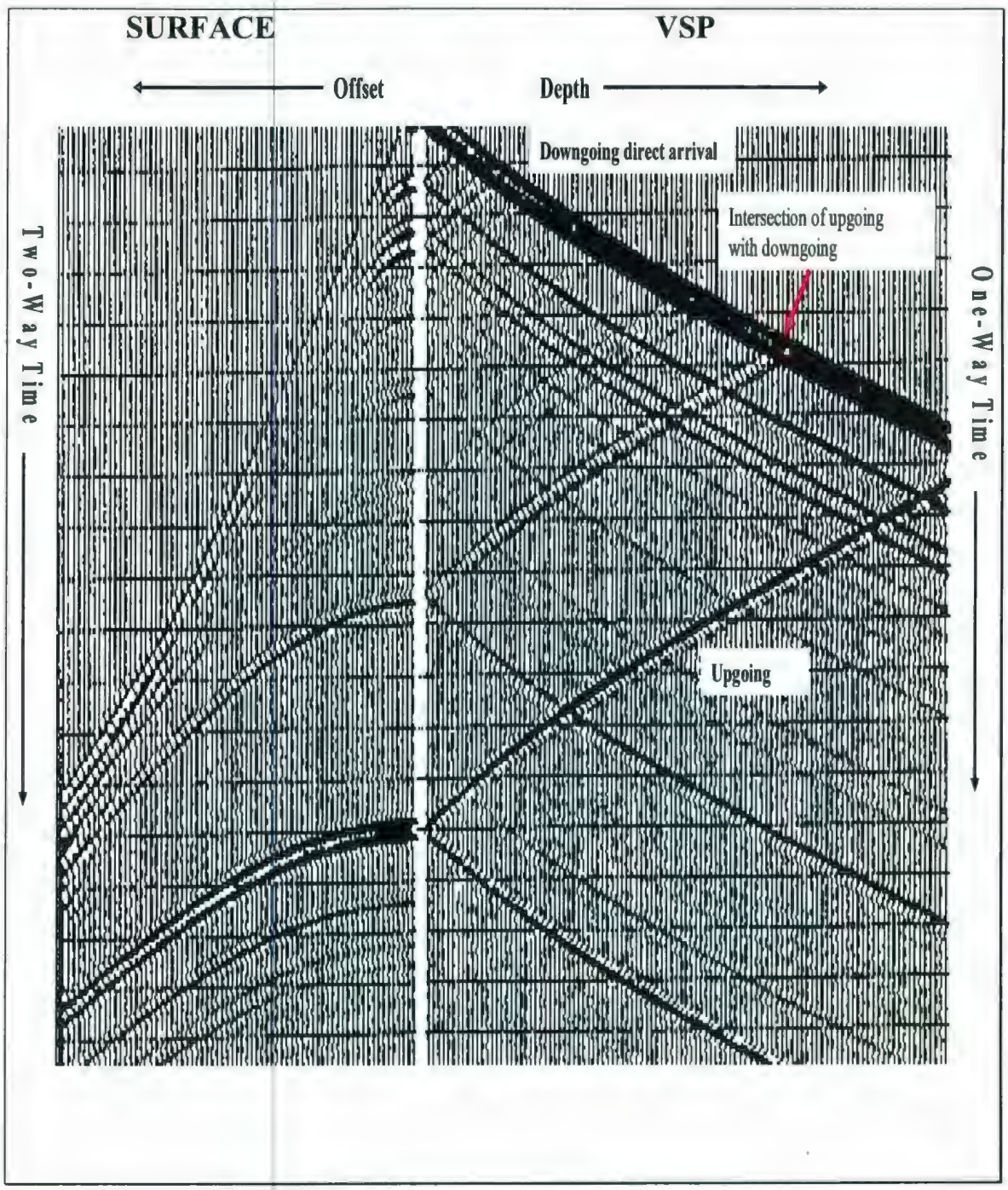

Figure 1.2.1 Comparison of a surface seismic trace gather (left) with a VSP trace gather (right) (Pearcy, 2000). Note the presence of the upgoing wave and how primary reflections are characterized by the coincident of the upgoing wave with the downgoing direct arrival indicated by the arrow.

1.3 The Application of Multicomponent Seismology in Vertical Seismic Profiling

When examining the applications of vertical seismic profiling as a seismic technique, there has been an apparent concentration on compressional or P-wave energy recorded on a vertical geophone in the borehole. However, many of the VSP tools that are used consist not only of a vertical geophone but also two horizontal geophones. More recently, the VSP tools consist of an array of three component geophone packages. This has allowed for the examination of shear waves or S-waves and mode-converted waves along with P-waves. Utilizing multicomponent recording requires distinction of the origins and elementary nature of the specific elastic waves of interest (P and S) that are observed. For an isotropic homogeneous media, particle motion associated with compressional wave (P-wave) propagation is oriented in the direction of propagation. Therefore, the particle motion is defined entirely by the ray geometry. Shear waves are associated with particle motion oriented perpendicular to the direction of propagation. Hence, the particle motion can be in any direction within the plane normal to the ray. The nature of the particle motion associated with a specific wave mode can also be referred to as its specific polarization.

For a visual understanding of these different polarized wave motions, **Figures 1.3.1**, **1.3.2.**, and **1.3.3** demonstrate the particle motion involved in the wavefields recorded by a three component vertical seismic profile survey. To simplify the figure, ray paths for the upgoing waves are shown for the source that is offset to the left of the well. For the source offset to the right of the well, the ray paths for the downgoing waves are shown.

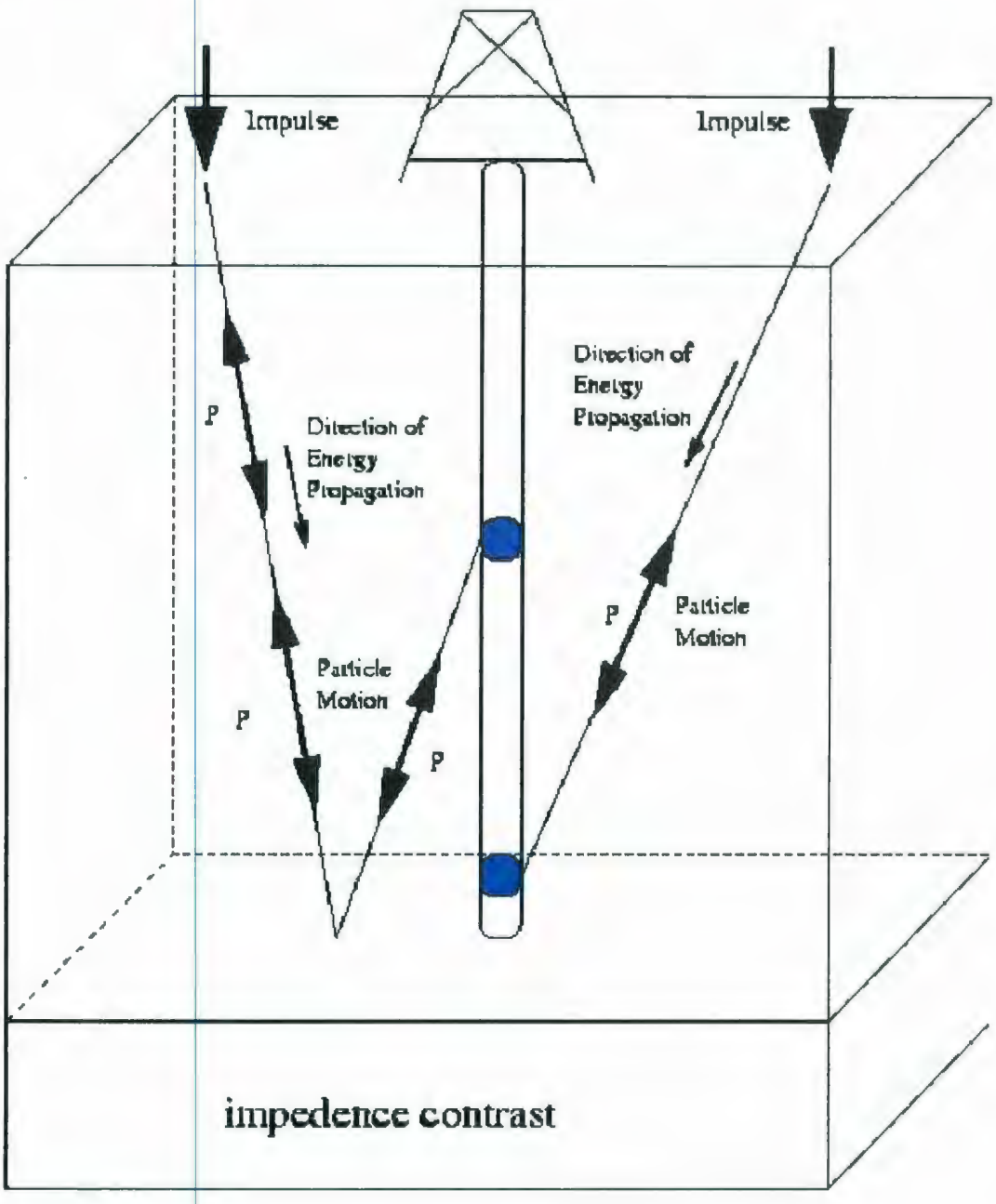

Figure 1.3.1 Direction of energy propagation and particle motion of an upgoing (left) and a downgoing (right) compressional (P) wave created by a vertically polarized impulse.

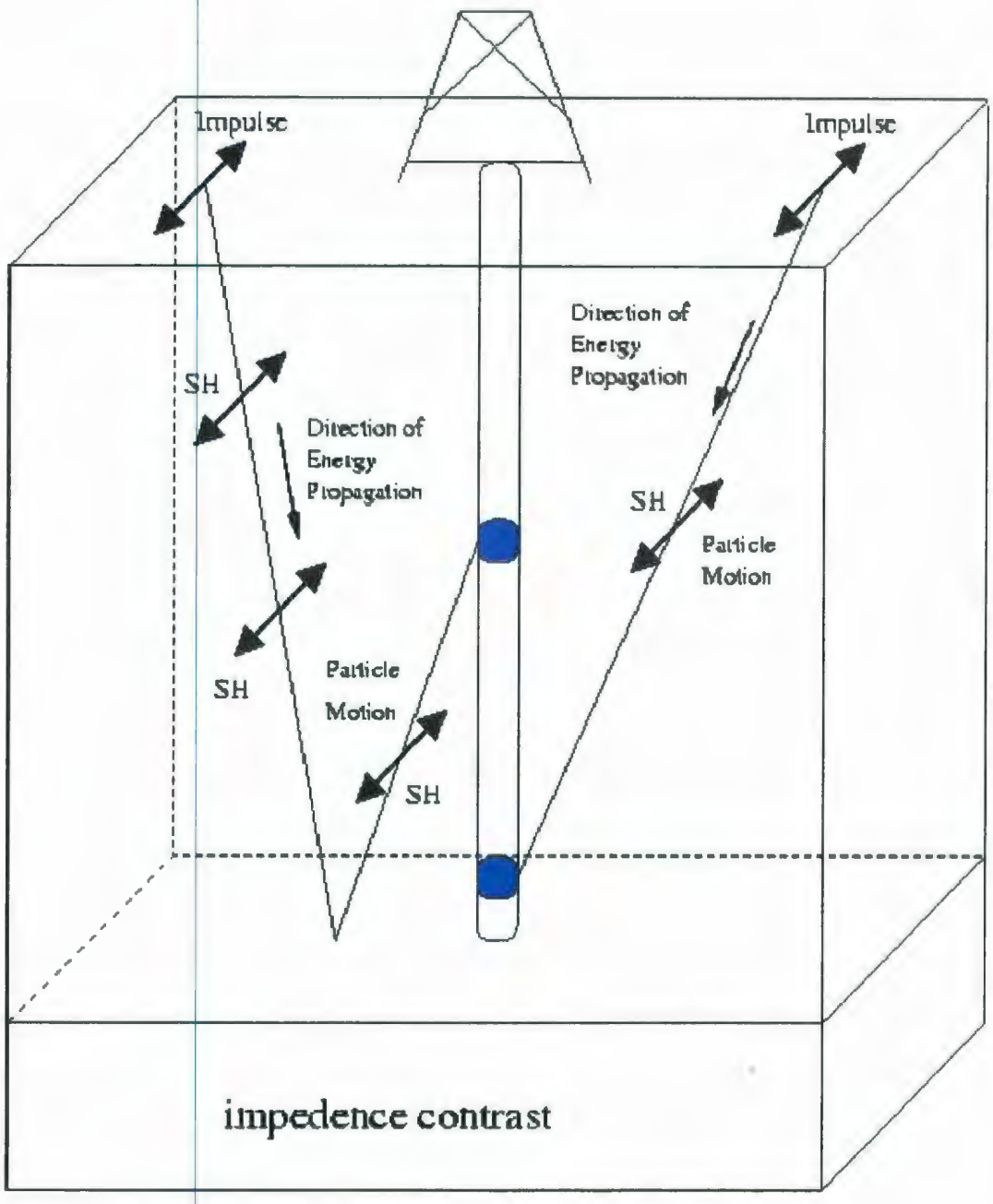

Figure 1.3.2 Direction of energy and particle motion of an upgoing (left) and a downgoing (right) SH shear-wave created by a source that is polarized perpendicular to the plane of incidence that is defined by the source, the three component geophone and the reflection point.

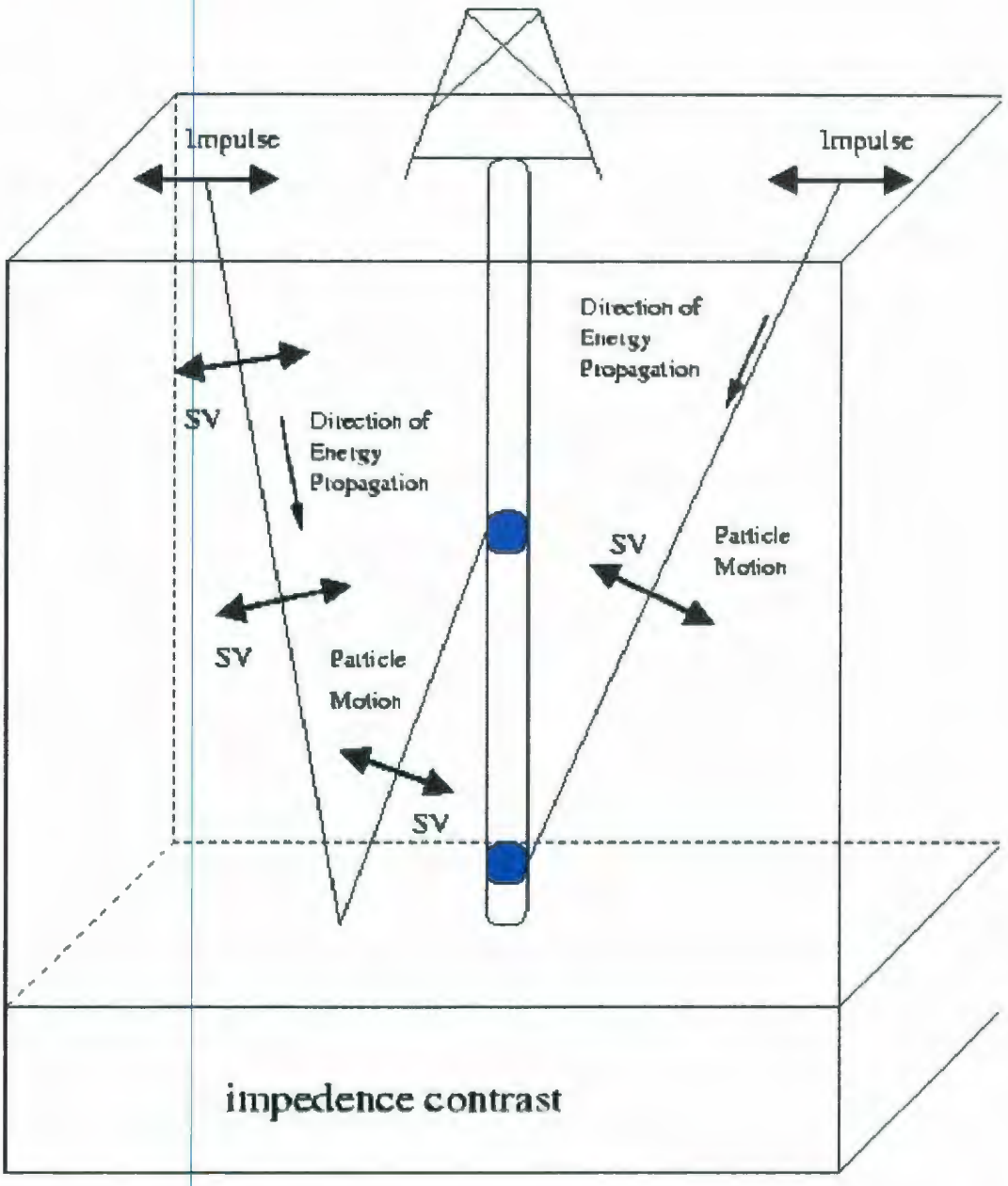

Figure 1.3.3 Direction of energy and particle motion of an upgoing (left) and a downgoing (right) SV shear-wave created by a source that is polarized in the direction of the plane of incidence that is defined by the source, the three component geophone and the reflection point.

The P-wave situation (**Figure 1.3.1**) shows a P-wave as a vertical impulse on the Earth's surface. This impulse leads to a P-wave that is reflected from a specific depth and recorded by a geophone within the borehole as an upgoing P-wave. This impulse also leads to a P-wave that travels to a geophone positioned within the borehole and recorded as a downgoing wave. The upgoing reflected ray and the downgoing direct ray lie in a plane which contains the source, the three component geophone and the reflection point. This plane, which is perpendicular to the reflecting surface, can be defined as the plane of incidence. For the P-wave propagation in a flat earth, particle motion or polarization of the wave is in the direction of the ray.

For S-wave propagation, the orientation of the source, or equivalently what direction the source is polarized, will have a strong effect on the particle motion and hence the polarized nature of the specific shear wave. The SH-wave situation in **Figure 1.3.2** demonstrates a horizontal impulse orientated/polarized perpendicular to the previously defined plane of incidence. This generates a shear wave with particle motion that is purely horizontal. This shear wave, categorized as a SH-wave, is polarized normal to the ray propagation direction and normal to the plane of incidence. Since the particle motion of this wave is purely horizontal, it is apparent why a three component geophone is required to record the complete wavefield.

The SV-wave situation in **Figure 1.3.3** demonstrates a horizontal source impulse oriented/polarized parallel to the plane of incidence. The resulting particle motion is perpendicular to the ray propagation and the motion within the plane of incidence. However, the particle motion is not necessarily vertical. Only when the ray is horizontal

will the motion be vertical. Therefore, this shear wave, categorized as a SV-wave, has a polarization nature that should be considered as lying in the plane of incidence, not as vertical particle motion. Due to the polarization nature of the SV-wave, the vertical component along with the horizontal components can record this wave. In each case portrayed in **Figures 1.3.1**, **1.3.2** and **1.3.3** the different waves were produced by a source that is also polarized in the specific direction with respect to the plane of incidence. However, there is another way to produce these different wave modes of interest, and that is by utilizing the phenomenon of mode conversion.

For a P-wave impinging upon a horizontal interface between two solids at some arbitrary angle other than 90° (**Figure 1.3.4**), four different waves are generated at the interface. They are a reflected P-wave and a reflected mode-converted SV-wave. Also there is a transmitted P-wave and a transmitted S-wave that has undergone mode conversion. However, the S-waves are propagating at a slower velocity. Since the P-wave particle motion is entirely in the plane of incidence, the S-wave particle motion is restricted to the same plane. Therefore, the mode converted S-waves are of the SV-polarization distinction.

In the case of a P-wave impinging upon a horizontal interface between a liquid layer over a solid layer (**Figure 1.3.4**), only three different waves leave the interface. Since the liquid will not support S-wave propagation, there will be no reflected mode converted S-wave, just a reflected P-wave. Also, there will be a transmitted P-wave and a transmitted mode converted S-wave with SV-polarization.

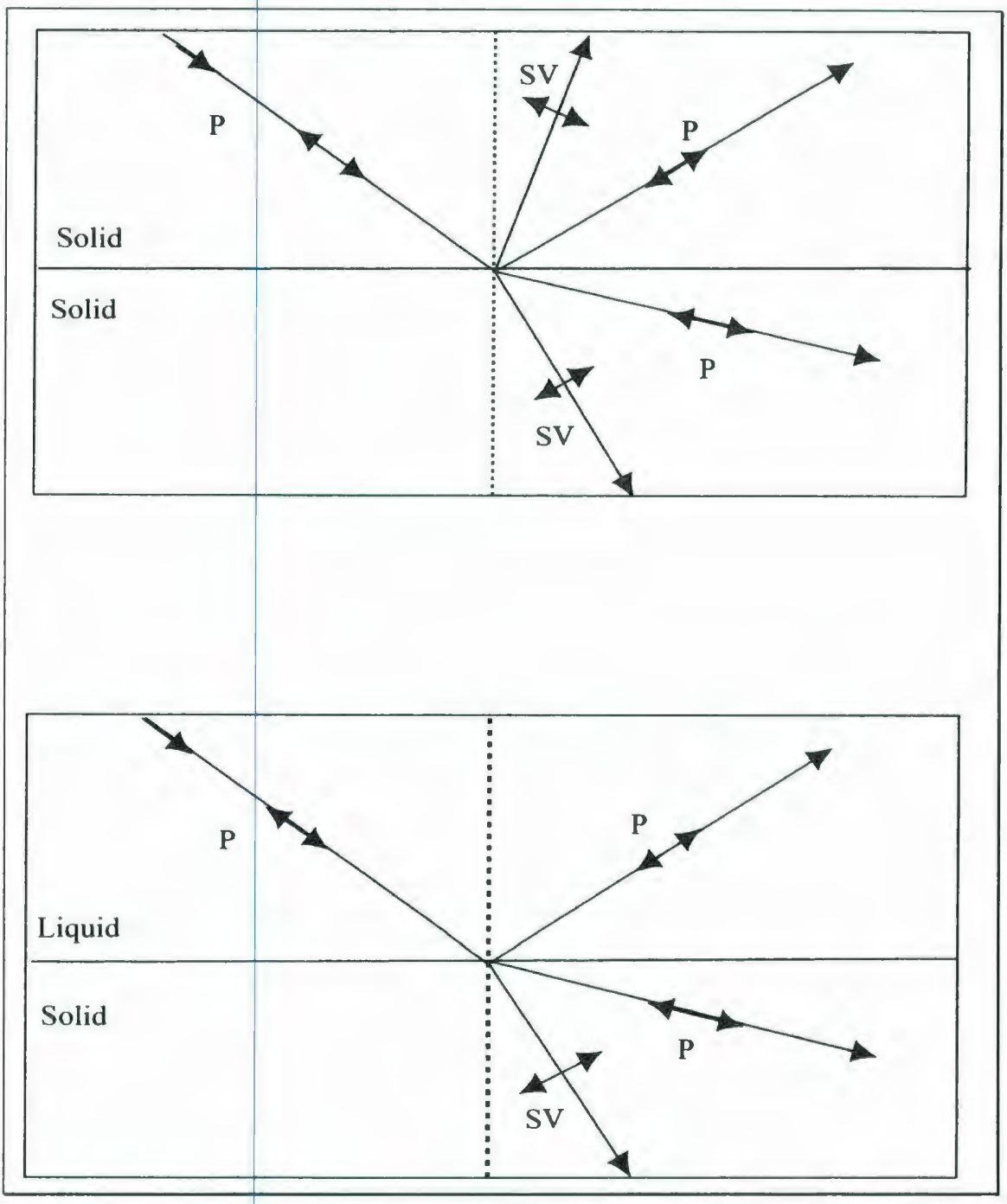

Figure 1.3.4 Partitioning of energy into different wave modes (P and SV) upon reflection between two isotropic solids (top) and between a liquid and an isotropic solid (bottom).

To exploit mode conversion for the acquisition of S-wave energy by utilizing P-wave sources, **Figures 1.3.5** and **1.3.6** show possible VSP field geometries. The case for mode conversion in a land environment portrayed in **Figure 1.3.5**, considers a P-wave source that causes a propagating P-wave to produce, at the boundary of two solids, a mode converted downgoing SV-wave and a reflected upgoing SV-wave. Also, a downgoing P-wave and a reflected P-wave is present. This P-SV reflection has an advantage in that it can be recorded in areas that are not accessible to cumbersome mechanical sources requiring a polarized wave motion to induce a SV-wave. In the specific marine example portrayed in **Figure 1.3.6**, the energy generated in the water, transmits as a P-wave and is mode converted to an SV polarized S-wave at the sea floor. It can then travel as direct downgoing waves, or continue to the reflecting interface as an SV polarized S-wave and P-wave. Both can then be reflected as a corresponding upgoing SV polarized S-wave and an upgoing P-wave. For a comprehensive study of multicomponent seismology, refer to Tatham et al. (1991). For more specific references on the use of multicomponent seismology in vertical seismic profiling, refer to Galperin (1985), Balch et al. (1984) and Hardage (2000). Now that the nature and origin of propagating elastic waves in the context of multicomponent vertical seismic profiling has been discussed, it is fitting to examine the different VSP survey configurations. The different configurations can allow for the study of specific rock attributes extracted from the elastic waves discussed in this section.

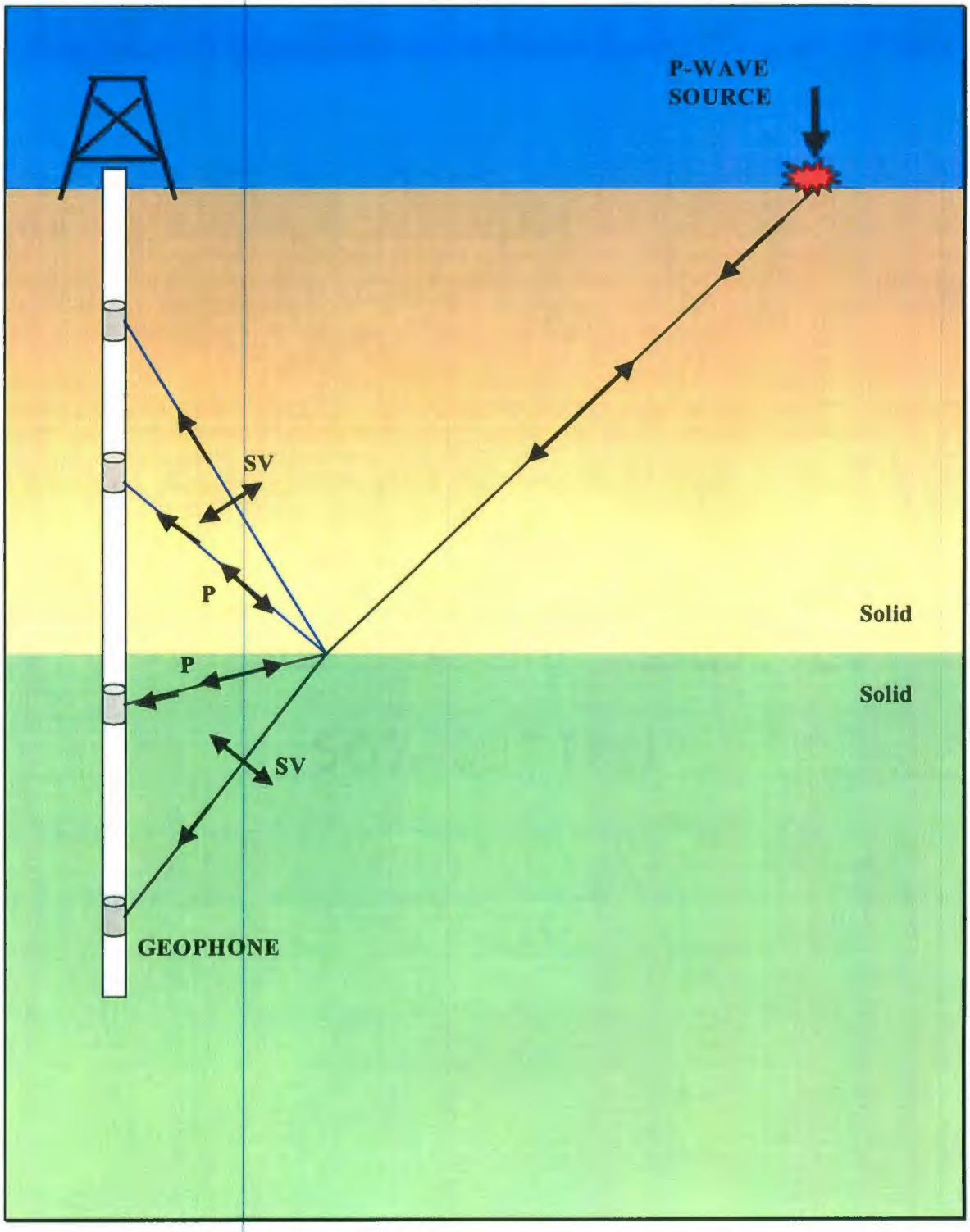

Figure 1.3.5 Possible land environment VSP field geometry for exploiting mode conversion created by a P-wave at the reflection point between two solids.

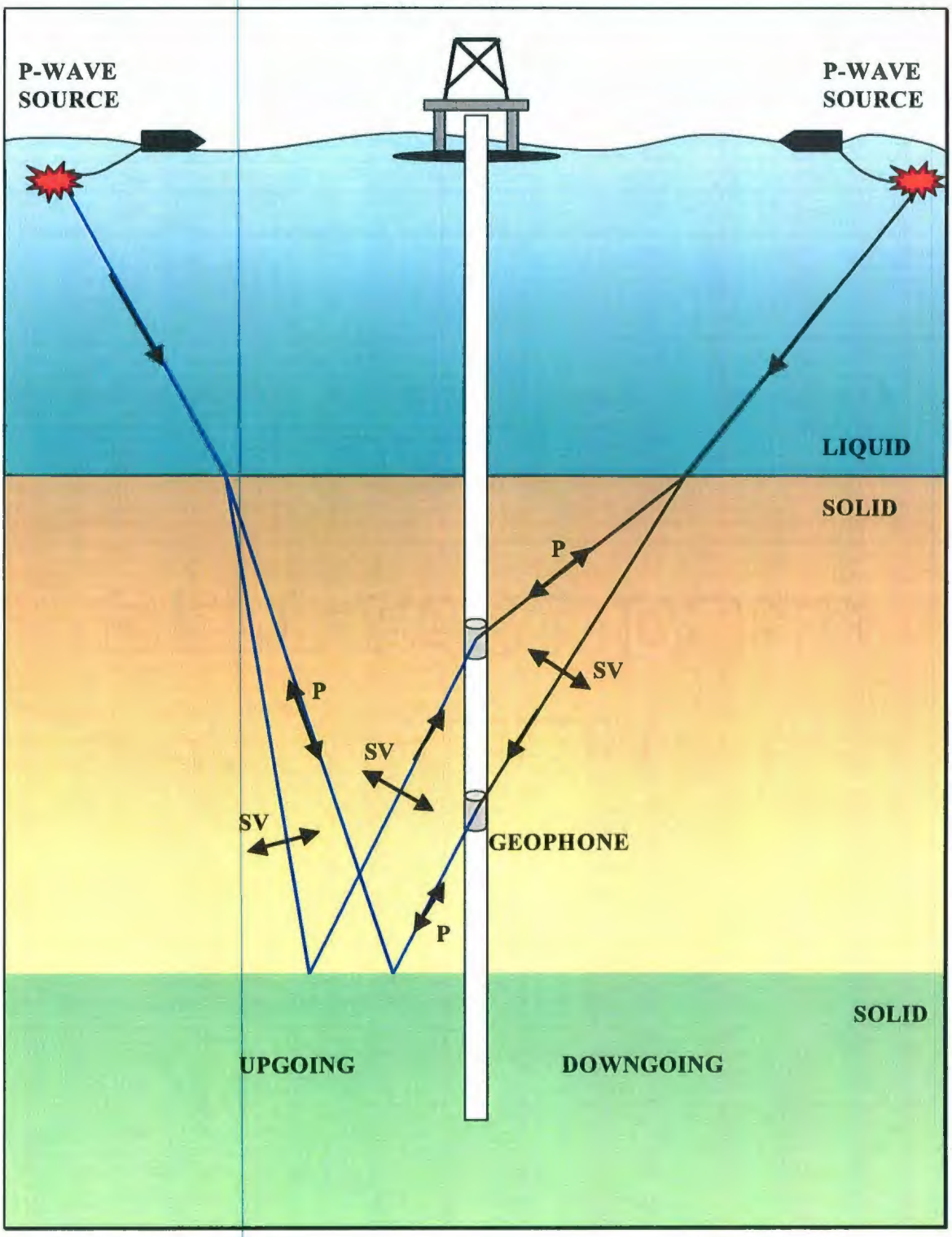

Figure 1.3.6 Possible marine environment VSP field geometry for exploiting mode conversion created at the contact point of a P-wave at the sea floor.

1.4 VSP Survey Configurations and Their Uses

To extract elastic wave properties from VSP data many survey configurations have been developed. Each of the survey configurations are designed to provide specific types of information about the subsurface.

The most basic VSP survey configuration is the checkshot survey. As mentioned in **Section 1.1**, it was the initial and is still a very important VSP configuration. The survey consists of measuring the direct arrivals from any type of source polarization at the surface to a geophone at specific levels within the borehole (**Figure 1.4.1**).

The checkshot survey allows for the acquisition of travel times which can be used to determine rock velocities. These travel times and associated velocities can then be used to determine depth-velocity models. The direct arrivals can also be used to derive seismic wavelets which can be used to create synthetic seismograms to be implemented in conjunction with surface seismics (Wyatt, 1981).

Another important use of the travel times obtained from the direct arrivals in a checkshot survey is to convert sonic log travel times so they can be used with surface seismic surveys. This procedure is practiced because sonic borehole tools emit a seismic source at frequencies in the ultrasonic range. Because of the frequency range used, the travel times on the sonic log will not correlate well if compared to surface seismic travel times. At these frequencies the seismic wave propagates differently and can be affected by small-scale rock characteristics more directly then the lower frequencies (0 to 250 Hz) associated with surface seismic sources. For further insight on the reasons for the discrepancies between sonic and seismic travel times, and techniques used to convert the

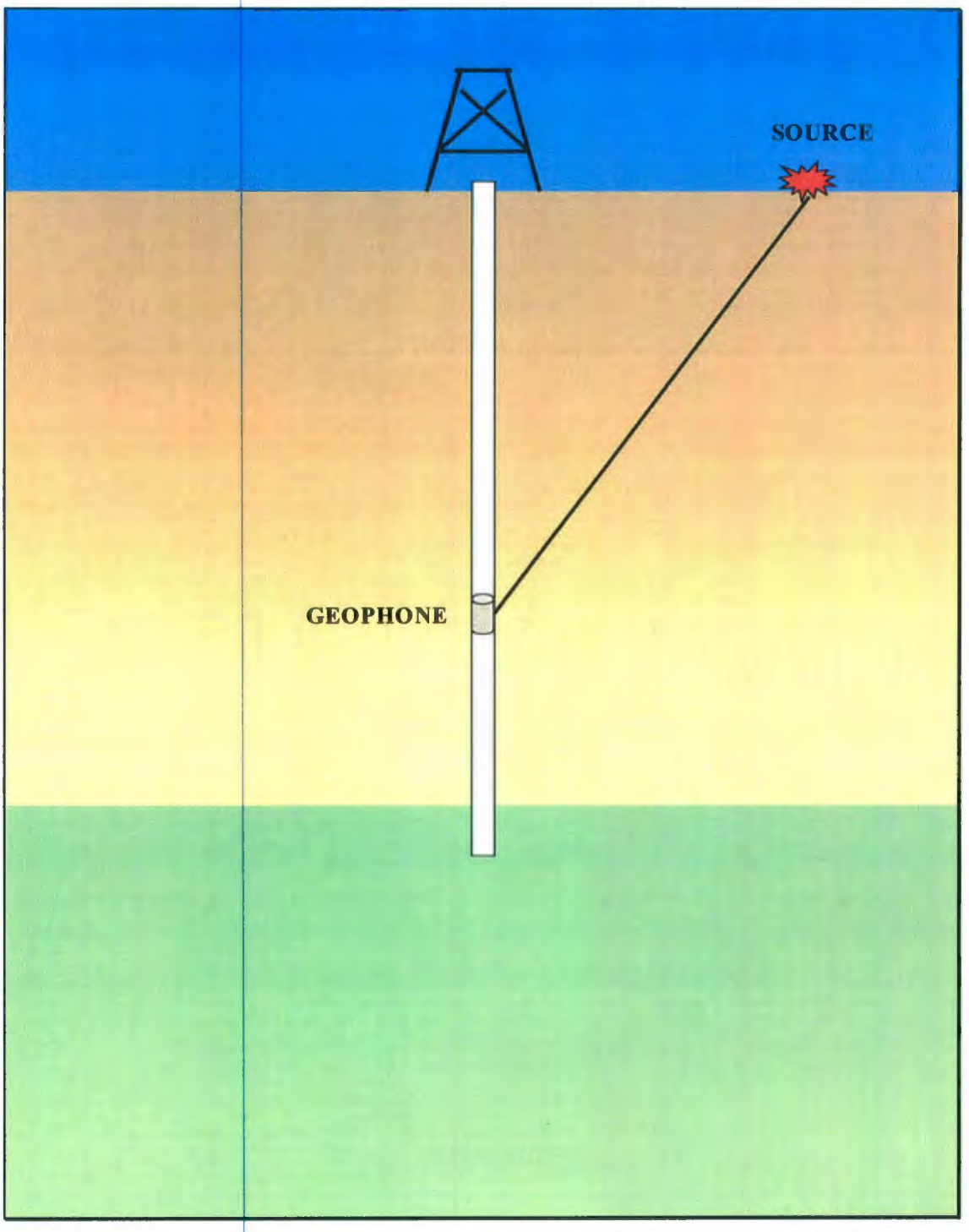

Figure 1.4.1 The checkshot survey depicting the recording of only a direct downgoing arrival within an isotropic medium.

sonic log into seismic travel times, refer to studies by Gretener (1961), Kennett et al.(1971), Strick (1971) and Stewart et al.(1984).

The zero offset VSP survey configuration is basically a checkshot survey, except the specific geophone recording locations are at smaller depth intervals (Stewart et al., 1984). There is a source at the surface that is kept stationary at a small offset (angle) with respect to the geophone in the borehole (**Figure 1.4.2**). However, the direct arrivals are not the only element of the wavefield investigated. The upgoing wavefields are also used for investigating stratagraphic horizon markers which can be correlated with surface seismic horizons. Also, patterns of multiple reflections can be identified and used to help in designing deconvolution operators to attenuate multiples in surface seismic data.

The configuration and uses of zero offset VSP survey can also be extended into situations where the borehole is considerably deviated or even horizontal. The modification is that in order to keep the source at a small offset with respect to the geophones in the borehole, the source has to be moved so that it is positioned above the geophone (**Figure 1.4.3**). This configuration, categorized as the vertical incidence survey, is also used to obtain information from the direct arrivals and the upgoing wavefields. One advantage of the vertical incidence survey is that the upgoing and downgoing wavefields can be used to image lateral coverage from beneath the well. Also, fault and dip identification of the formation around the well is possible (Hardage, 2000). However, the disadvantage to this type of survey configuration is that great care has to be taken to ensure that the source and receivers are vertically aligned. This is time consuming and expensive.

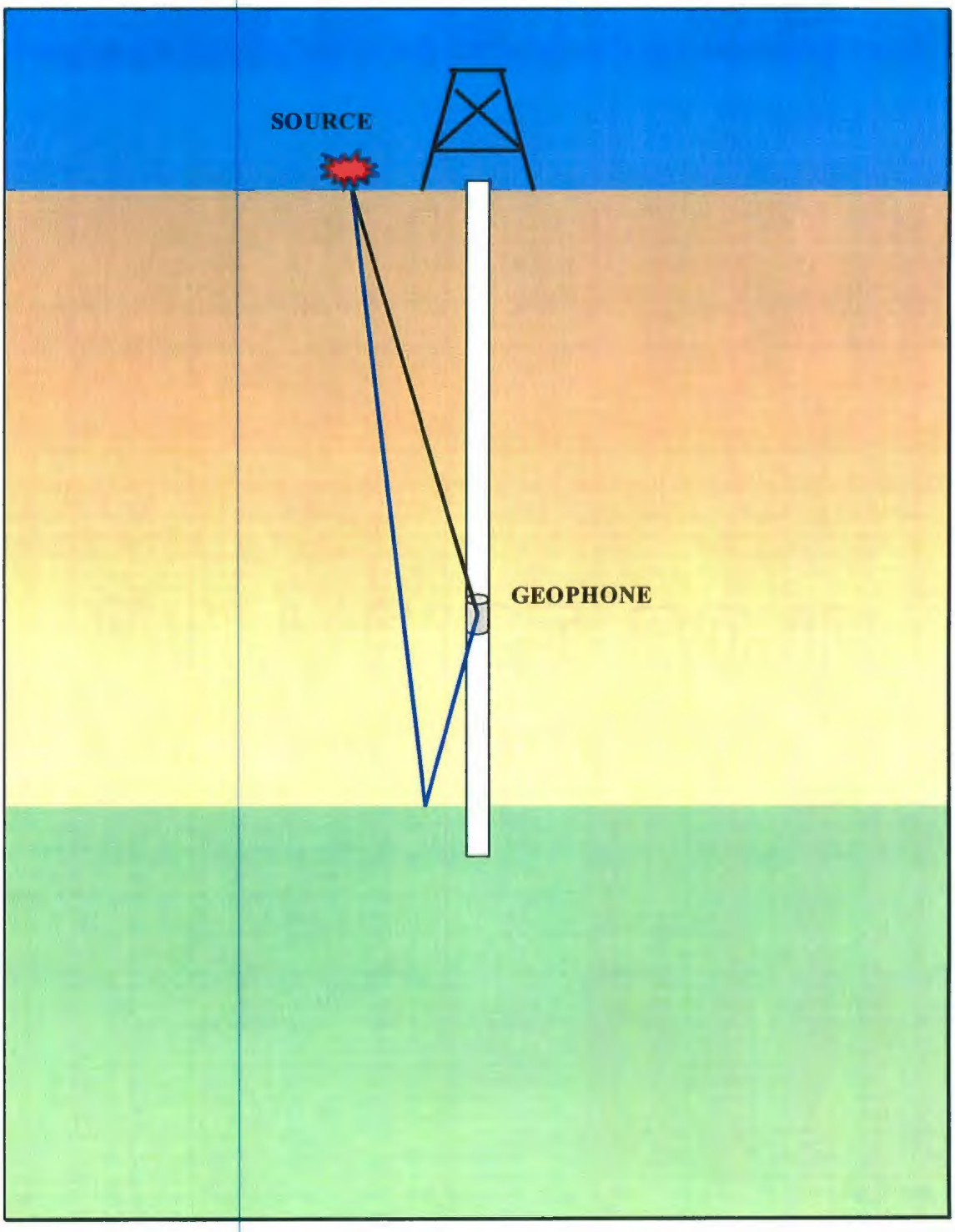

Figure 1.4.2 The zero offset survey depicting the recording of a direct downgoing arrival and a primary upgoing arrival within an isotropic medium.

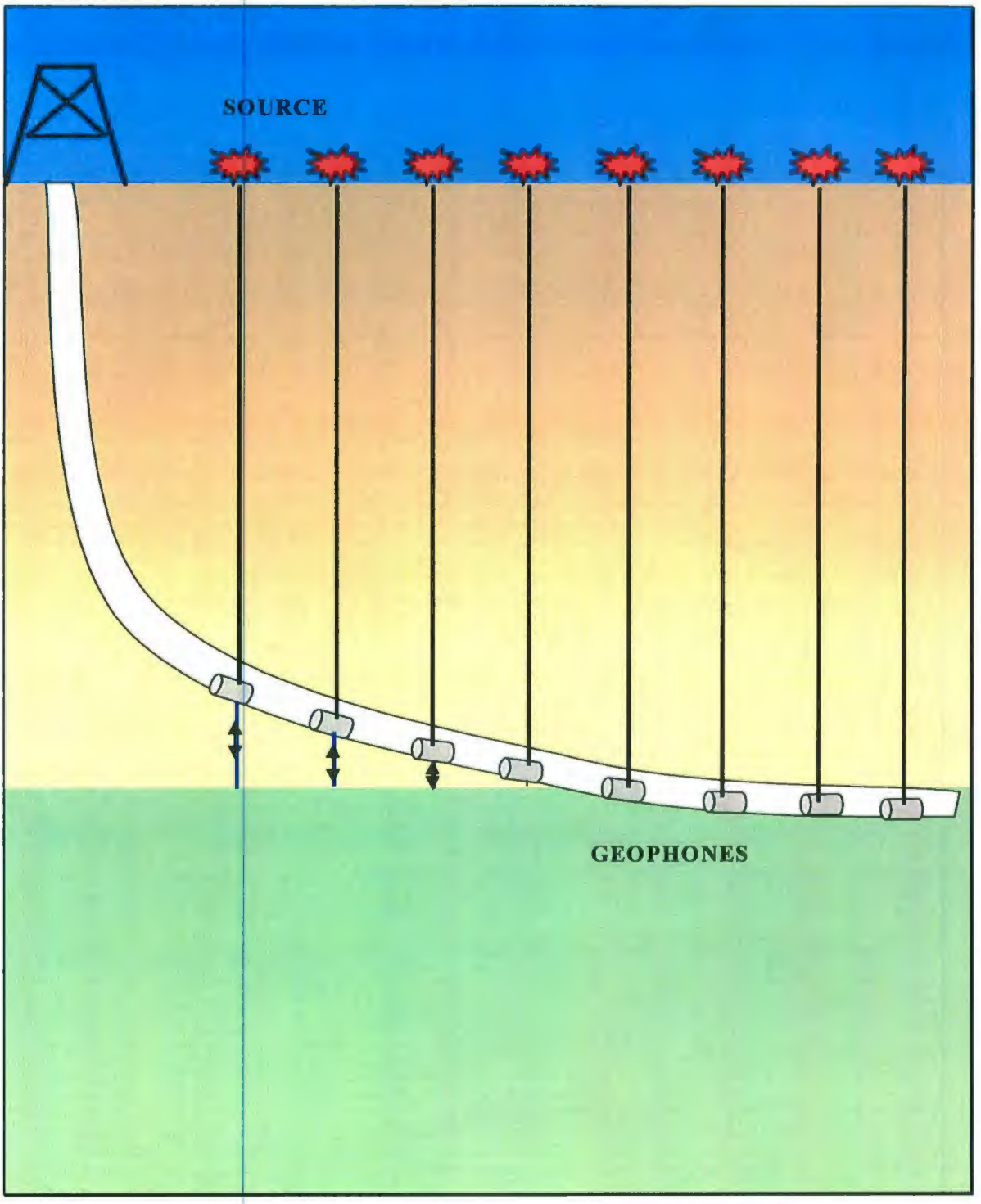

Figure 1.4.3 The vertical incident survey configuration depicting the recording of a direct downgoing arrival from each source-geophone pair within an isotropic medium. Also, note the existence of primary upgoing arrivals recorded by geophones located above the interface between the two mediums.

In both vertical and deviated wells, the offset VSP configuration is widely used. The survey configuration consists of a source placed at some offset beyond near normal incidence with respect to a number of receiver positions within the borehole (**Figure 1.4.4**). This survey configuration is quite common when a VSP survey is acquired offshore in a deviated well. The source can be hung off the side of the rig and kept there throughout the course of the survey.

The offset VSP configuration can be used for acquiring many of the same attributes about a formation as the zero offset VSP. This configuration is also commonly used for investigating mode conversion. It can lend itself to SV shear wave analysis and allows for the possibility of acquiring information about the recorded SV wave when a vertically polarized (P-wave) source is used.

The walkaway survey (**Figure 1.4.5**) is a survey configuration that also lends itself to acquiring more insight into the propagation of P and SV elastic waves if a vertically polarized (P-wave) source is used. This survey configuration consists of a single receiver or a number of receivers kept stationary at a specific depth in the borehole. Then a number of sources ranging from zero offset to far offset are fired at some azimuth to the receivers. Data is commonly acquired from far to zero source offsets on both sides of the receivers.

This configuration can also be used to acquire the same attributes as the offset VSP. However, since it is common practice in walkaway surveys not to acquire data at many depth levels, this allows for more in-depth investigation of a specific area of the target rocks. Because of the range of source offsets, this survey configuration is

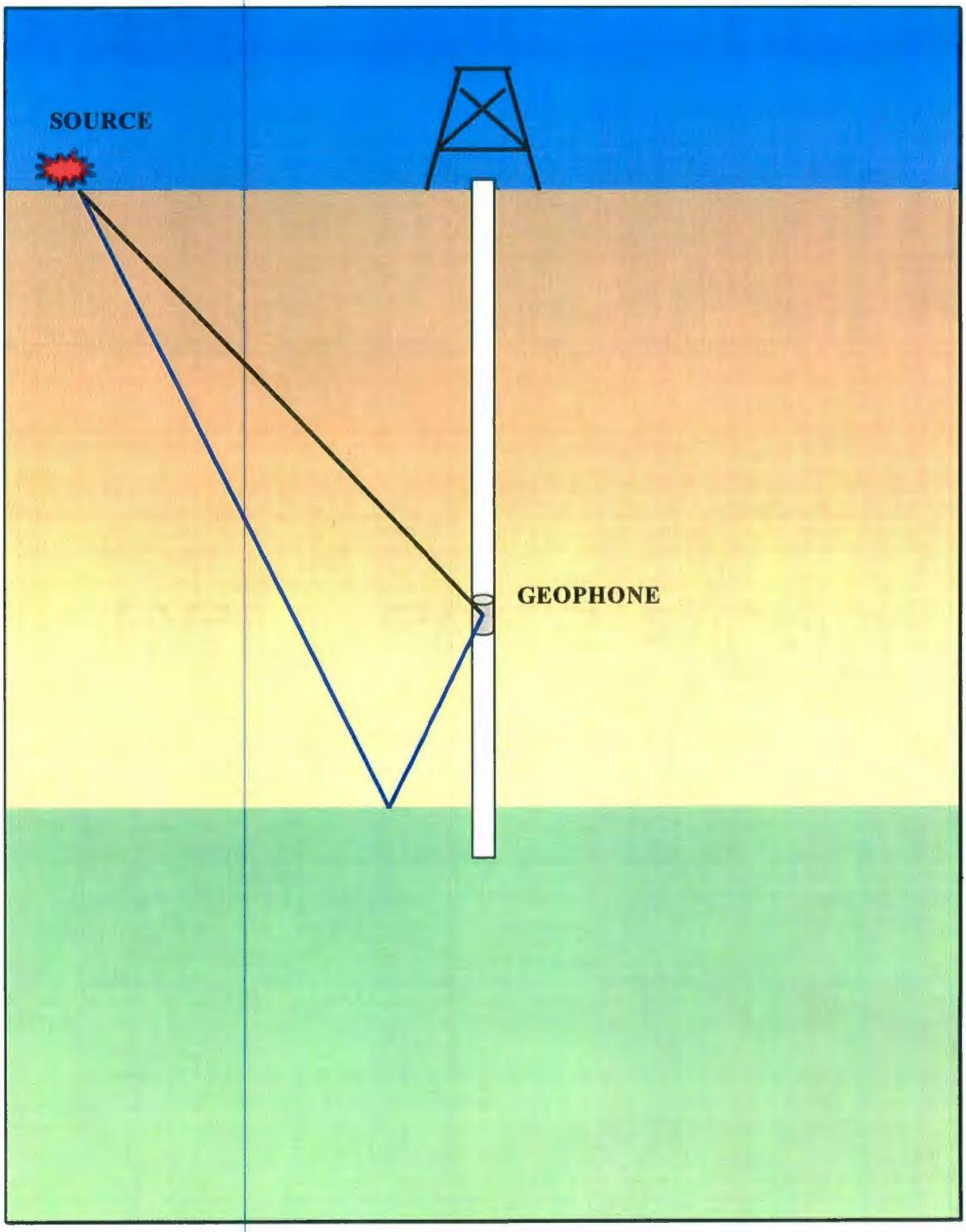

Figure 1.4.4 The offset survey configuration depicting the recording of a direct downgoing arrival and a primary upgoing arrival within an isotropic medium.

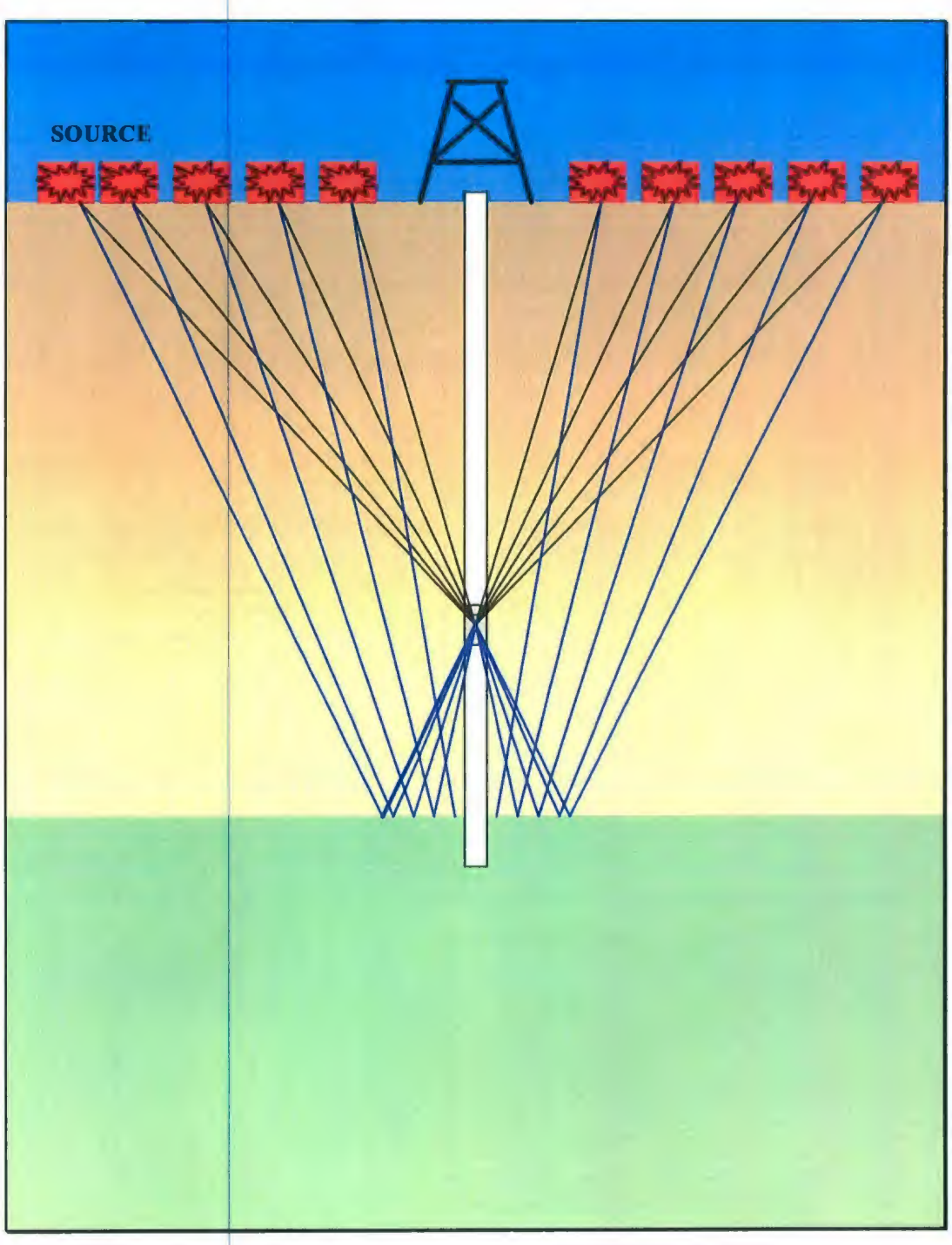

Figure 1.4.5 The walkaway survey configuration depicting direct downgoing arrivals for each source and primary corresponding upgoing arrivals within an isotropic medium.

commonly used for amplitude variation with offset (AVO) analysis (Coulombe, 1993). Also, this is quite useful for acquiring a range of anisotropic attributes that are associated with a specific rock unit within a reservoir.

CHAPTER 2 VSP Survey Characteristics for This Study

2.1 Vertical Incidence and Walkaway Survey Locations

The Hibernia oil field is located 315 kilometers southeast of St. John's, Newfoundland, Canada in 80 meters of water. This Field was discovered by a Chevron-operated well in 1979 (Sydora, 1999). The Hibernia oil field consists of many fault blocks as characterized by **Figure 2.1.1**. These fault blocks have been drilled by a number of wells that originate from a gravity-based structure (GBS). As indicated in **Figure 2.1.1**, there are oil producing wells and gas or water injector wells.

For this study the location concentration will be on the Q and R blocks. **Figure 2.1.1** demonstrates that the Hibernia Q and R fault blocks are located near the center of the field, to the northeast of the GBS. The vertical incident survey data used for this study were acquired in the B-16_2 well drilled into the Q block. The walkaway data were acquired in the B-16_4z well drilled into the R block. These wells are cased deviated producing wells that at reservoir depth are separated by approximately 1.5 kilometers. For a more three-dimensional understanding of the specific area of the Hibernia field that the VSP surveys were acquired in, **Figure 2.1.2** show the two deviated wells with their position relative to the GBS.

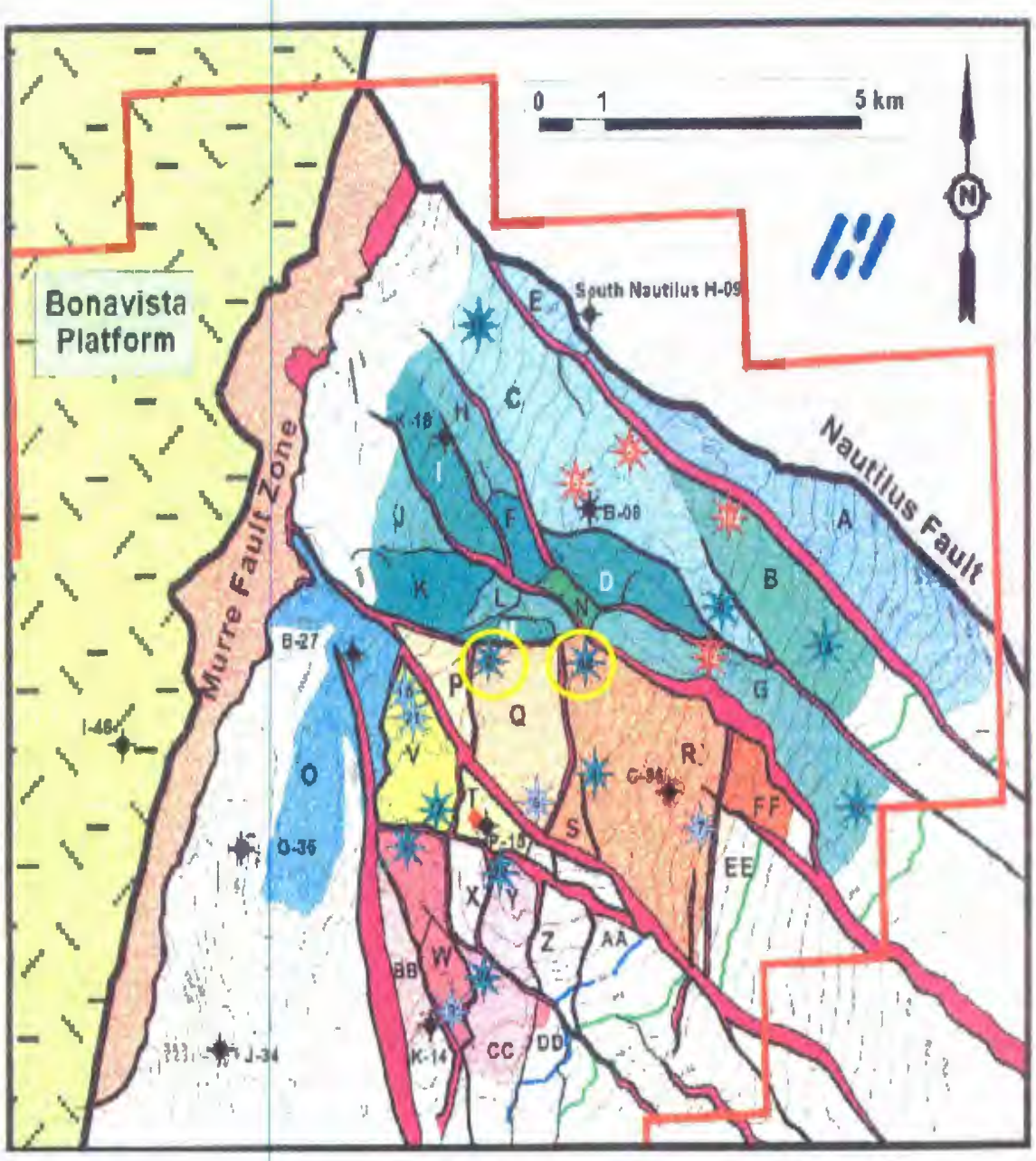

Figure 2.1.1 Hibernia fault block map showing the position of the Q and R blocks and the location of each well (B-16_2, B16_4z) within each block. These blocks are denoted by the peach and orange colors respectively. The green stars represent wells which are oil producers, while the red and blue stars represent gas and water injector wells. The location of the GBS is denoted with the red cross.

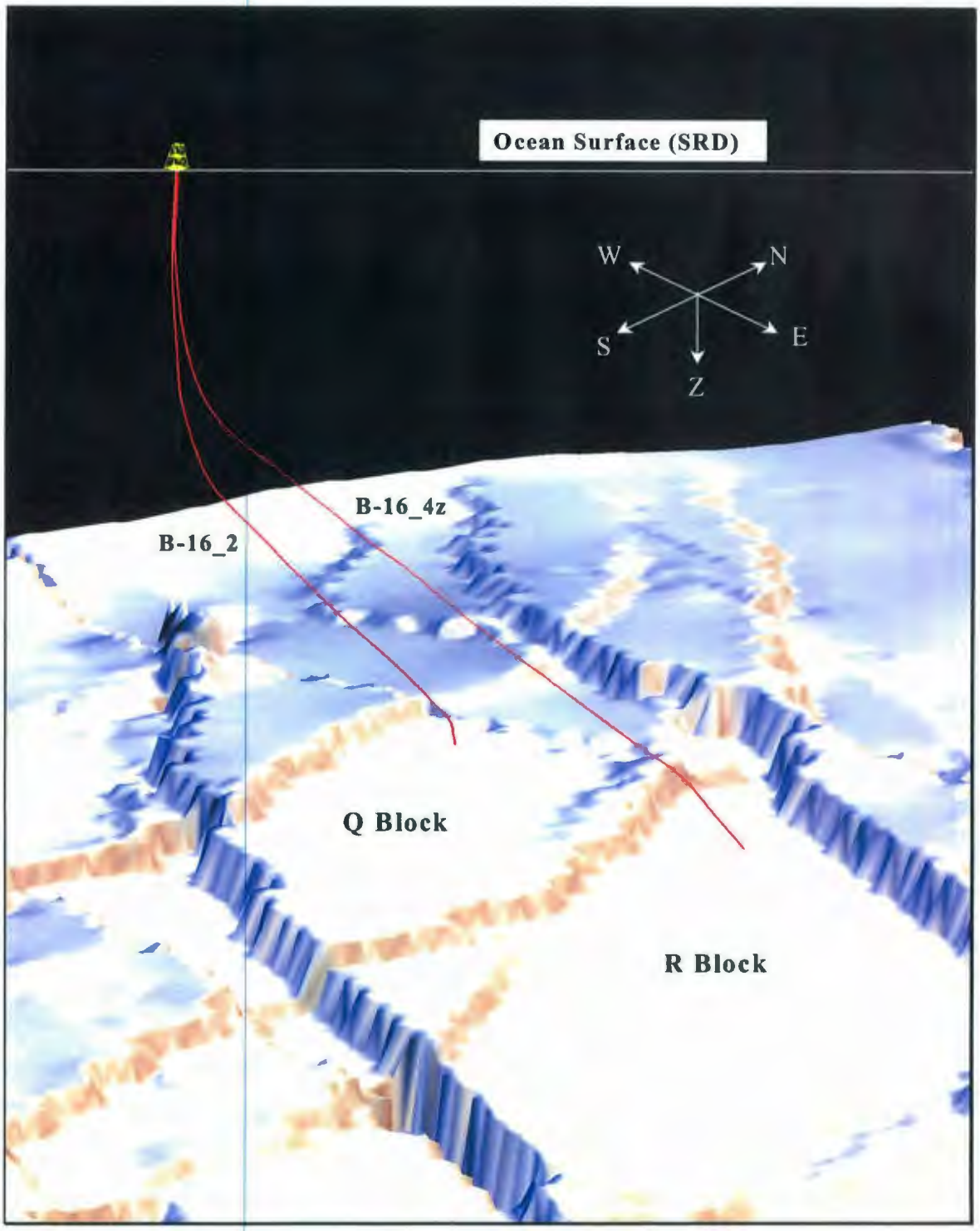

Figure 2.1.2 A three-dimensional view of the base of the Hibernia Reservoir showing the Q and R fault blocks and the B-16_2 and B-16_4z production wells.

2.2 Distinctive Survey Characteristics for VSP's Conducted in Deviated Wells

For any VSP survey acquired in a vertical or deviated well, there is standard acquisition terminology associated with it. The depth measurements taken to determine the position of the VSP tool in the well are first acquired at the kelly bushing (KB). This is the name given to a specific bushing that is located just over the hole on the drill floor of the oil rig. In the case of an offshore rig, the kelly bushing (KB) can be several tens of meters above sea level. Hence, it is convention to convert all the depth measurements relative to sea level. This common datum is referred to as the standard reference datum (SRD). The depths quoted for this study will all be referenced to SRD.

The length of wire attached to the VSP tool that is spooled out during the progression of the survey gives the measured depth (MD) of the geophones at the specific survey points. In a vertical well, the measured depth of the geophones should be equal to their true vertical depths because the amount of wire spooled out will be equal to the depth of the geophones. However, for a deviated well these values represent distance along the borehole and the measured depths of the geophone positions will be greater than the true vertical depths. **Figure 2.2.1** illustrates the distinction between these two depth measurements in a deviated well. The true vertical depths of the geophones are determined by comparing the geophone positions in the well (measured depth) with the calculated true vertical depths of the well. This is determined from a direction-inclination survey conducted during the drilling process.

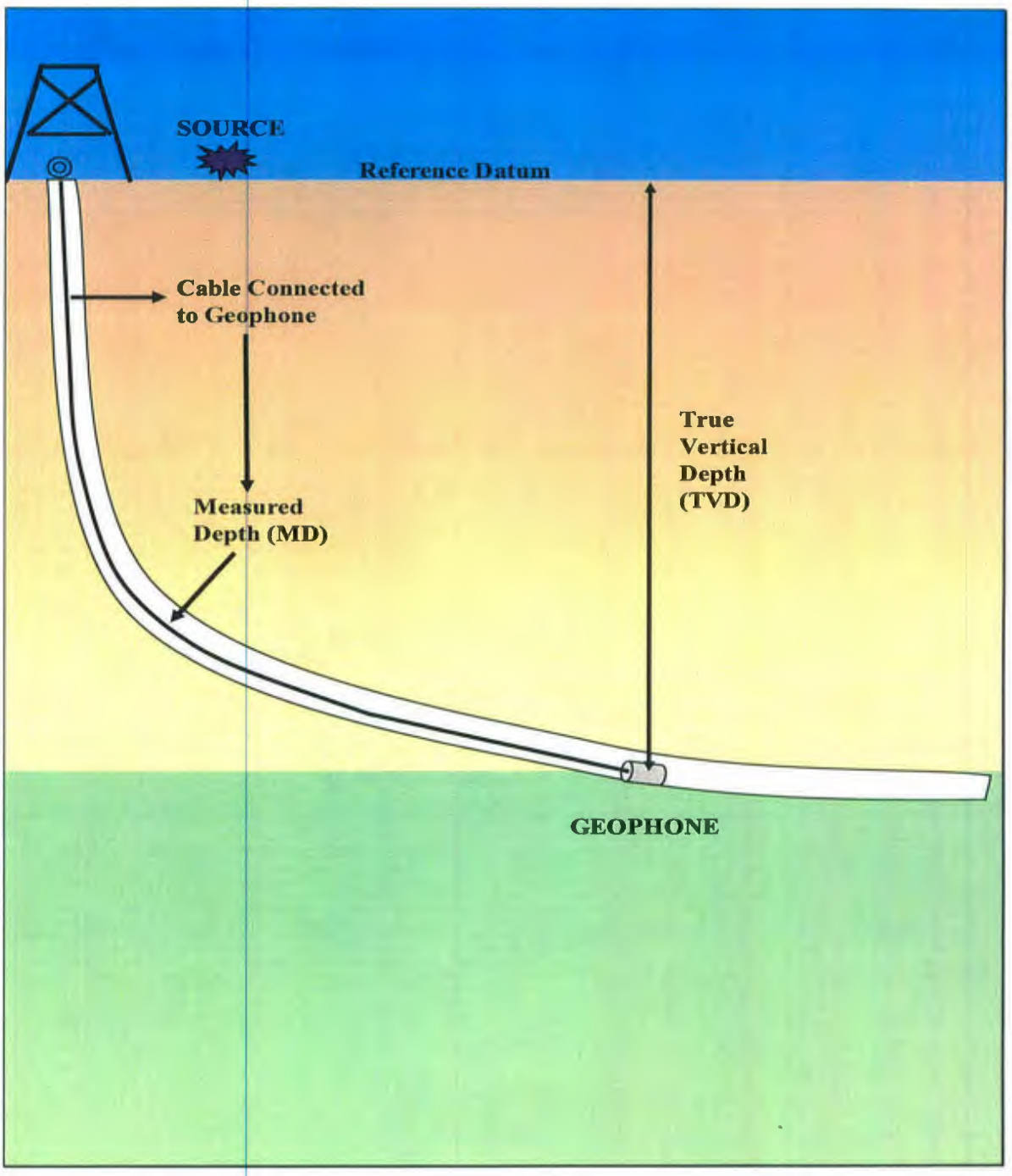

Figure 2.2.1 The distinction between the two depth measurements, measured depth (MD) and the true vertical depth (TVD), acquired during a VSP survey conducted in a deviated well.

CHAPTER 3 Signal Processing of the Vertical Incidence Survey for Travel Time - Depth Measurements

As discussed in **Section 1.2**, vertical seismic profiling was first used to measure travel times to define a time-depth relationship within the rock column. As the technique of vertical seismic profiling evolved, allowing for many different formation attributes to be investigated, the significance of acquiring basic travel times has remained.

Initially, these travel time measurements were obtained through VSP surveys acquired in vertical wells. However, highly deviated boreholes have become common practice in the hydrocarbon industry since the 1970's. Yet, there is very little literature discussing processing considerations when trying to acquire precise travel times in deviated wells. This chapter focuses on processing issues and their potential effect on deriving travel times from three component vertical incidence data. The chapter starts with a description of the experimental survey configuration. It then proceeds with possible geometric and signal processing considerations for the purpose of acquiring precise travel times. This gives theoretical insight into why rotation of the vertical component signal is performed. The travel times acquired after rotation of the vertical component are then compared to the raw vertical component travel times. Finally, the chapter concludes with observations and final remarks.

3.1 Vertical Incidence Survey Configuration

The vertical incidence survey data was acquired using Schlumberger's Array Seismic Imager (ASI) borehole tool (Kawahara et al.,1990) in the B-16_2 cased production well. The ASI tool consists of a string of five sensor packages mounted on a special bridle cable with a separation of 15 meters and connected to a mother cartridge (**Figure 3.1.1**). Each sensor package contains three mutually orthogonal geophones so that the complete seismic wavefield was recorded.

The vertical incidence survey was acquired from a measured depth (MD) range of 4369.0 meters to 634.0 meters from the standard reference datum (SRD). This measured depth range is 3682.4 meters to 633.0 meters in true vertical depth (TVD) from SRD. The survey begins at a measured depth of 4369.0 meters (3682.4 meters TVD). This is the position of the last geophone on the array, and the other four geophones in the array are positioned at 15 meter intervals above the last. This allows the array to extend an interval of 60 meters. Because of the magnetic clamping, it is assumed that the tool anchors to the bottom curvature of the deviated well. A source-boat carefully positioned the source (air-gun) above the middle of the array at a depth of 3 meters. A number of shots for each 60 meter interval were fired to try to obtain a consistent source wavelet and increase the signal to noise ratio. The sampling rate was 1ms and the recording time was five seconds. **Figure 3.1.2** gives an indication of how the survey was implemented by showing how the shots were positioned over the first two levels of the survey consisting of five geophones each and at a measured depth range (MD) of 4369 to 4309 meters and 4294 to 4234 meters.

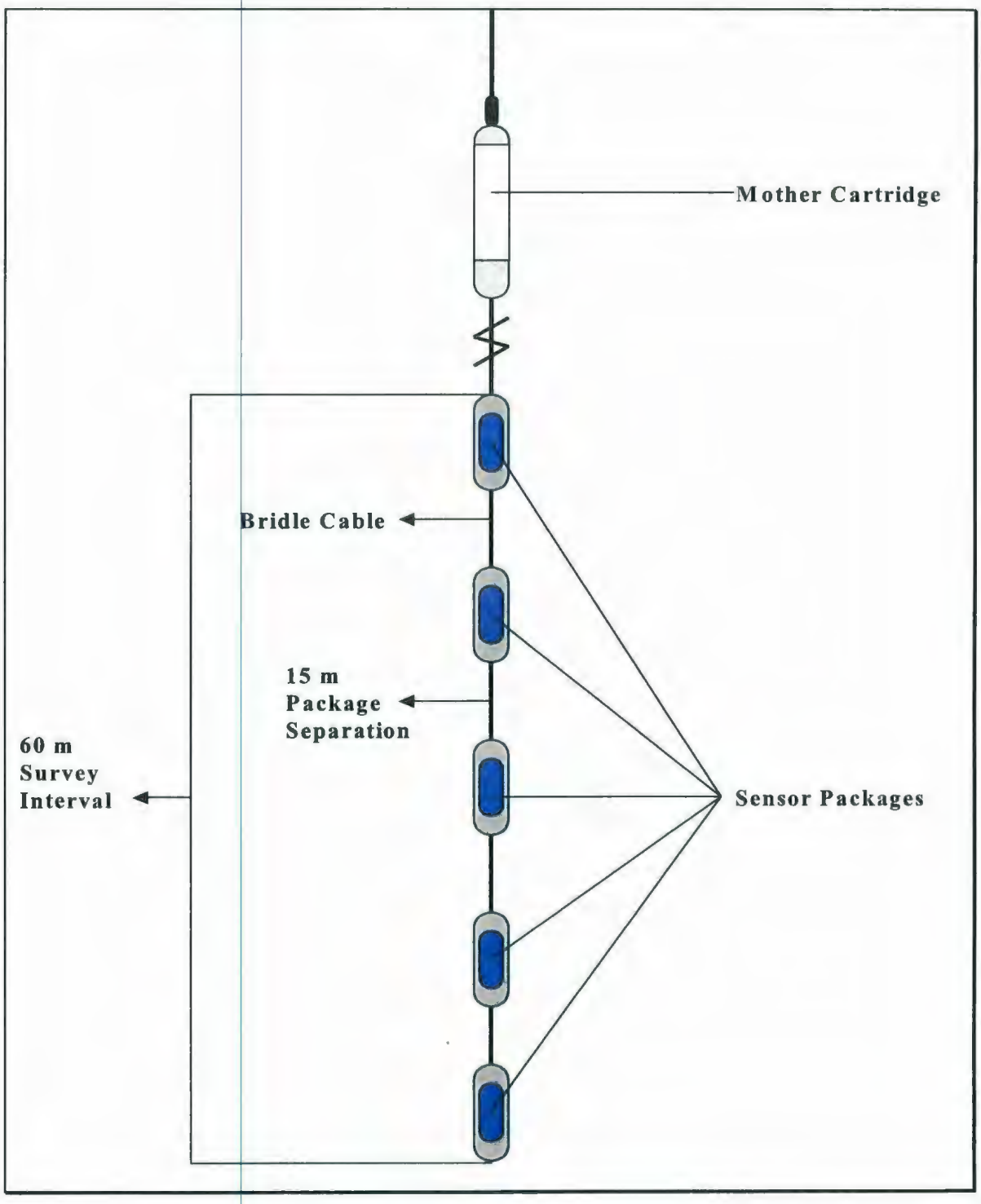

Figure 3.1.1 The Array Seismic Imager (ASI) tool configuration. Each sensor package contains three mutually orthogonal geophones and a magnetic clamping device.

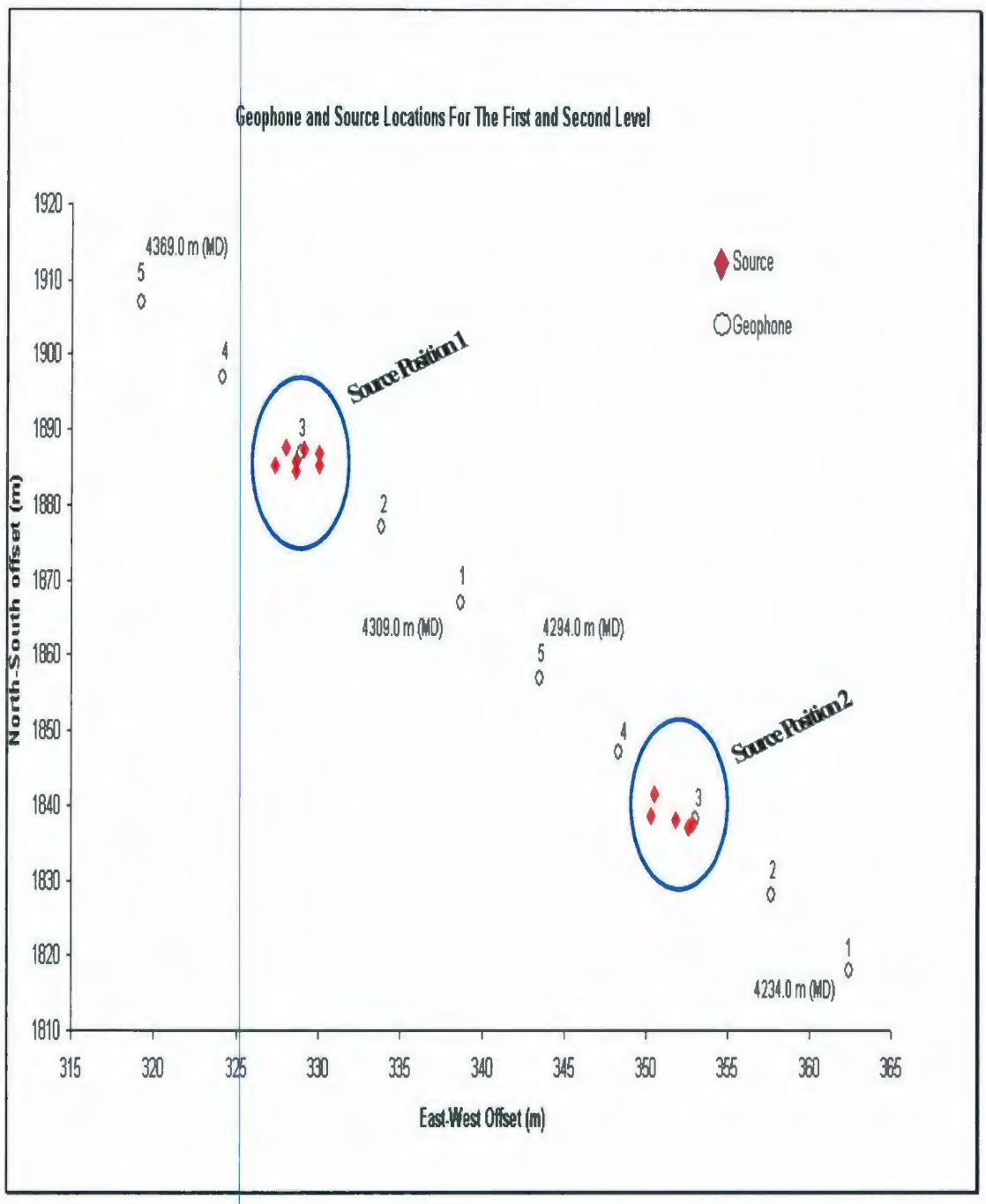

Figure 3.1.2 Shot positions over the first two levels of the vertical incident survey. The offset coordinates are with respect to a point projected to the ocean surface (SRD) 76 meters directly below the kelly bushing (KB) of the GBS.

The geophones were unclamped and then pulled up the well so that the last geophone was 15 meters above the position of the first geophone in the previous 60 meter interval. The survey proceeded as indicated until a measured depth of 1834.0 meters (1773.3 meters TVD) after which the survey interval changed from 15 meters to an inconsistent interval. This interval varied from 80, 90 and 100 meters for the last eight five geophone 60 meter intervals. **Figure 3.1.3** shows a plan view of the geophones with respect to the track of the borehole and a 3-dimensional representation of the geophone positions at true vertical depths.

3.2 Processing Considerations When Acquiring Travel Times from a Vertical Incidence Survey

3.2.1 Geometric Considerations

The geometric considerations for processing a vertical incidence survey to acquire precise travel times can be established by first investigating the near normal incidence survey conducted in a vertical borehole. One of the main properties of the near normal incidence survey that allows for the consistent acquisition of precise travel times, is that the vertical component of a three-component geophone package is in-line with the downgoing P-wave particle motion. Hence, the vertical component is in a common coordinate frame defined by the particle motion of the P-wave and therefore the signal is maximized onto that component. If this common coordinate frame were not established for each source-receiver pair, then the downgoing P-wave would be sampled, to different degrees, on all three components.

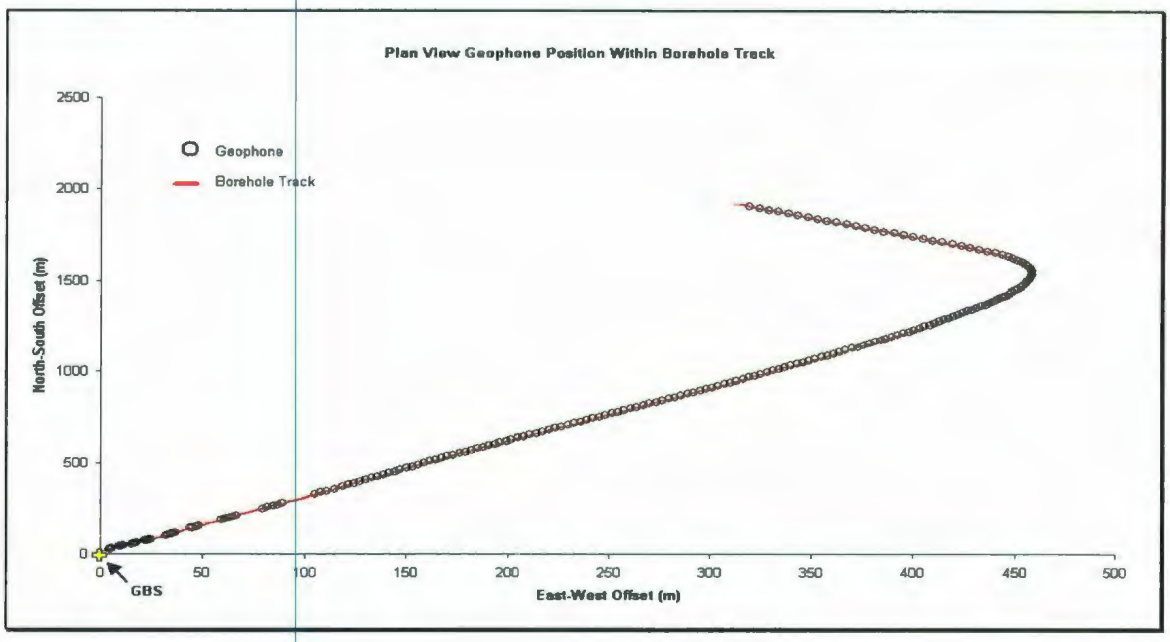

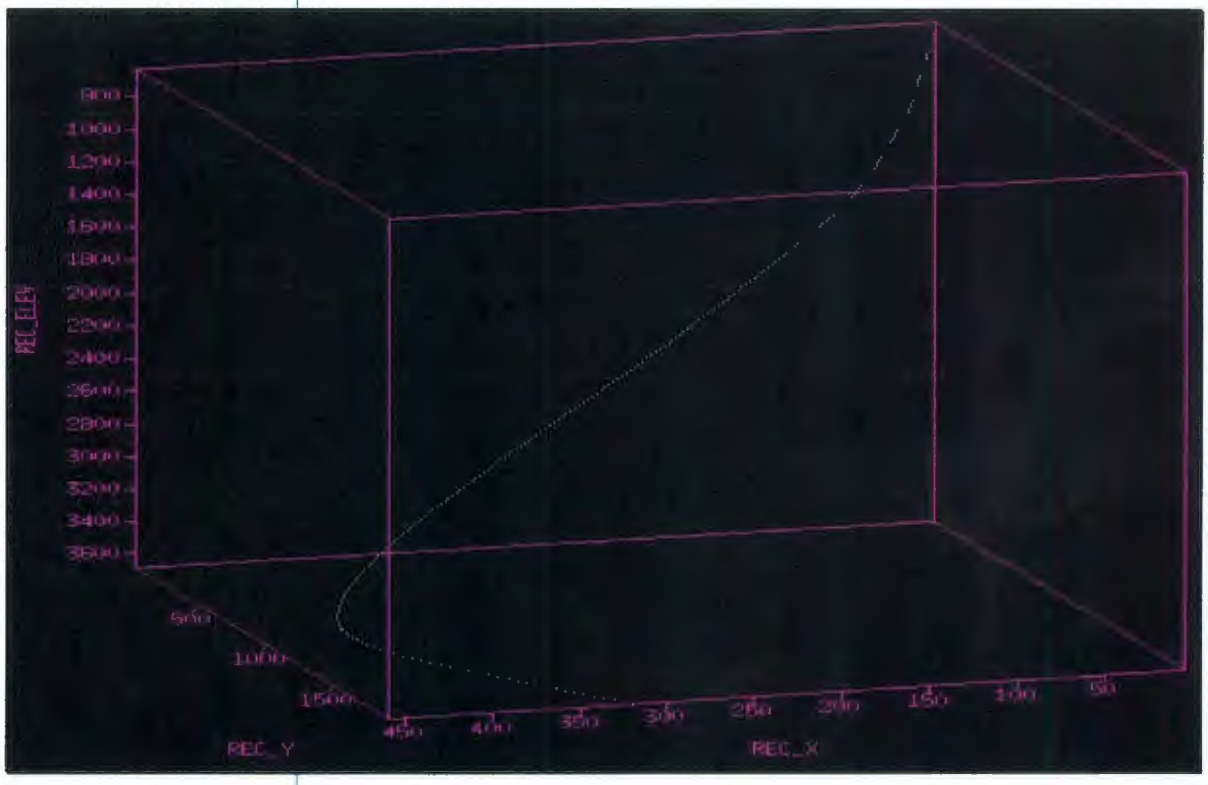

Figure 3.1.3 A plane view of the geophone positions with respect to the track of the borehole (top), accompanied by a 3-dimensional representation of the geophone positions at TVD (bottom).

This raises some significant questions. Can an unresolved measurement of a near normal incident downgoing P-wave without resolution into a common coordinate frame affect the precision of acquired travel times? Can the absence of a common coordinate frame affect the ability to acquire precise travel times even if there is a near normal incidence source-receiver configuration? Can an unresolved P-wave signal in a near normal incidence configuration cause a change in the shape of a first arrival wavelet so it is harder to identify its onset or even phase shift it?

Literature that could give some insight on these questions seems to be nonexistent. However, when processing the signal from a vertical incidence survey these questions should not be ignored. This is because the vertical component is not in-line with the direct downgoing P-wave particle motion, rather, it is at an angle dictated by the deviation of the borehole. Also, because of the rotational torque in the connecting cable attached to the tool, the horizontal components rotate freely as the survey progresses. Consequently, all three components are in a different coordinate frame for each survey level and not in-line with the P-wave particle motion. Therefore, within a three component vertical incident survey, measurements of the downgoing P-wave particle motion are **not** recorded predominately on one component, but to different degrees, on all three.

When acquiring travel times from VSP data acquired when the source is beyond near normal incidence (ie. the offset or walkaway survey), it is common practice to rotate the vertical component to lie in-line with the P-wave particle motion. This is because source is always at an angle to the receiver. Therefore, the vertical component is not in-

line with the P-wave particle motion. However, rotation is not common practice when processing vertical incidence data even though the vertical component is not in-line with the direct downgoing P-wave. In the context of this argument, it would be good practice to obtain a common coordinate frame defined by the P-wave particle motion when acquiring travel times from a vertical incident survey. This can be done by rotating the vertical component - using the signal from all three components - vertically in-line with the downward P-wave particle motion. This will ensure that the P-wave signal is predominately on the vertical component, establish a common coordinate frame for each source-receiver pair and possibly increase the reliability of the acquired travel times.

The remainder of this chapter demonstrates the implementation of the rotational process on the vertical incidence signal. The discussion following this demonstration is aimed at shedding some light on determining if there is a need for rotation of the vertical component into a common coordinate frame when trying to acquire precise travel times from a vertical incidence survey conducted in a deviated well.

3.3 Vertical component processing

3.3.1 Geometry assignment and Trace Editing

As outlined in **Section 3.1**, the vertical incidence survey data used for this study was conducted in the B-16_2 deviated cased production well using Schlumberger's ASI borehole tool. The survey depth range is from a true vertical depth (TVD) of 3682.4 meters to 633.0 meters from the standard reference datum (SRD). The B-16_2 well is at a maximum deviation of 48 degrees from the vertical.

Assigning the vertical incidence survey geometry recreates the source-receiver survey configuration, borehole path and the shot-to-receiver azimuths. East-west (x) and north-south (y) positional coordinates are needed. These positional coordinates denote the offset (in meters) from a point directly below the kelly bushing at SRD (76m). Even though there is a small range of source positions over the middle geophone in the array (**Section 3.1**), a single source position with the same offset coordinates as the middle geophone is used for each progressive survey level. Trace quality control is then performed by comparing entered and computed data.

Figure 3.3.1 shows the full upgoing and downgoing wavefields recorded. Several events can be identified in these data. The downgoing P-wavefield and the upgoing P-wavefield are labeled P and P-P respectively. The large change in the slope of the first breaks at the upper levels (shallower depths) of the survey is due to changes in level spacing. The prominent steeply sloping downgoing event is identified as a tube wave which propagates along the well bore.

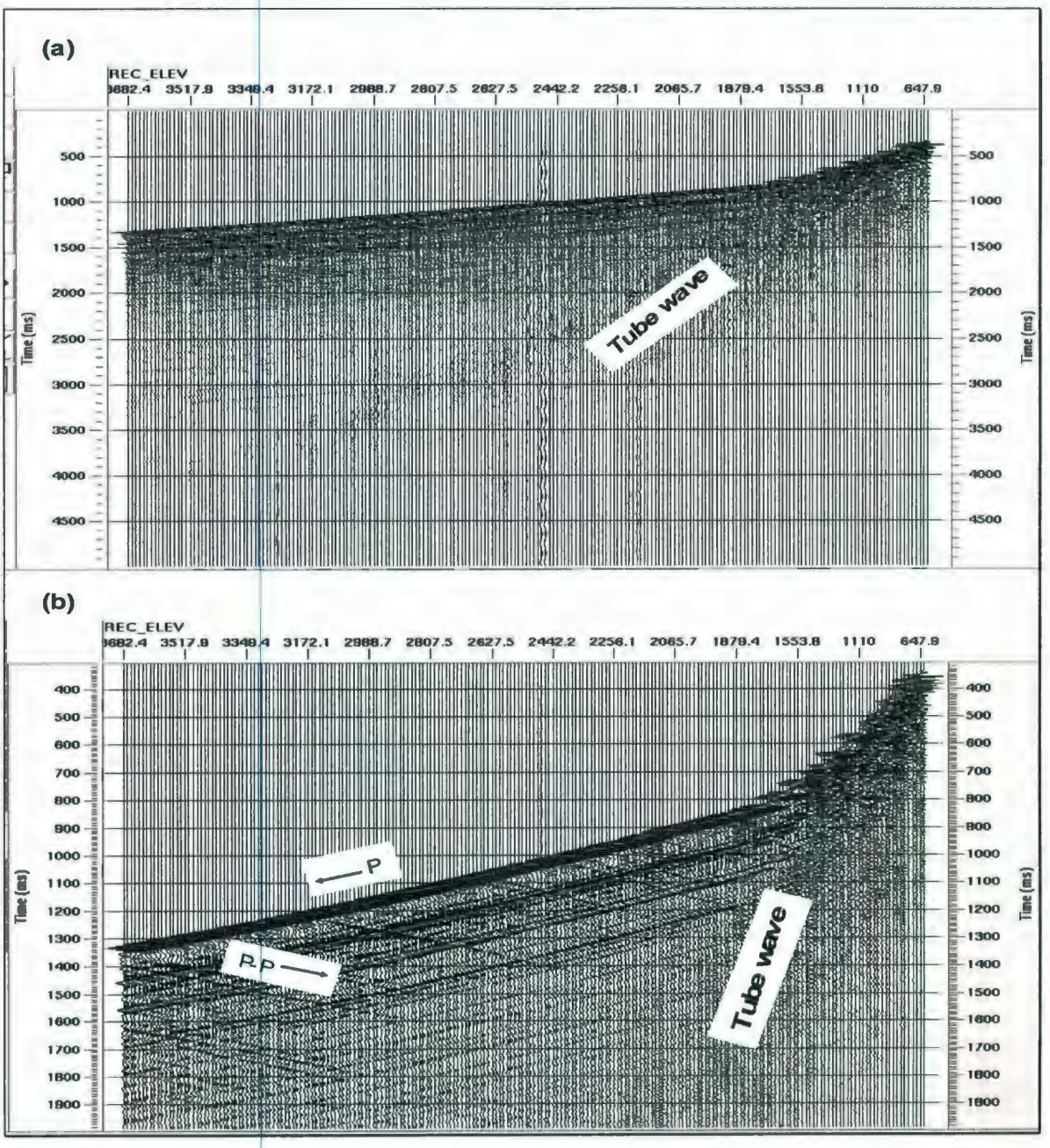

Figure 3.3.1 (a) Raw vertical component trace gather of the full vertical incidence survey from true vertical depth (SRD) of 647.9 meters to 3682.4 meters and recording time from 0 to 5000 ms showing upgoing and downgoing waves in addition to the tube wave. (b) Vertical component trace gather showing the same depth range as (a), however, emphasizing a recording time range of 300to 2000 ms respectively.

After further examination of **Figure 3.3.1 (b)**, the majority of the ensemble traces show little noise. Editing of these traces in order to better determine a time pick from the first break downgoing P-wave would probably be ineffective. To solidify this, **Figure 3.3.2** shows the traces of the first three stages of the survey (TVD range of 3682.4 meters to 3538.6 meters). There is a clear representation of the onset of the direct (downgoing) P-wave without any additional noise.

3.3.2 Acquiring First Break Travel Times

Acquiring the first break travel times from the onset of initial downgoing P-wave involves the use of a first break picking algorithm. A time gate is picked before and after the onset of the first break downgoing P-wave. Examining the onset of the first break energy reveals that most of the energy lies within a time envelope of 100ms. Care is taken to pick a time gate that encompasses the first break energy and does not exceed 100ms. This prevents additional recorded signal from being used in the first break determination. In **Figure 3.3.3**, the time gate is shown for the first 15 recorded traces (TVD 3682.4 m to 3538.6 m).

Trying to determine the time gate for the shallow part of the survey (TVD 1820.8 m to 647.9 m), where the survey depth interval varies from 80, 90, or 100 meters, is of concern. Confidence in determining the onset of the first break energy is much lower (**Figure 3.3.4**). Examining these traces and using the more prominent traces as a guide, it is determined that a 100 ms time gate can also be used. However, for this part of the survey confidence in specific picks is low.

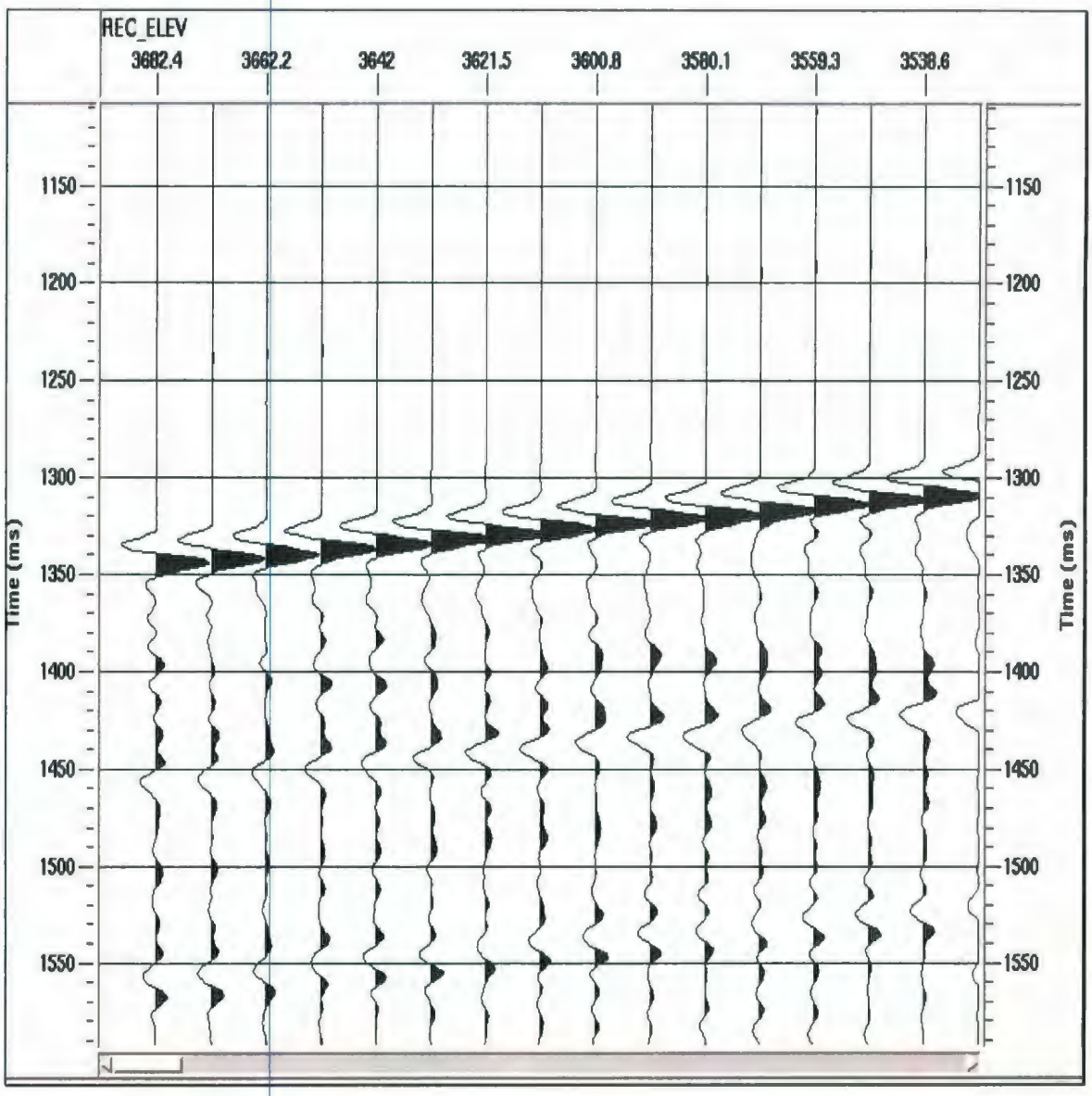

Figure 3.3.2 Trace ensemble of the vertical component for the first three levels of the survey. True vertical depth range of 3682.4 meters to 3538.6 meters and time range of 1100 to 1600 ms respectively. The onset of the first break downgoing wave is very identifiable.

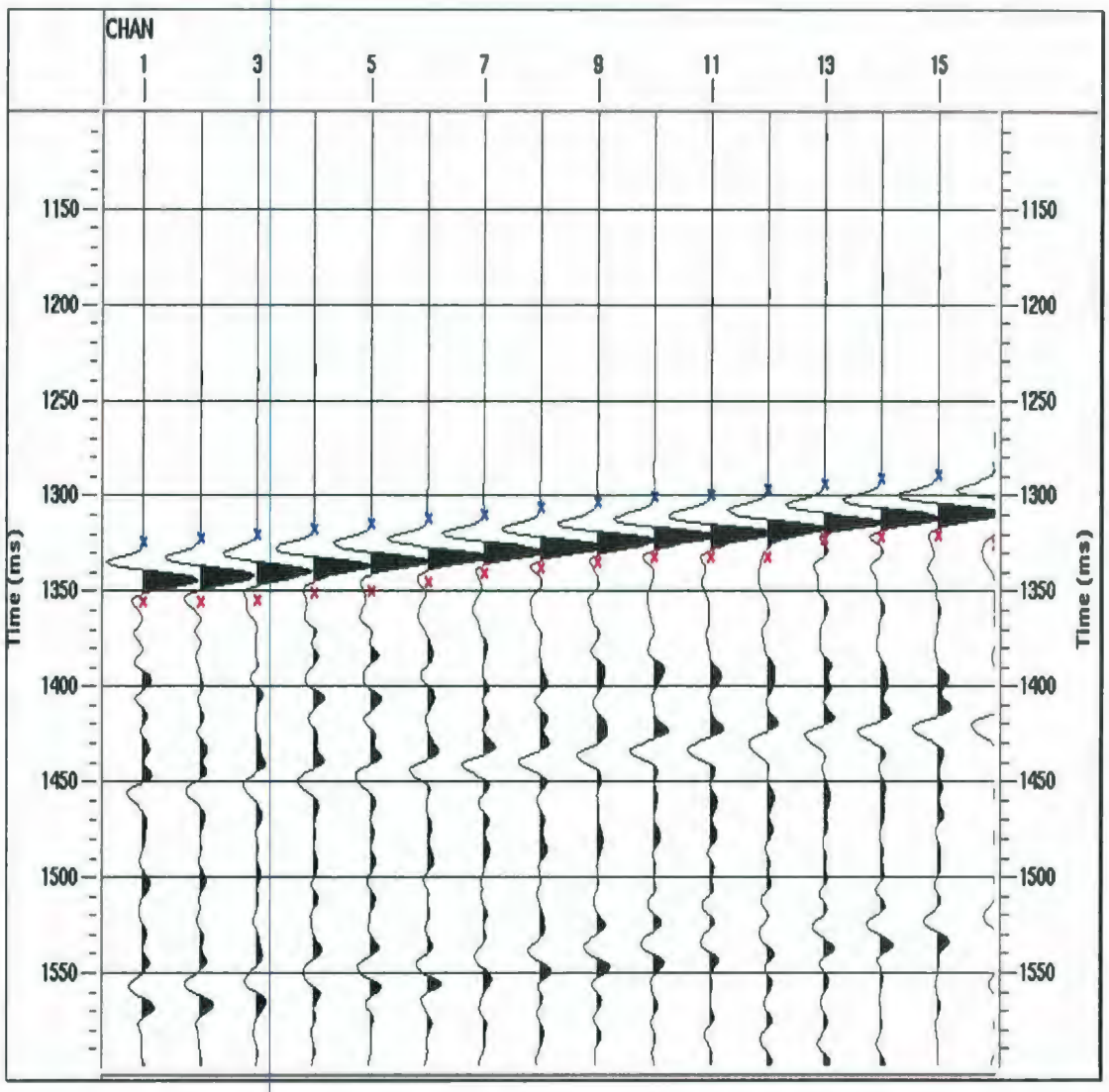

Figure 3.3.3 Trace ensemble of the vertical component for the first three levels of the survey (TVD 3682.4m to 3538.6m) showing the time gate used for the first break algorithm.

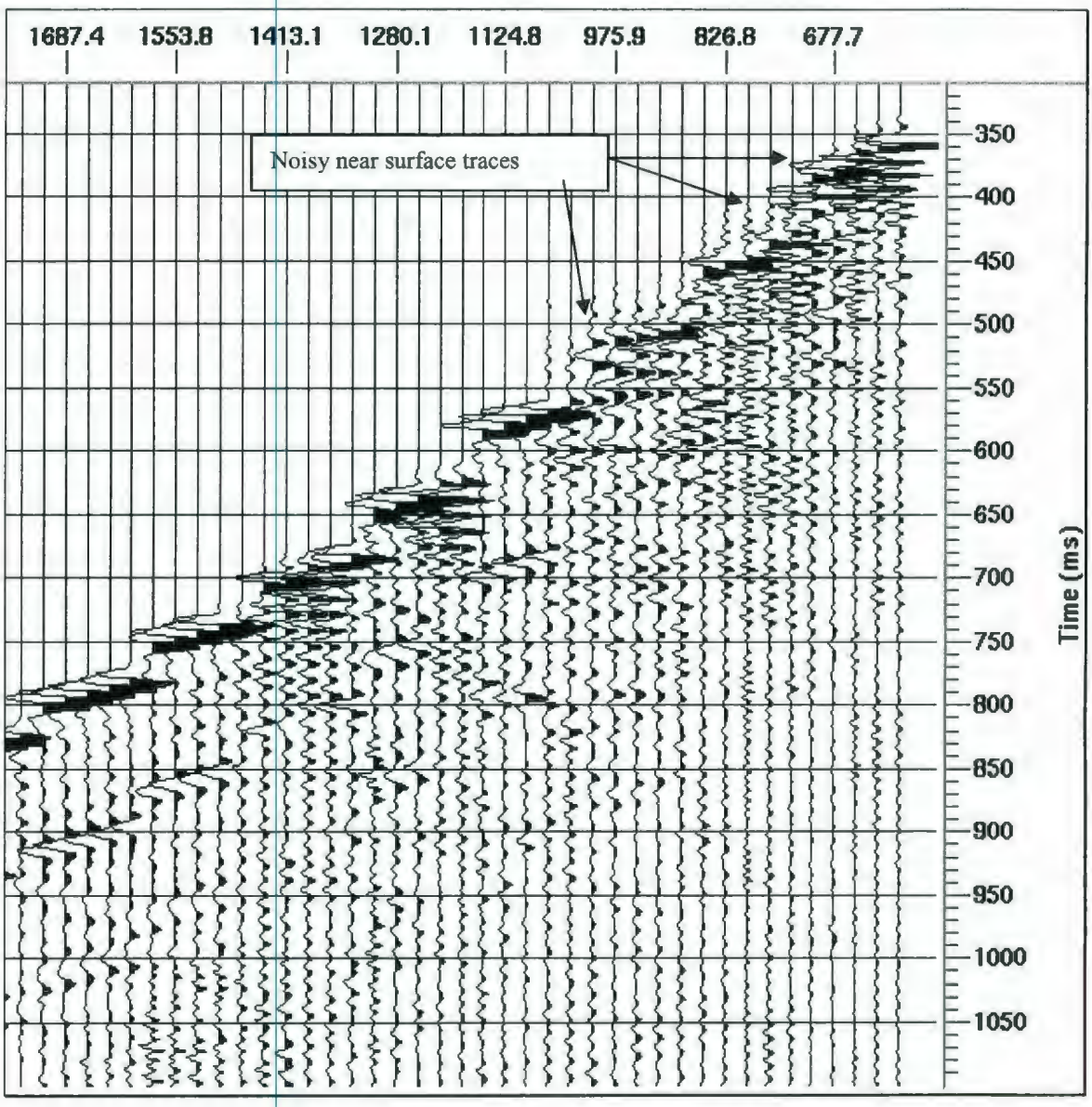

Figure 3.3.4 Trace ensemble of vertical incidence survey showing shallow section of the survey (TVD 1820.8 m to 647.9 m). Note the increase of noise around the onset of the first breaks.

From these travel time picks, a time-depth relation **(Figure 3.3.5)** is created. Since there was very little processing of the signal before these travel times were obtained, travel times acquired after the rotational process is compared to these "raw" travel times. This reference is needed in order to assess if rotating the vertical component should be considered when acquiring travel times from a vertical incidence survey conducted in a deviated well.

3.4 Three Component Processing

3.4.1 Geometry Assignment and Trace Editing

Assigning the geometry to all three components is much the same as assigning the geometry to just the vertical component. For each component, the same source coordinates and calculated source-to-receiver offsets are used. However, the azimuth and the inclination of the borehole from North also enter the calculation. These data are obtained from the direction and inclination measurements taken during the drilling process. The measured depth associated with the direction and inclination data is paired up with the same measured depths (MD) of the survey. The appropriate corresponding direction and inclination data are then used. In some cases, the measured depths taken during specific samples of the direction and inclination survey are not an exact match to the vertical incident survey. Therefore, the closest direction and inclination measurements to the vertical incidence's measured depths are used.

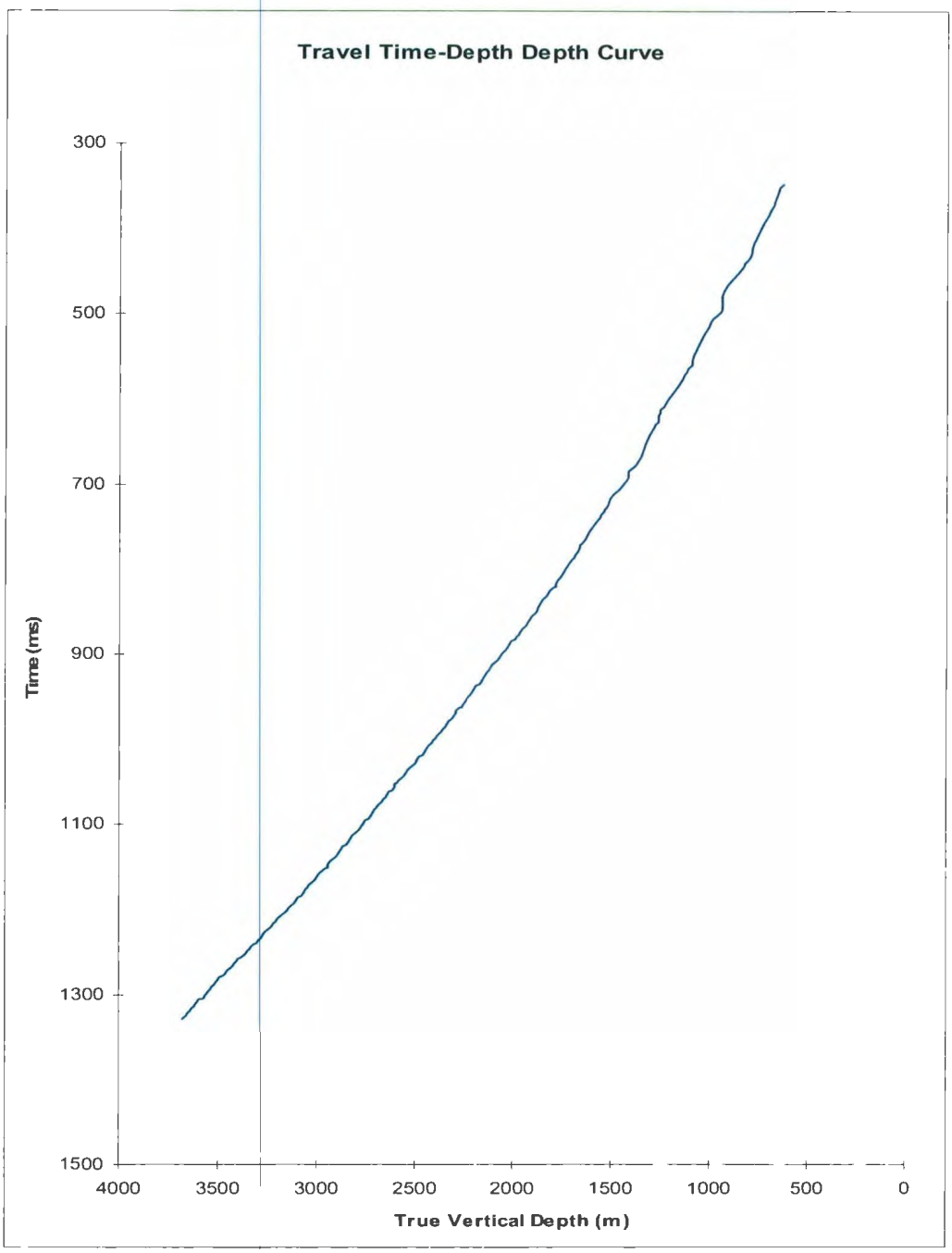

Figure 3.3.5 Travel time depth curve obtained form the downgoing first break travel times of the vertical incident survey.

For this study, the x-component of the geophone package is assigned the number one (1), the y-component is assigned the number two (2), and the z-component (the vertical component) is assigned the number three (3). To process the three component data effectively, other calculations such as the azimuth of each component are needed. This is calculated from the source-to-receiver azimuth in the same way outlined in **Section 3.3.1**. These calculations allow for the display of the raw component trace gathers (**Figure 3.4.1**).

On first inspection of the x and y-components, they seem to be slightly noisier than the z-component. Additionally, the downgoing P-waves are not as prominent. Also, zooming in closer on the individual traces of the y-component reveals a reversal in the polarity of every fourth or fifth trace (**Figure 3.4.2**). The polarity of these traces is reversed before rotational analysis can be performed.

3.4.2 Rotational Analysis

The purpose of rotational analysis is to reorientate or rotate three component seismic data to a new coordinate frame that is defined by the nature of the experiment. As with the vertical incident data used for this study, this process can allow for the rotation of the vertical component into the plane of the downgoing P-wave particle motion. This will maximize the P-wave signal onto the vertical component. To determine what angles are needed for component rotation, the concept of a hodogram is used.

A hodogram is a plot of seismic amplitudes recorded in a plane as a function of time. **Figure 3.4.3 (a)** illustrates two seismic receiver components at right angles to one another with a simplified planer seismic wavefront approaching at a 45 degree angle to both receivers. **Figure 3.4.3 (b)** illustrates a hodogram plot of data that could possibly

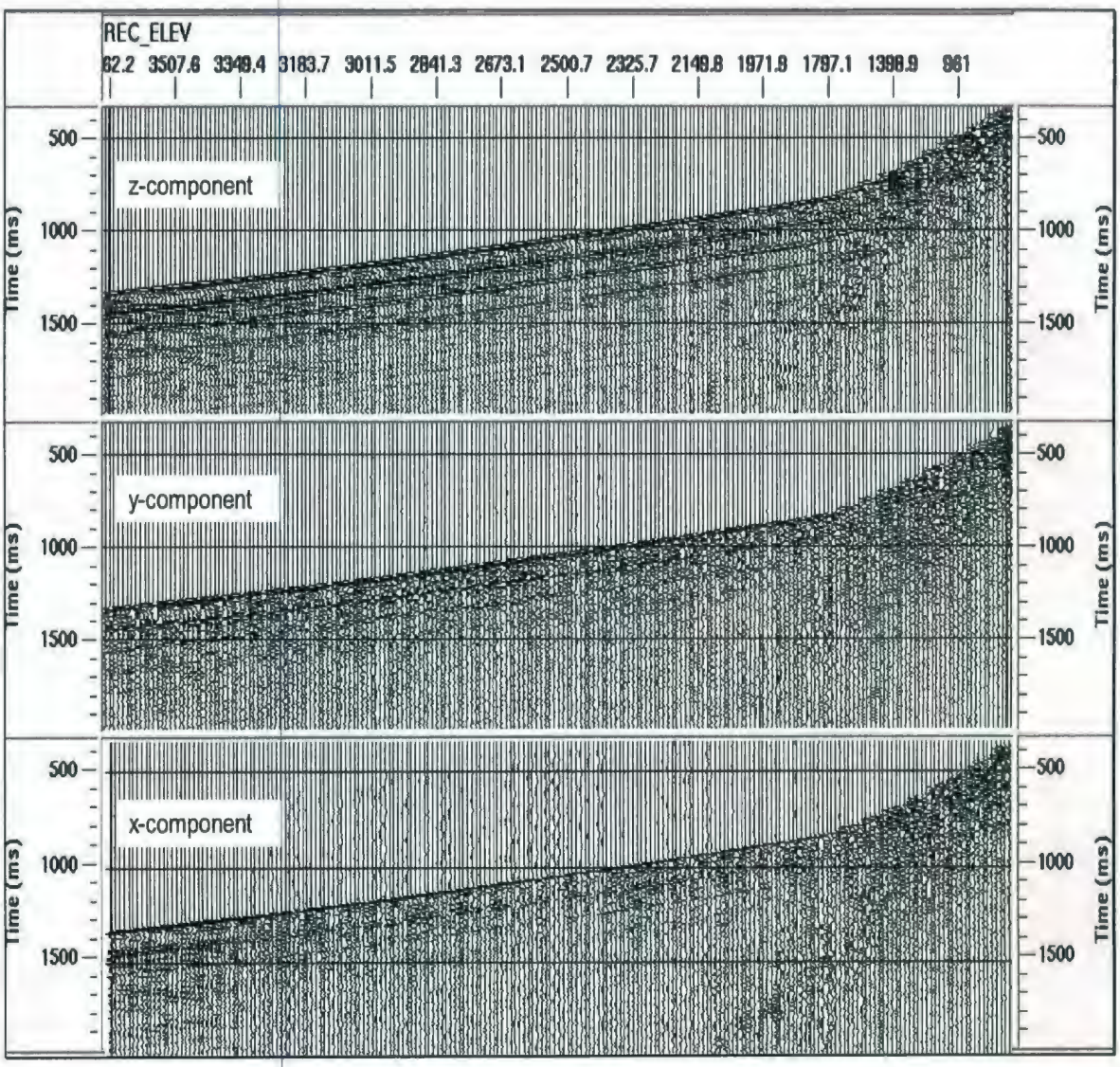

Figure 3.4.1 Three panel trace ensemble of the x, y and z-components for the full depth range of the survey and an emphasized recording time range of 300 to 2000 ms respectively.

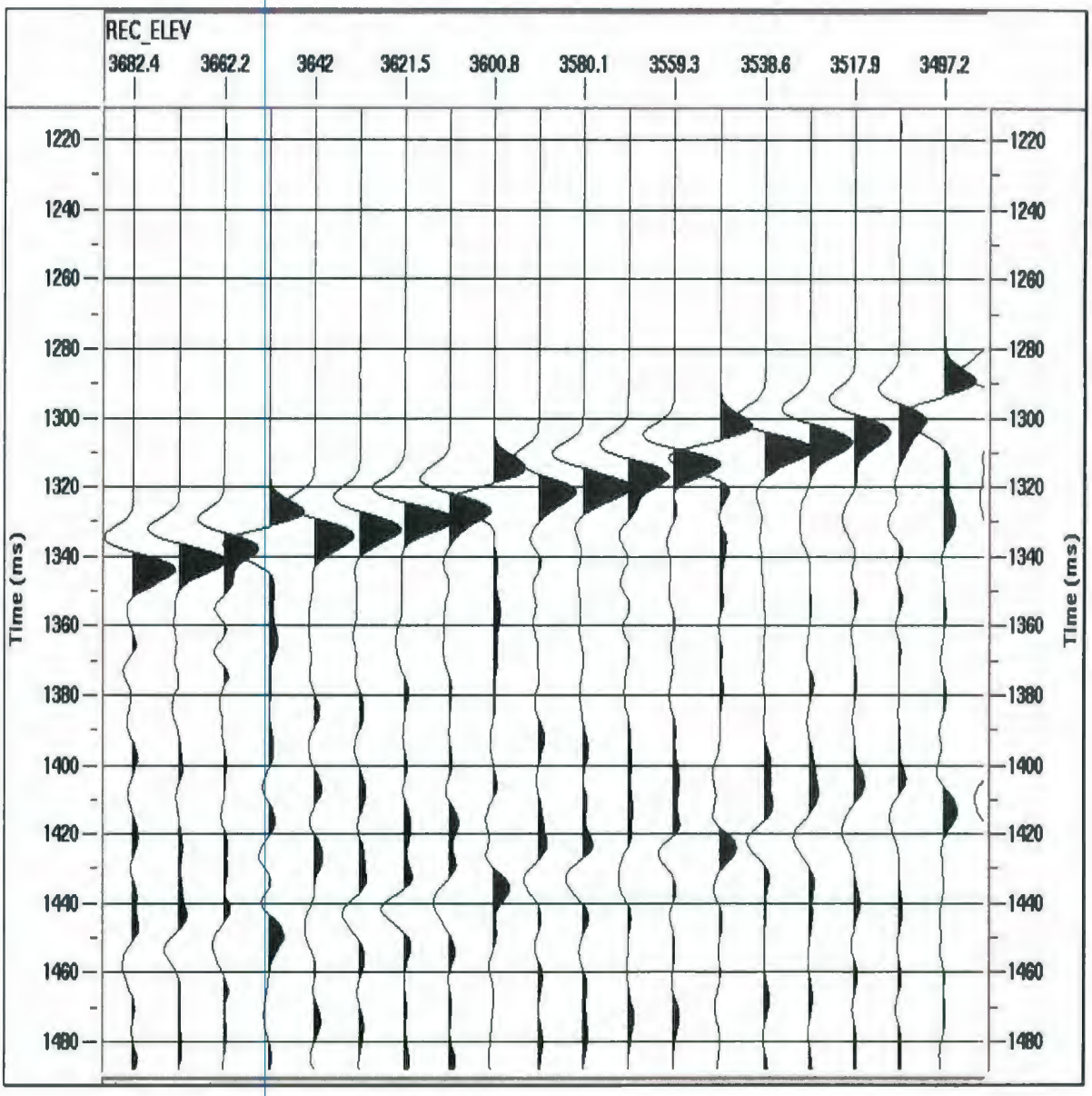

Figure 3.4.2 Trace ensemble of the y-component for the first four levels of the survey (TVD 3682.4 m to 3486.8 m) showing the reversed polarity fourth or fifth trace. This continues throughout the entire ensemble.

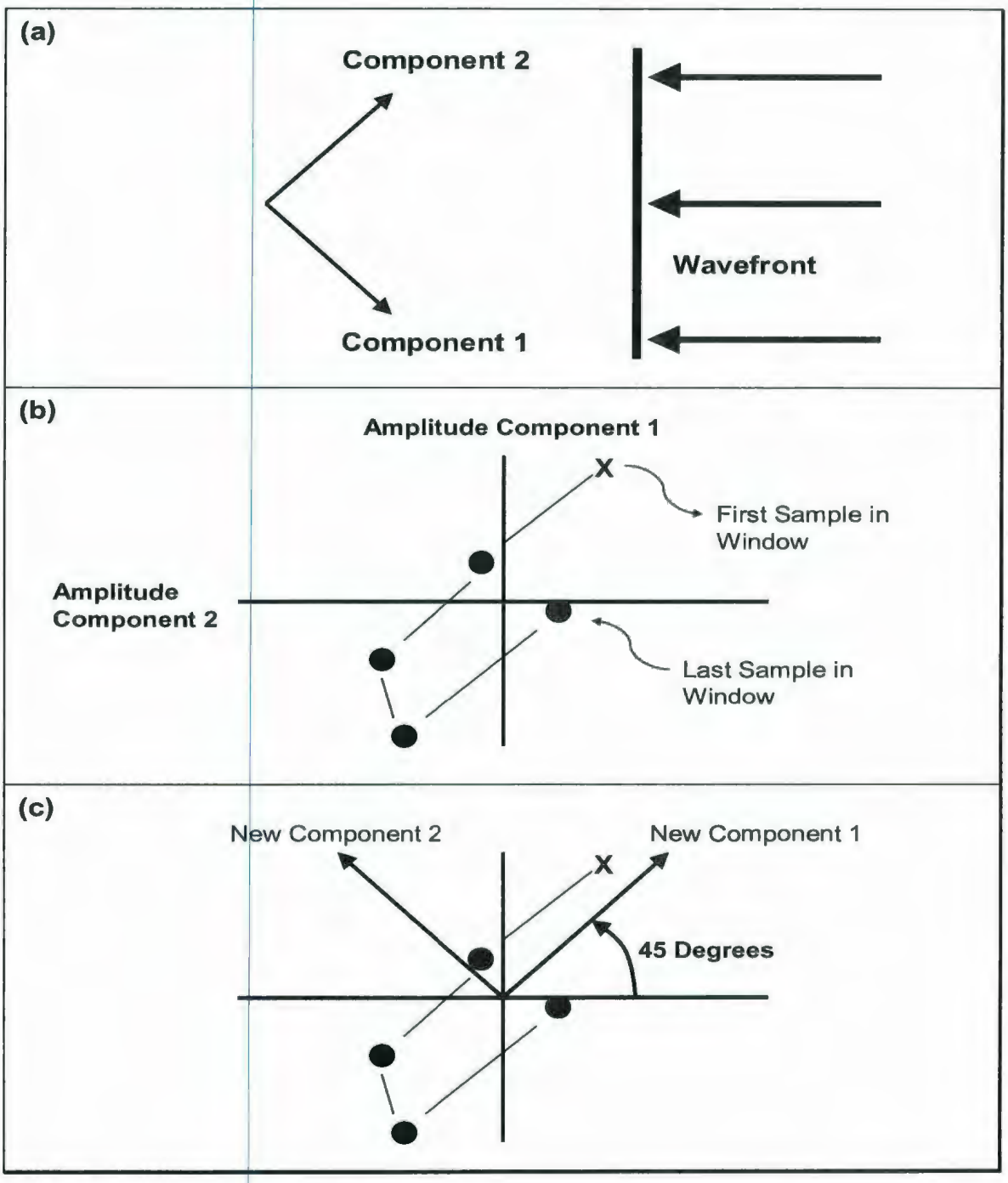

Figure 3.4.3 Illustration on the concept of the hodogram. (a) Planer Wavefront approaching receiver components at right angles to each other. (b) Hodogram of five samples recorded on component 1 and 2 in (a). (c) New receiver axes after 45 degree rotation counter-clockwise.

have been recorded on the two receivers in **Figure 3.4.3 (a)**. Each point in the hodogram is a plot of the amplitude on Component 1 versus the amplitude on Component 2 within a given time window. The five points in the hodogram plot represent the amplitudes of five sequential samples from the recorded data traces. The first time sample in the time window is marked by an "X" and sequential samples are connected with a line. If Component 1 of the receivers in **Figure 3.4.3 (b)** had been orientated directly toward the approaching wavefront, the majority of the energy in the five samples would have been recorded on Component 1. Component 2 would have been perpendicular to the particle motion of the wavefront, therefore, relatively little of the energy would have been recorded on this component. **Figure 3.4.3 (c)** illustrates a new set of components after rotation (solid lines) which maximizes the power on the new Component 1. For the purpose of this study, the new Component 1 can represent the vertical component and its rotation into the plane of the downgoing P-wave energy.

Before using the concept of the hodogram to rotate the vertical component in-line with the downgoing P-wave particle motion, specific component labeling has to be introduced in order to follow the rotations performed by the hodogram algorithm used for this study. The x-component is given the label H1, the y-component is given the label of H2 and the vertical component (z) is labeled V1. Throughout the rotational processes, it is assumed that the H1 component is 90 degrees in a clockwise direction from the H2 component when viewed from above the H1-H2 plane (right-handed coordinate system).

The three-dimensional coordinate rotation of the three geophone components is decomposed into two separate two-dimensional rotations. For these data a rotation in the horizontal plane (H1-H2) is followed by a rotation in the plane defined by the vertical component and the rotated H1 component. **Figure 3.4.4 (a)** illustrates how the rotation of H1 and H2 through an angle theta is performed. The H1-axis is rotated through an

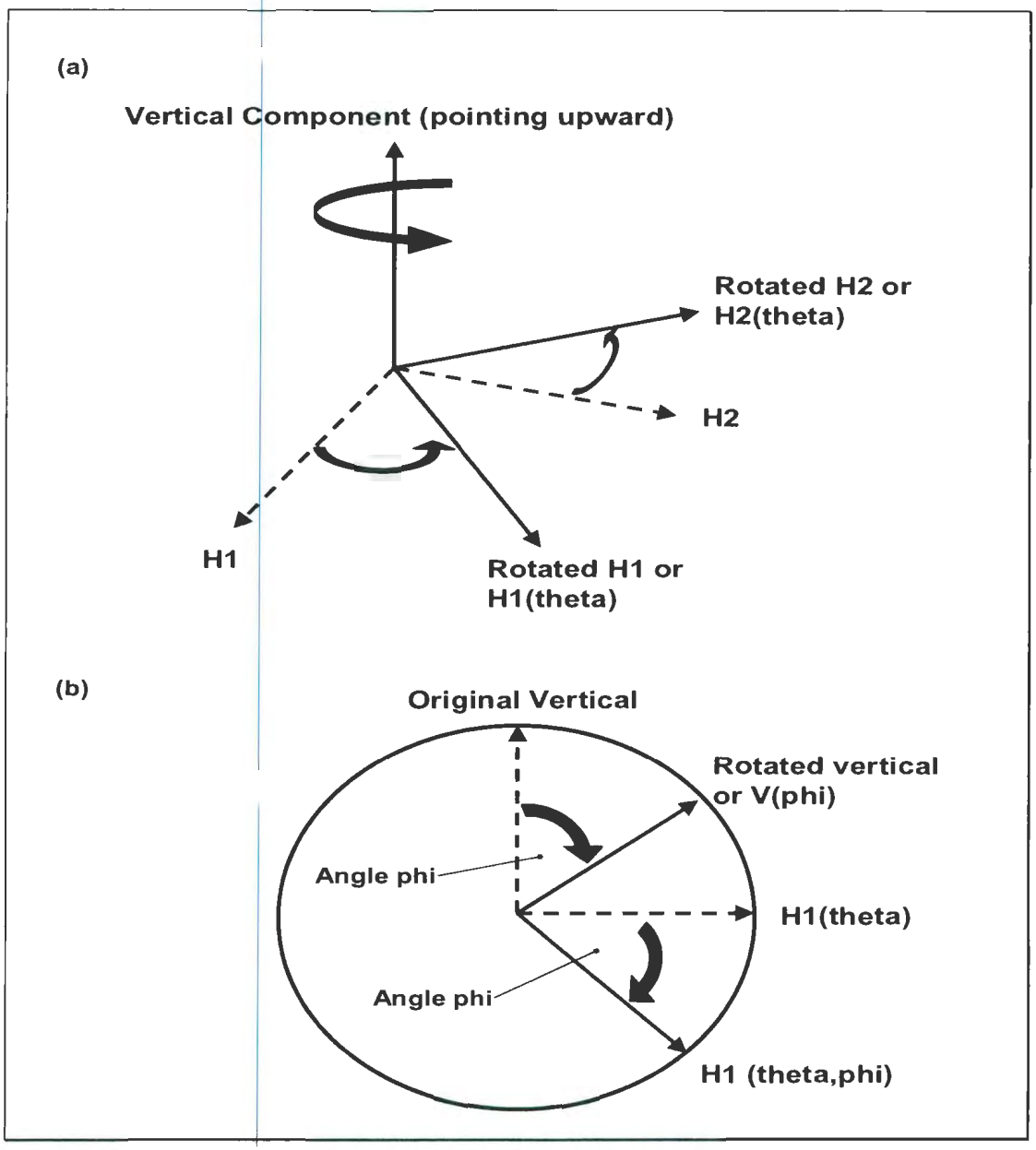

Figure 3.4.4 A depiction of the rotations performed on the three component vertical incident data for this study. (a) Illustrates the first set of rotations in the H1-H2 plane. Note the vertical component is orientated upward for clarity. (b) Illustrates the second set of rotations around H2. The new coordinate axes after the rotation are solid lines and the original positions of the axes are dashed lines.

angle theta in the direction of the H2-axis (counter-clockwise). Note that the direction of the vertical component is unaffected by this rotation.

The second rotation is performed in the plane defined by the vertical-axis and the rotated H1-axis which is denoted as H1 (theta). In this case, the angle phi is measure from the vertical-axis in the direction of H1 (theta). **Figure 3.4.4 (b)** illustrates the phi rotation looking down the rotated H2-axis which is denoted as H2 (theta). Note that this rotation leaves the direction of the rotated H2 component unchanged. The vertical axis after rotation through the angle phi is referred to as V (phi), and the H1(theta) axis after rotation through the angle phi is referred to as H1(theta,phi). After these rotations are performed, the coordinate frame of the geophones is now aligned with the P-wave signal.

3.4.3 Acquiring First Break Travel Times after Rotation of the Vertical Component

Considering all three components at one time for every geophone position, the hodogram algorithm used for this study allows for the examination of the power recorded on all three components with respect to the axes of the specific component rotation performed. A time gate that encompasses the first break downgoing P-wave for each component is initially determined. Multiple interpretations of different time gates, 10ms before and 40ms after the initial trough of the first break allows for a number of samples that can determine the P-wave particle motion with confidence.

Another useful feature of this hodogram algorithm is that it displays the horizontal and vertical traces before and after the rotation in real time. This can increase confidence in the rotations performed on the data because it is possible to visually interpret the

effectiveness of the processing step for each trace. This is especially useful for the shallow levels which contain more noise. **Figure 3.4.5** displays the hodograms for the first level (five geophones) of the survey. The particle motion of the downgoing P-wave is well defined. Hence, the new component axes are picked with a high degree of confidence. **Figure 3.4.6** displays the hodograms for the first level (five geophones) after the rotation is performed. These hodograms show that the vertical component has a concentration of the first break energy from all three components. The vertical component is now pointed directly towards the impinging P-wave and in a vertical plane with the source.

To be certain of this, the inclination angle of the vertical component (define by the borehole inclination) before rotation is compared with a calculated vertical component inclination relative to the vertical plane after rotation. This calculation consists of subtracting the angle phi for which the vertical component is rotated through with the original inclination angle. The inclination calculations for the first two levels are found in **Table 3.4.1**. The vertical component for the first three levels is now in a vertical plane of incidence and therefore in-line with downgoing P-wave. The full data set of the rotation angles used for the rotation of the vertical component can be found in **Appendix A** of this study.

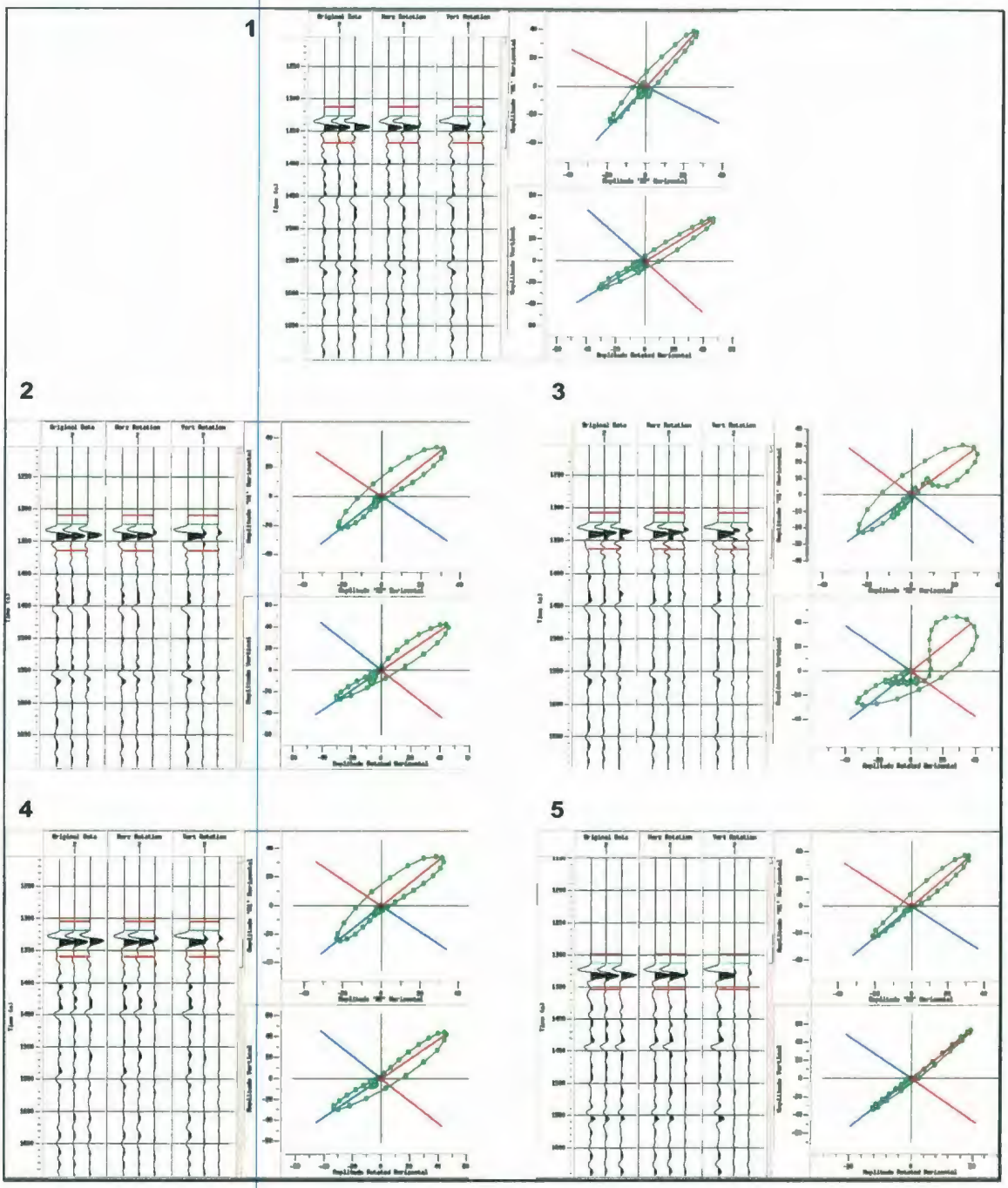

Figure 3.4.5 Hodogram display of the first five geophones of the survey before rotation. Note the traces before and after each rotational operation. Consequently, the vertical trace is left with maximum power. The first trace in the original three trace ensemble (far left) is the vertical component. Second, is the y-component (H2) and the third trace is the x-component (H1).

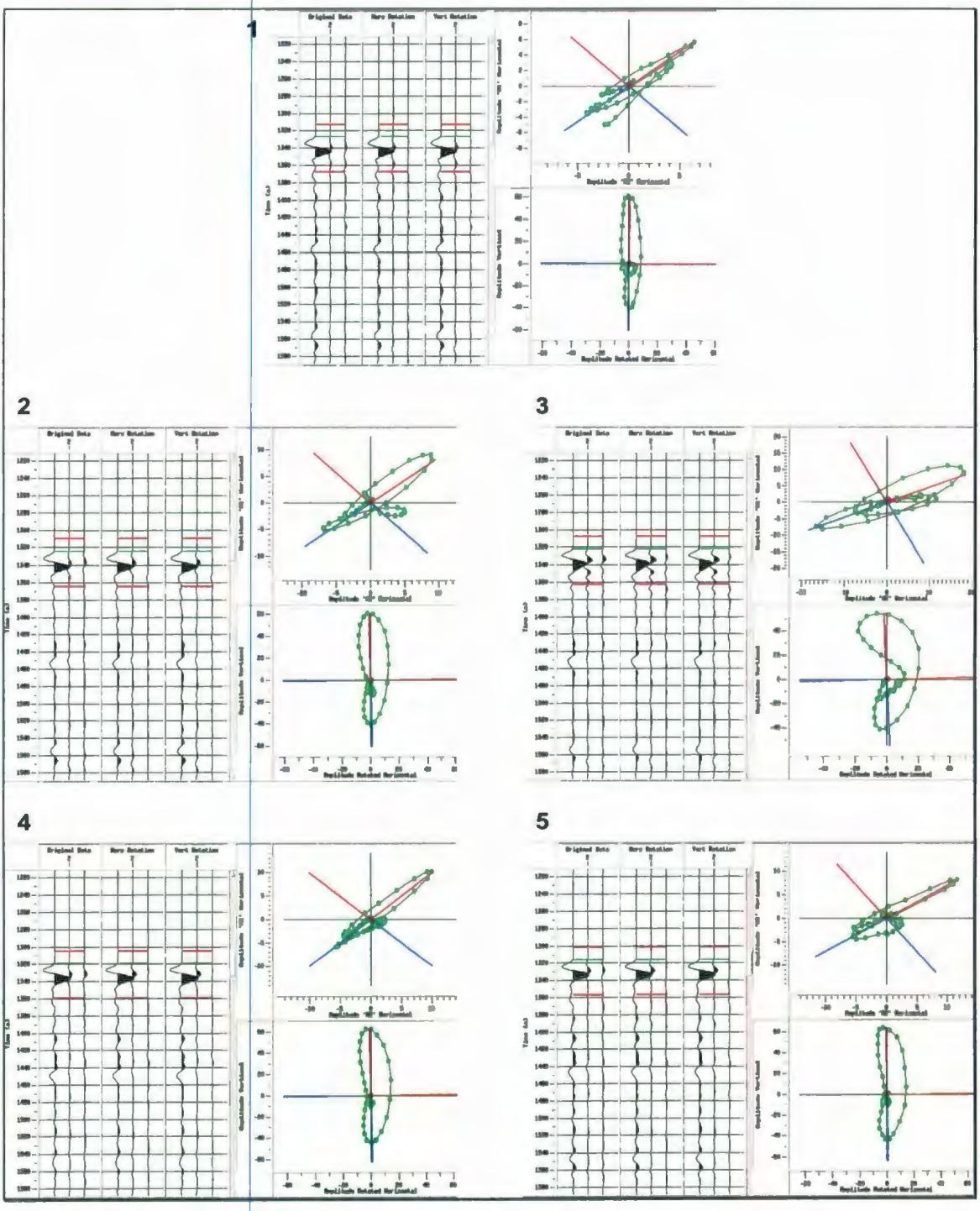

Figure 3.4.6 Hodogram display of the first five geophones of the survey after rotation. The bottom right hand corner of each display prominently shows that the vertical component contains most of the power after rotation. Hence, it must be pointed towards the source.

Table 3.4.1 Inclination Calculations Relative to the Vertical Plane Before and After Rotation of the Vertical Component for the First Two Levels (10 traces -- TVD 3682.4m to 3590.4m).

Trace Number	Inclination Before Rotation From Direction and Inclination Survey (degrees)	Inclination After Rotation (degrees)
1	47.70	3.70
2	47.70	0.01
3	48.00	5.00
4	48.00	1.00
5	47.40	0.69
6	47.40	4.41
7	46.80	2.80
8	46.20	4.19
9	46.20	4.20
10	46.00	0.40

Displaying the trace ensembles of all rotational operations performed on the three components (**Figure 3.4.7**) also gives an indication of how the vertical component has been rotated through an angle phi. The amplitudes of the first arrivals show that the power is maximized on the vertical component and that the x and y-components have been rotated out of the P-wave's plane of incidence. However, it is hard to directly comment on whether or not the rotations will improve the ability to pick travel times from the first arrivals when compared to raw vertical component. Travel times are acquired using the same method as in **Section 3.3.2**.

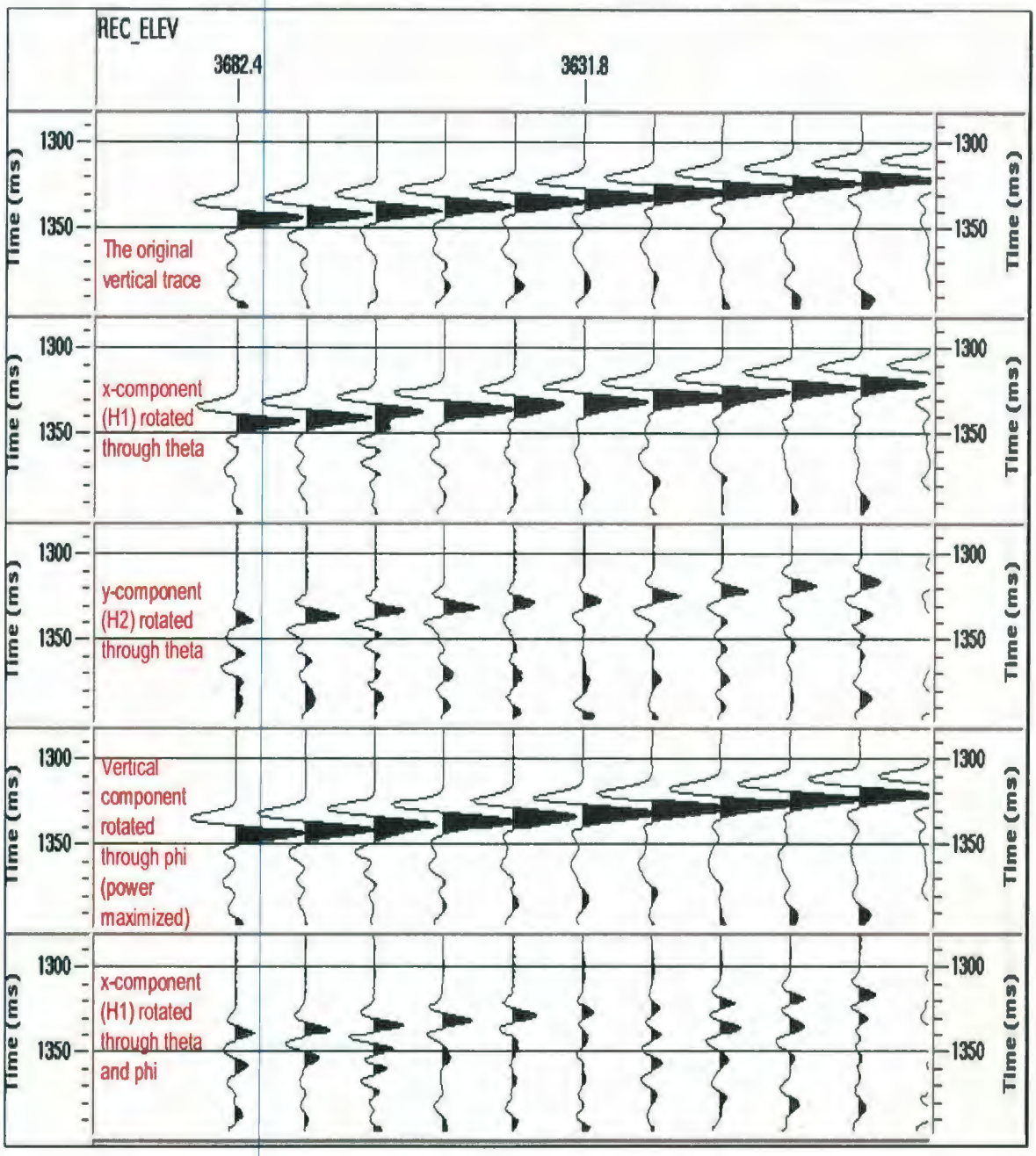

Figure 3.4.7 Five ensemble display demonstrating the final outcome after rotation of the components into a new coordinate axes. The five ensembles are the first two levels of the vertical incident survey (TVD 3682.4 m to 3590.4 m) and time interval 1280ms to 1400ms respectively.

3.5 A Comparison of Travel Time Measurements

Initial comparisons between the raw and rotated vertical component travel times (**Appendix B**), indicates only small variation between them. To detect any variance that warrants further examination the difference between the raw and rotated travel times are calculated (ie. (rotated travel time) – (raw travel time)).

To establish a definition of a difference between the raw travel times and the times acquired after rotation of the vertical component, the precision at which we are able to sample the downgoing P-wave needs to be discussed. The precision is dictated by the sample rate at which the signal was recorded. The vertical incidence survey data was acquired with a sampling rate of 1ms (**Section 3.1**). Therefore, a travel time difference of less than ± 1ms, after rotating the vertical component, cannot be detected. Hence, travel times beyond ± 1ms are considered a difference in travel time measurement after rotating the vertical component.

For an initial understanding, the magnitude of the average of the differences between rotated vertical component travel times with respect to the corresponding raw vertical component travel times (ie. |(rotated travel time) – (raw travel time)|) is calculated to be 0.45 ms. The value is less than 1 ms, therefore, initially I conclude that there is minimal difference between the rotated and raw vertical component travel times. This suggests that the process to compensate for well deviation by rotating the vertical component in-line with the P-wave particle motion does not affect the first arrivals within the trace ensemble. However, a closer examination is needed because averaging the travel times could possibly smooth or average any time differences (> 1 ms). To show specific travel time differences at each geophone level, **Figure 3.5.1** displays these differences between the raw travel times and travel times acquired after rotation of the vertical component.

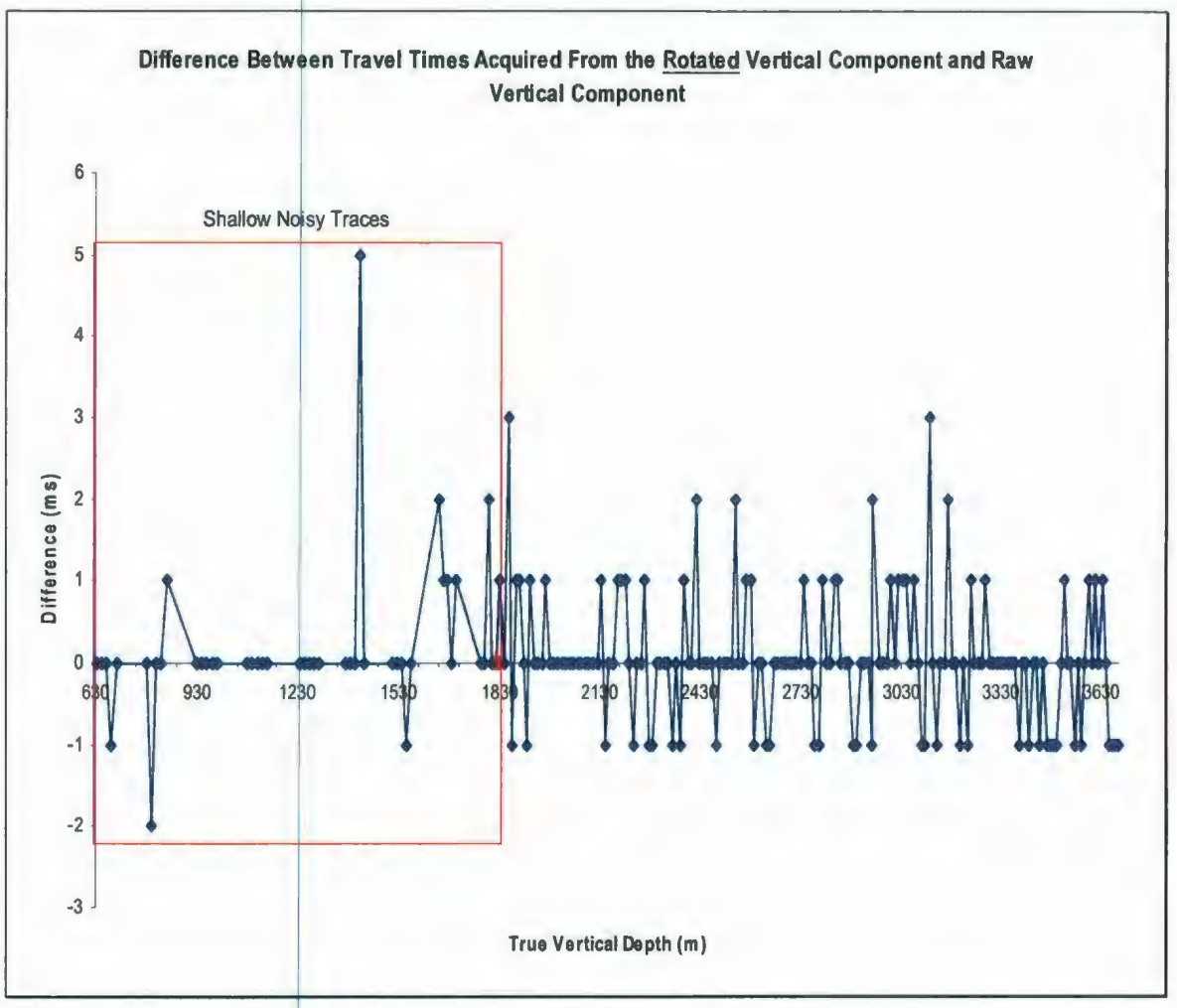

Figure 3.5.1 Differences between the raw travel times and travel times acquired after rotation of vertical component.

Examination of **Figure 3.5.1** indicates bias towards more positive than negative differences, implying rotation resulted in larger travel times. I was unable to determine any specific reason for this bias. Nevertheless, these results indicate that rotating the vertical component caused 10 traces to have travel time differences > 1 ms. However, five of these are associated with travel times acquired from the noisy shallow traces (TVD 1820.8 m to 633.0m) where confidence in some of the picks is low.

Differences beyond the shallow picks indicate that the rotation of the vertical component could be exposing inaccuracies in the raw travel times. This poses a problem because the picks have an affect on calculated average and interval velocities. To determine if these differences do have an affect, the average velocities before and after rotation of the vertical component is calculated.

Figure 3.5.2 illustrates that the average velocities correlate very well. However, the shallow section shows a wide range of average velocities. This suggests that confidence in the ability of the picking algorithm to acquire precise travel times from specific noisy traces is low for both raw and rotated data sets, therefore, resulting in irregular average velocities. Nevertheless, the travel time differences found throughout have very little affect on the average velocities. The highest travel time difference of 5 ms, only equates to an average velocity difference of 9 ms^{-1}. These results correspond to the smoothing associated with continually averaging as the depths increase and are relatively insensitive to small travel time variation. However, calculated interval velocities show velocity changes over specific depth intervals and should be more sensitive to travel time differences.

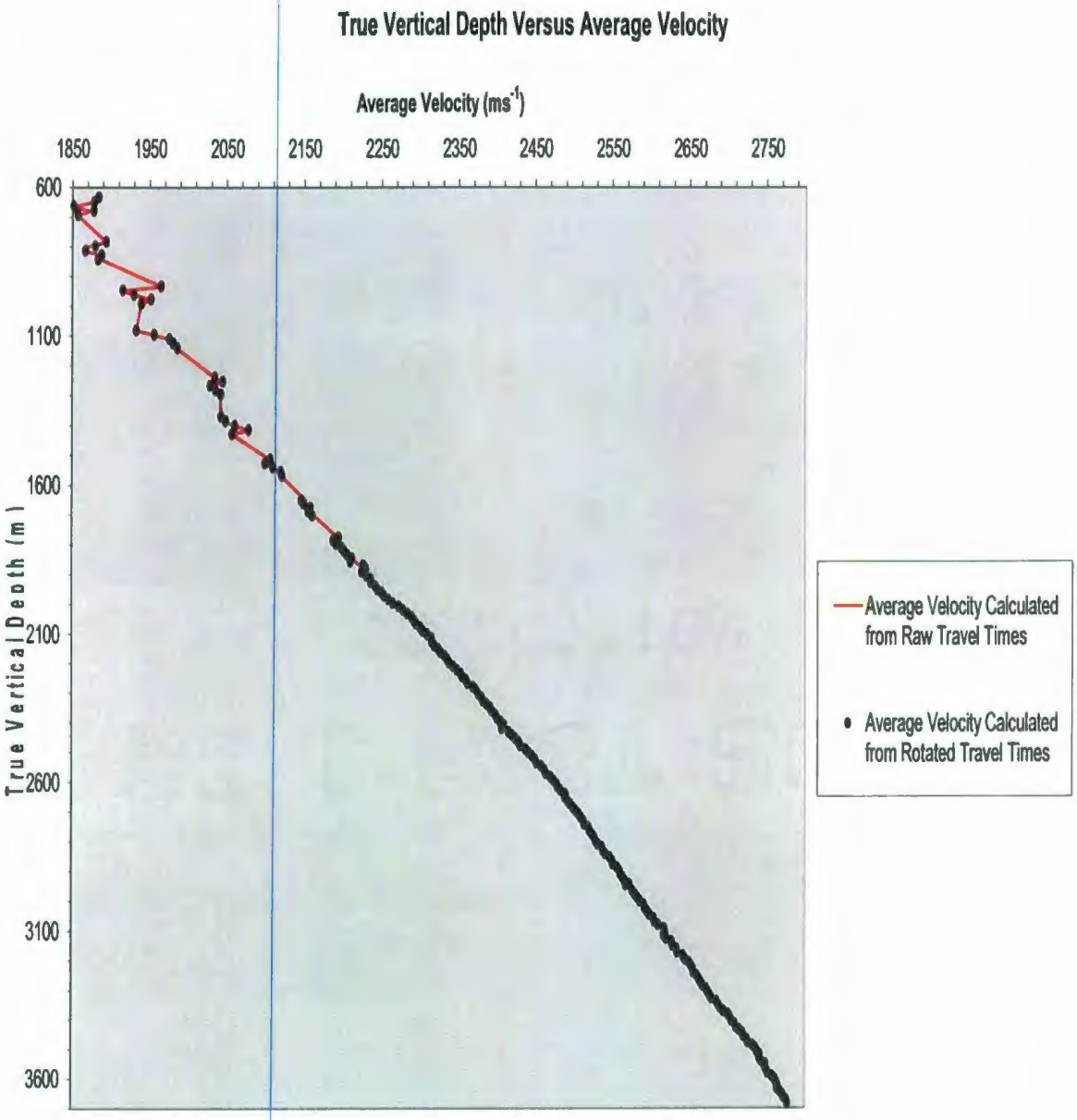

Figure 3.5.2 Comparison of average velocities calculated from raw vertical component and rotated vertical component travel times.

Using the raw and rotated travel times to calculated interval velocities, **Figure 3.5.3** illustrates that very little information can be acquired and irregular unrealistic interval velocity differences occur. This suggests that for this data set the calculation is very sensitive to any travel time variations over the depth interval between two receivers. To try to reduce the instability of the calculated interval velocities, and thus possibly reveal important trends, the average of the interval velocities over each five receiver depth interval is calculated. **Figure 3.5.4** illustrates that this procedure was able to produce consistent realistic velocities and shows that both sets of averaged interval velocities correlate well. The shallow section shows a wide range of interval velocities and again suggests that confidence in the ability of the picking algorithm to acquire precise travel times from specific noisy traces is low for both raw and rotated data sets.

After examining the differences in interval velocities, it is found they range from 100 ms^{-1} to 900 ms^{-1}. However, it is not possible to determine if these interval velocity differences are associated with travel time differences greater than 1 ms. To try to determine an interval velocity difference that is associated with a 1 ms travel time difference, I decide to choose depths and travel times that correspond to average velocities around the mean average velocity for both data sets (2411 ms^{-1}). Using these depths and times, a travel time difference of 1 ms will give an interval velocity difference of approximately 250 ms^{-1}. Hence, excluding interval velocity differences $\geq$ 250 ms^{-1} reveals that travel time differences greater than 1 ms generate small, seemingly random, clusters that on average have interval velocity differences ranging from 350 to 650 ms^{-1}. Unfortunately, without access to interval velocities derived from a sonic log, I am unable

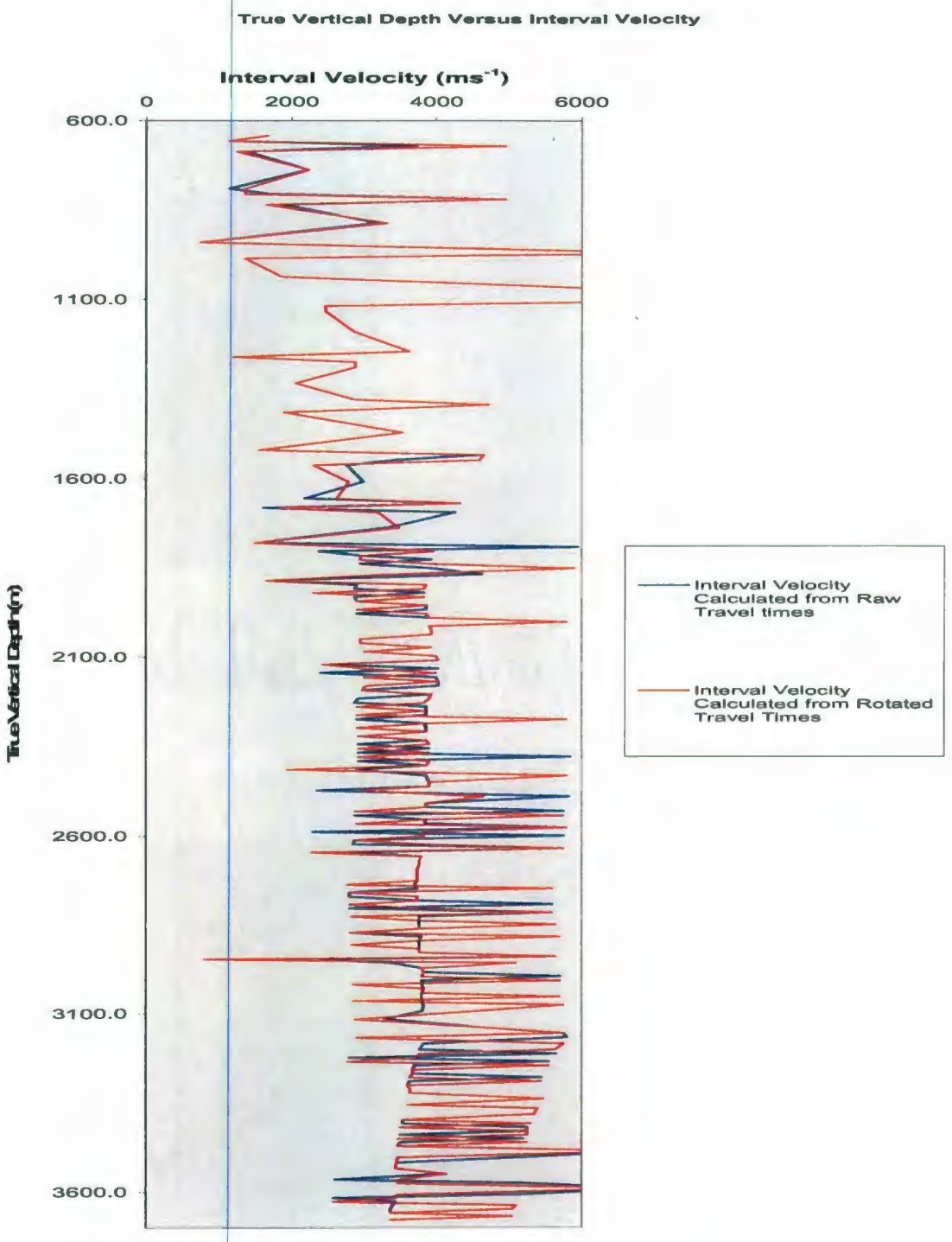

Figure 3.5.3 Comparison of interval velocities calculated from raw travel times and rotated vertical component travel times.

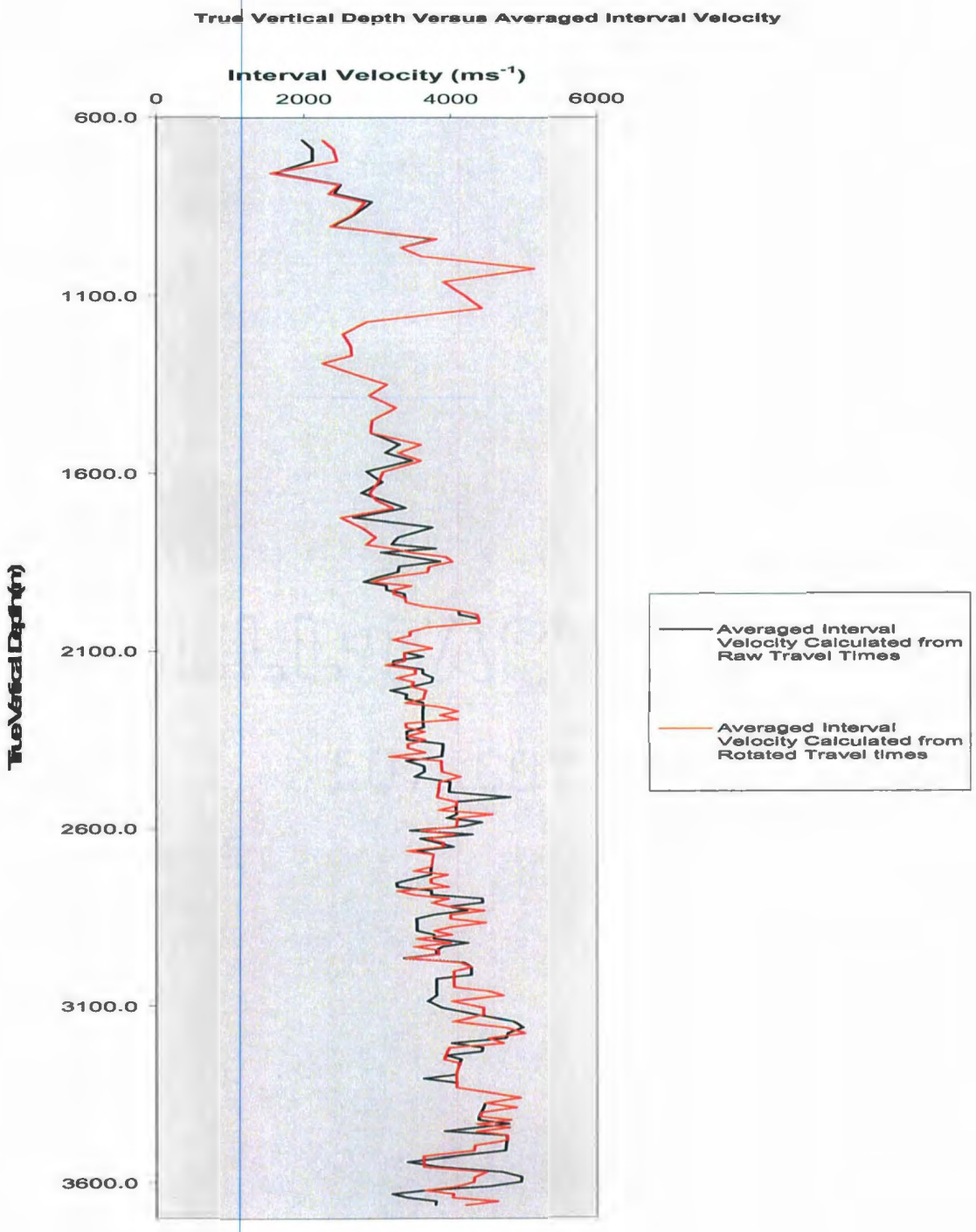

Figure 3.5.4 Comparison of the average interval velocities over a five receiver interval calculated from raw travel times and rotated vertical component travel times.

to determine which set of travel time measurements produce interval velocities that correlate best, and thus should be used for further applications.

3.6 Remarks

Examination of the issue of whether special processing considerations needs to be made when trying to obtain precise travel times from a vertical incidence survey conducted in a deviated well has lead to inconclusive results. Only slight variations are found when comparing the first break travel times acquired from the vertical component orientated along the axis of the borehole with that of the rotated vertical component orientated in-line with the P-wave particle motion.

Nevertheless, to suggest that there will be no difference in travel times in all cases concerning vertical incidence surveys is a quick assumption. I think the arguments brought forth in **Section 3.2.1** gives the theoretical support that for these survey situations the deviation of the well cannot be easily dismissed. Presently, due to the availability of rotational analysis software, a loss in productivity is not an issue. If it is found for another similar data set that there are differences in the travel times after rotational analysis is performed, then the procedure has demonstrated its value.

Attempting a rotational analysis on a vertical incidence survey in a highly deviated well should not be overlooked. This is especially true when these travel times can be essential to the continued integrated processing within a reservoir exploration and development program.

CHAPTER 4 Signal Processing of the Walkaway Survey for Travel Time Measurements

Operationally, a walkaway survey is quite different than a vertical incidence survey. A walkaway survey is conducted over a small depth interval with sources positioned at a range offsets with angles ranging from normal incident to as much as 65 degrees. This survey configuration allows for the measurement of travel times with respect to a change in angle of incidence. Whereas, for the vertical incidence survey, the measured travel times give a vertical time-depth relationship.

One of the most active areas of current seismic research and development involves understanding qualitatively and quantitatively the effects of velocity anisotropy on seismic imaging and velocity analysis. Vertical seismic profiling has shown great promise as a technique to investigate velocity anisotropy because the measurements are taken within the rock under investigation. Furthermore, the dependence of seismic anisotropy on velocity differences as a function of angle has proven to be a specific requirement that can be obtained from VSP survey configurations like the walkaway (Ahmed et al., 1986). Therefore, the importance of precise travel times is fundamental in acquiring anisotropy information.

There are processing considerations when trying to acquire precise travel times from a walkaway survey. For example, the geometry for this type of source-receiver configuration poses an issue. Since the offset for each source is changing as the source-receiver offset changes, the source-receiver coordinate frame will be different for each shot position. This is true for a walkaway survey conducted in a vertical or deviated well. Therefore, the direct downgoing P-wave particle motion is not necessarily recorded

predominantly on one component of a three component geophone package. If the vertical component is used to acquire travel times, and its orientation is not taken into account, possible phase shifting of the first arrival onsets or changes in shape and amplitude of the first arrival wavelets are issues that cannot be ignored. Therefore, the ability of a first break picking algorithm to acquire precise travel times would be in question. Hence, because of the survey geometry, it is appropriate to rotate the vertical component toward the direction of the P-wave particle motion when acquiring travel times from a walkaway survey. However, horizontal displacements of subsequent geophones, due to well deviation, leads to additional processing considerations. This is because, in a vertical well for the same source there is a common source-receiver plane for each survey level. Whereas, when the well is deviated, there will be a slightly different source-receiver plane for each survey level due to these horizontal displacements. This chapter investigates these additional considerations through a discussion of the three component processing techniques required to obtain precise travel times from a walkaway survey conducted in a deviated well.

The chapter begins with this study's walkaway survey configuration. It then proceeds with the processing of the three-component data. Further, first break travel times are acquired and final remarks are given. The operational theory of the algorithms used to process the walkaway data (e.g. First break algorithm, Hodogram algorithm) was previously addressed in **Chapter 3** and will not be discussed.

4.1 Walkaway Survey Configuration

The walkaway survey data was also acquired using Schlumberger's Array Seismic Imager (ASI) borehole tool. The tool was lowered down the B-16_4z cased production well and anchored at fixed depths (**Table 4.1**) throughout the duration of the survey. Again, it is assumed that the tool anchors to the bottom curvature of the deviated well.

Table 4.1 Measured Depths, True Vertical Depths and Geophone Inclinations of the Walkaway Survey Conducted in the B-16_4z Deviated Cased Production Well. All Depths are With Respect to SRD.

Geophone Number	Measured Depth (meters)	True Vertical Depth (meters)	Geophone Inclinations (degrees)
1	4384	3482.73	35.5
2	4399	3494.81	35.8
3	4414	3506.90	36.0
4	4429	3518.99	36.2
5	4444	3531.08	36.3

A source - boat maneuvered the source (air-gun) to create a line of 160 source positions at approximately 100 meter intervals (**Figure 4.1.1**). On the North-West side of the receivers 81 source positions were acquired at a source-receiver azimuth of 108 degrees; this was calculated by the clockwise angle created from a specific source position to the receivers. The offset from the receivers ranged from a far offset of 8128.9 meters to a near offset of 28.44 meters. There was then a 200 meter interval between the first near offset source to the North-West of the receivers and the first near offset source to the South-East of the receivers which was at an offset of 75.77 meters. There were 79 source positions to the South-East of the receivers which ended at an offset

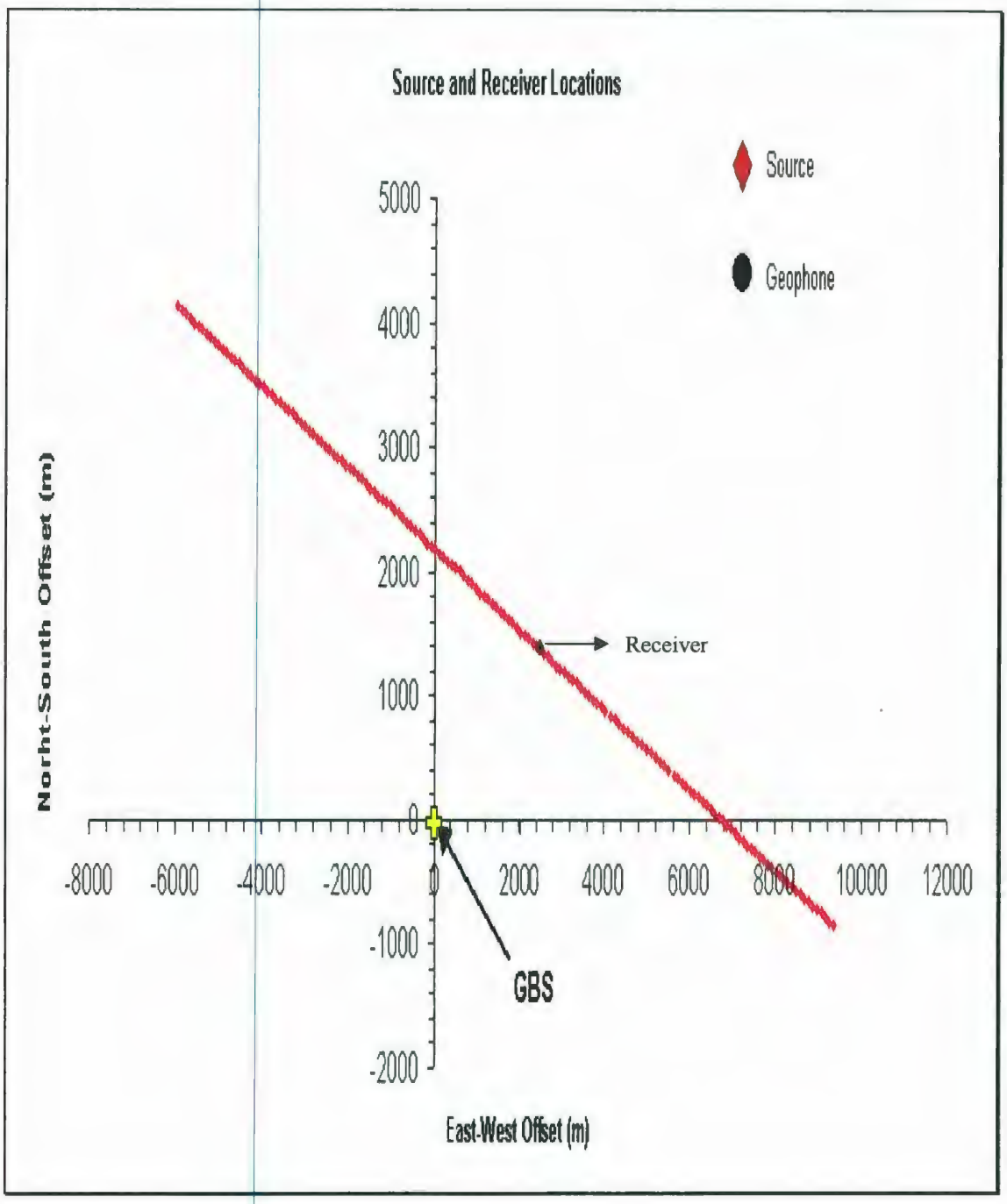

Figure 4.1.1 Source-receiver locations for the walkaway survey. The offset coordinates are with respect to a point projected to the ocean surface (SRD) 76 meters directly below the kelly bushing (KB) of the GBS.

of 7977.12 meters and created a source-receiver azimuth of 287 degrees calculated by the clockwise angle created from a specific source to the receivers.

4.2 Three Component Processing

4.2.1 Geometry Assignment and Trace Editing

Assigning the acquisition geometry to the walkaway survey primarily consists of the same procedure as outlined in **Section 3.3.1** for the vertical incidence survey. However, since the geophones are kept in the same position for the duration of the survey, the quantity of geophone positional data to enter is much less.

The geometry assignment requires the source-to-receiver offsets, as well as the inclination and azimuth of the borehole over the specific survey depths. These data are obtained from the direction and inclination data measurements for the depth section of the well that correspond to the survey depths. The x-component of the geophone package is assigned the number one (1), which signifies the H1 horizontal component. The y-component is assigned the number two (2), which signifies the H2 horizontal component. The z-component is assignment the number three (3) to distinguish it as V1, the vertical component. The data were inspected after geometry assignment to confirm that the geometry was assigned correctly.

Inspection of each component in each survey level indicates that there is a + 40 ms time shift on each trace after source 106 (**Figure 4.2.1**). The reason for these time shifts cannot be determined from field notes or header statements. Therefore, these traces

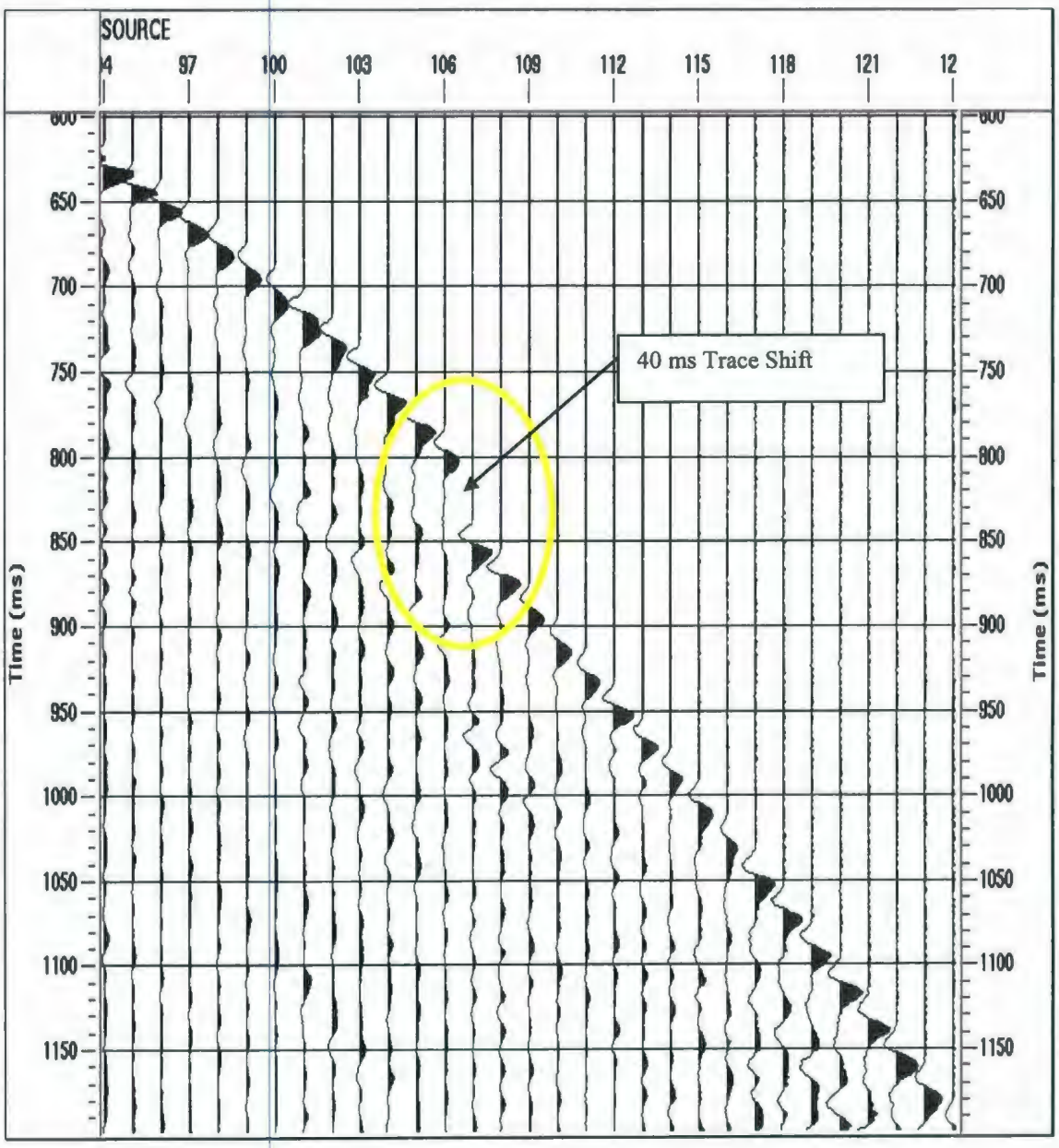

Figure 4.2.1 Trace ensemble of level 1 (TVD 3482.73 meters) displaying sample of 40 ms trace shift that occurs on each component in each level after trace 106 of the walkaway survey. Trace ensemble displaying traces before DC removal and bandpass filtering.

on each level are time shifted by - 40ms, after which, a trace DC removal and butterworth bandpass filter (8-18-36-80 Hz) is performed in order to properly display the trace ensembles.

Further inspection indicates prominent noise spikes occurring in level 1 (TVD 3482.73 m) and level 4 (TVD 3518.99 m) of the x-component trace ensembles and in level 3 (TVD 3506.90 m) of the z-component trace ensemble (**Figure 4.2.2**). The reasons for these noise bursts cannot be determined from field notes or header statements. Spike and noise burst edit algorithm is performed; however, further inspection of these noise bursts do allow for the acquisition of first break travel times since their onsets coincide with the first break energy.

After preliminary editing of the data, the trace ensembles for each component that correspond to the survey levels can be displayed (**Figure 4.2.3**). One noticeable feature is the signal obtained from the level 4 (TVD 3518.99 m) z-component. The coherent signal is very low and no reason could be determined for why level 4 was different, hence, it is difficult to obtain travel times from the z-component. Attempts at bandpass filtering provided little or no improvement. Therefore, the original data shown in **Figure 4.2.3** is used for the rotational analysis.

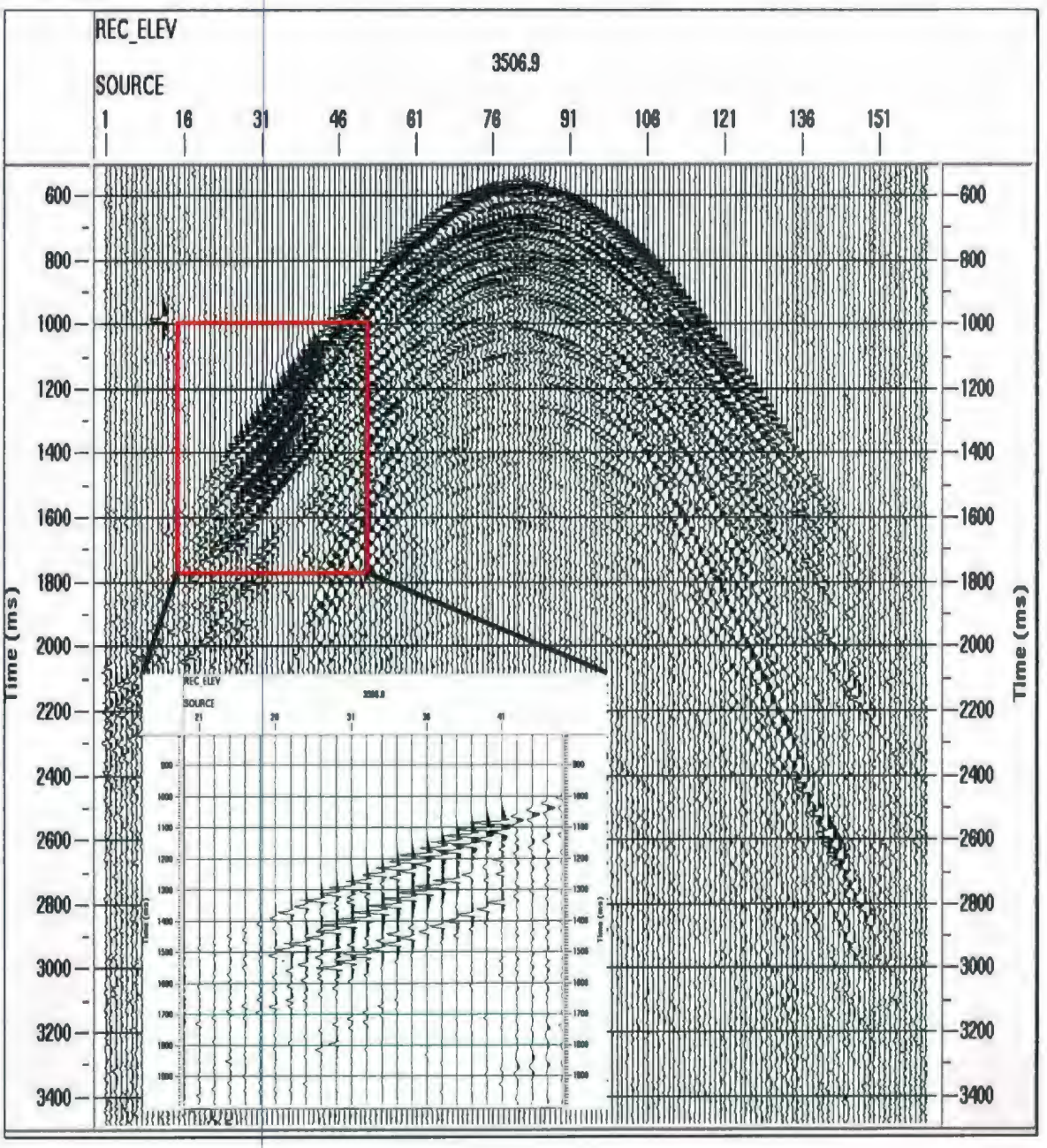

Figure 4.2.2 Trace ensemble of level 3 (TVD 3506.9 meters) z-component displaying example of prominent noise spikes. Noise spikes also occur on the x-components of levels 1 (TVD 3482.73 m) and 4 (TVD 3519.99 m) respectively (not shown).

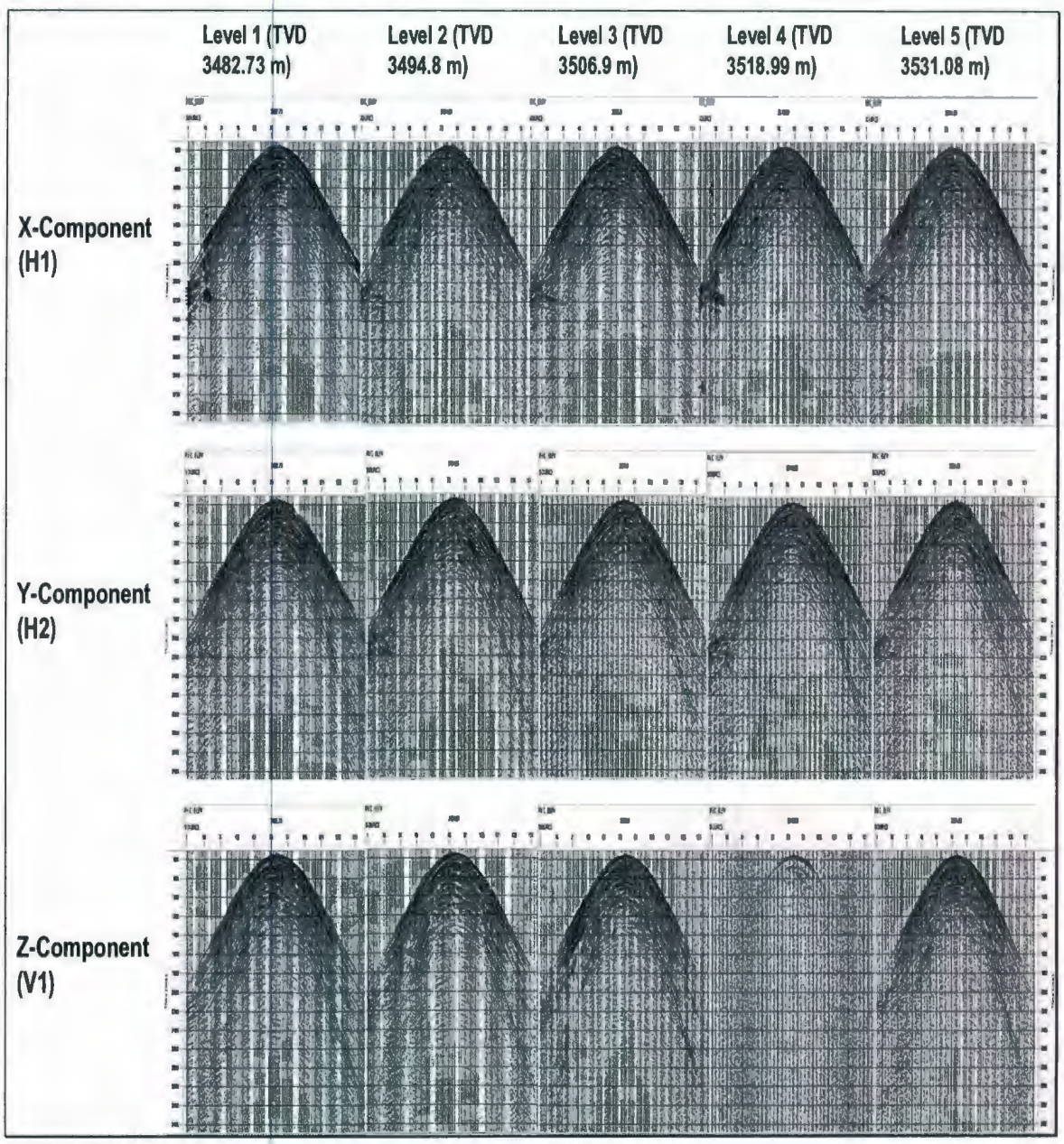

Figure 4.2.3 Fifteen trace ensembles displaying the all five geophone levels (TVD 3482.73, 3494.81, 3506.90, 3518.99 and 3531.08 meters from SRD) for each component (H1, H2 and V1) of the walkaway survey. H1, H2 and V1 are all displayed with the same scaling factor.

4.2.2 Rotational Analysis

The theory of the rotational analysis performed on the walkaway survey is the same as the vertical incidence survey. However, there are some differences when performing a rotational analysis on a walkaway data set. For the vertical incidence data, the final result was to have the vertical component in line with the impinging P-wave by maximizing power transferred from all three components to the z-component. The walkaway survey is considerably different in design. Since the source can be at significant offsets, and at an azimuth to the geophone package, the hodogram analysis requires more in-depth interpretations of the results. Final orientation of the z-component is not predetermined as it was for the vertical incidence survey (i.e. vertically up). Therefore, the final orientation of the z-component will be different for each shot taken. The overall result of this rotational procedure is illustrated in **Figure 4.2.4** for a vertical well situation. In the context of a deviated well situation the same procedure is performed. The horizontal component (H1) is rotated, through an angle theta, around the vertical component into a plane that contains the source and the receiver. Then the vertical component is rotated, through an angle phi, around the horizontal component (H2). This leaves the vertical component pointing directly at the impinging P-wave originating from the source at a specific azimuth.

Through iterative examination of different time gates, an optimal time gate was determined for the majority of the traces in each level. A window 10ms before and 40ms after the first break produces hodograms that allow for confident interpretation of the

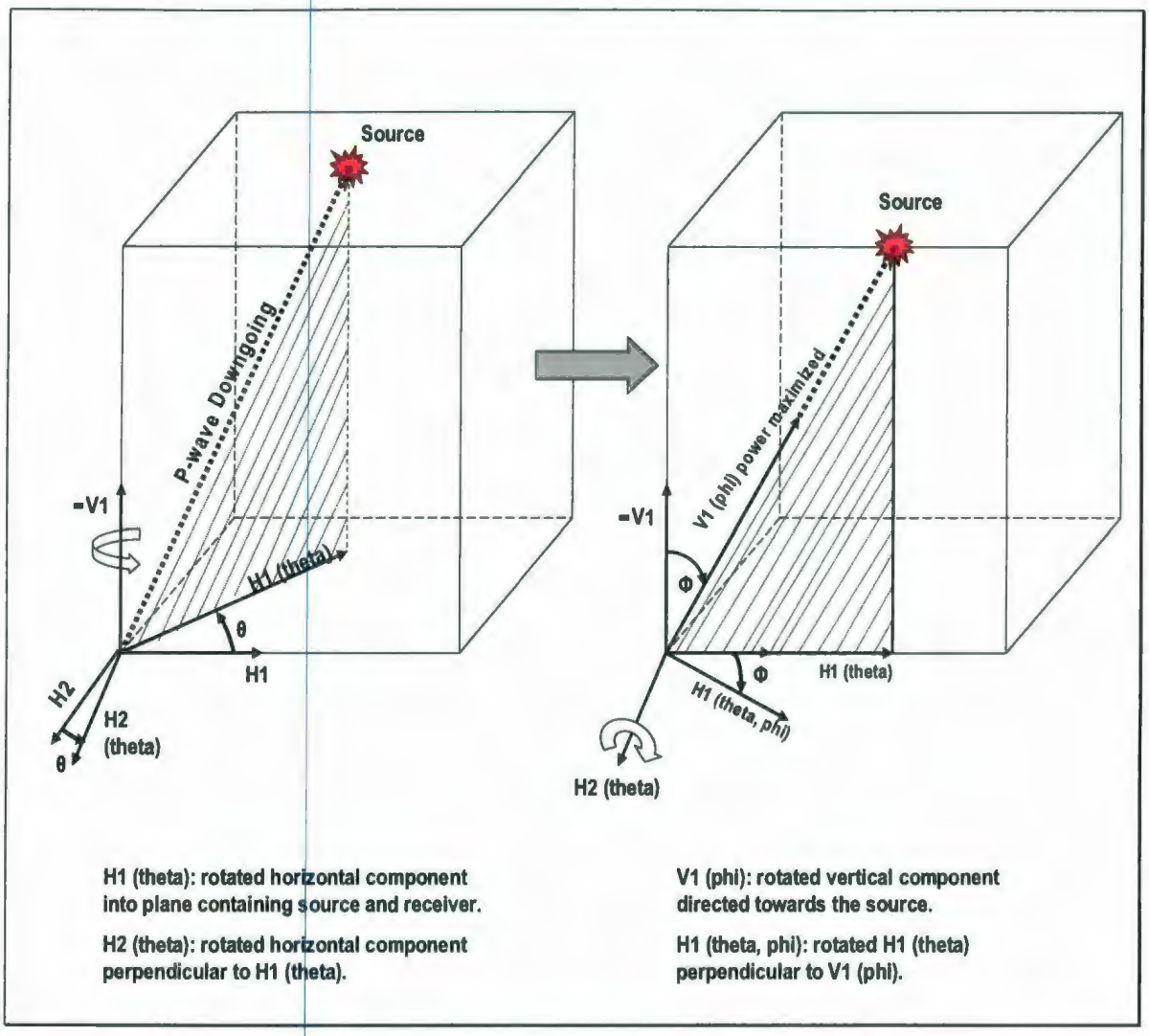

Figure 4.2.4 An illustration of the rotations performed on the three component walkaway data used for this study; Rotation of H1 into the source azimuth which is defined as the plane that contains the source and the receiver (left); After which the vertical component is rotated a specific inclination so that it is now pointing at the source (right).

rotation angle required to rotate the vertical component (**Figure 4.2.5**) towards the impinging direct downgoing P-wave.

Examination of **Figure 4.2.6** shows a significant improvement in the P-wave signal recorded for level 5 (TVD 3531.08 meters) of the walkaway survey. These rotations also diminished the presence of the SV-shear waves in the original vertical component ensemble. This is as equally true for level 1 (TVD 3482.73 m), level 2 (3494.94 m) and level 3 (3505.90 m).

This routine also proved to be appropriate when dealing with the problem of the low and noisy signal displayed within the ensemble corresponding to the vertical component of level 4 (TVD 3518.99 meters). Since the horizontal components are primarily used for the rotation, the first break energy displayed on these components was used without the inspection of the vertical component. Final results show that the rotation using only the horizontal components for the rotational analysis can still produce a power maximized vertical component ensemble (**Figure 4.2.7**).

4.2.3 Acquiring First Break Travel Times after Rotation of the Vertical Component

Determining the first break travel times from the onset of the initial downgoing P-wave after rotation of the vertical component into a source-receiver plane of incidence for each receiver level involves the same use of the first break algorithm utilized in **Chapter 3** for the vertical incidence survey. Examining the first break energy revealed that most of the energy lies within a time envelope of 50ms. The travel time picks were then acquired (**Appendix C**).

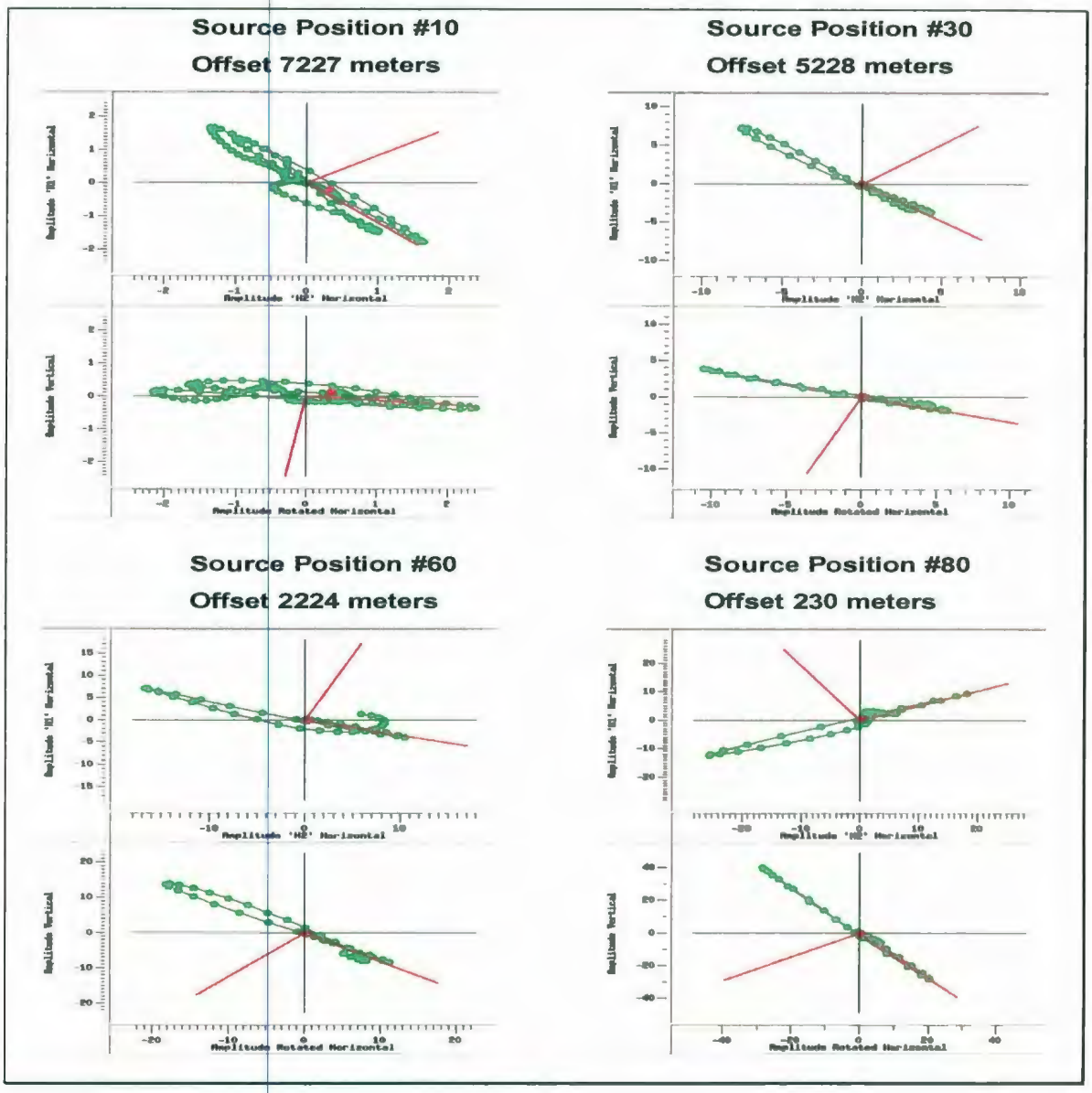

Figure 4.2.5 Hodogram display of specific source positions throughout the North-West side of level 5 (TVD 3531.08 meters) trace ensemble. Note for the far offset (shot 10) very little energy is recorded on the vertical component. This directly correlates with the low signal recorded at far offsets on the vertical component. This observation is the same for all the previous levels of the walkaway survey.

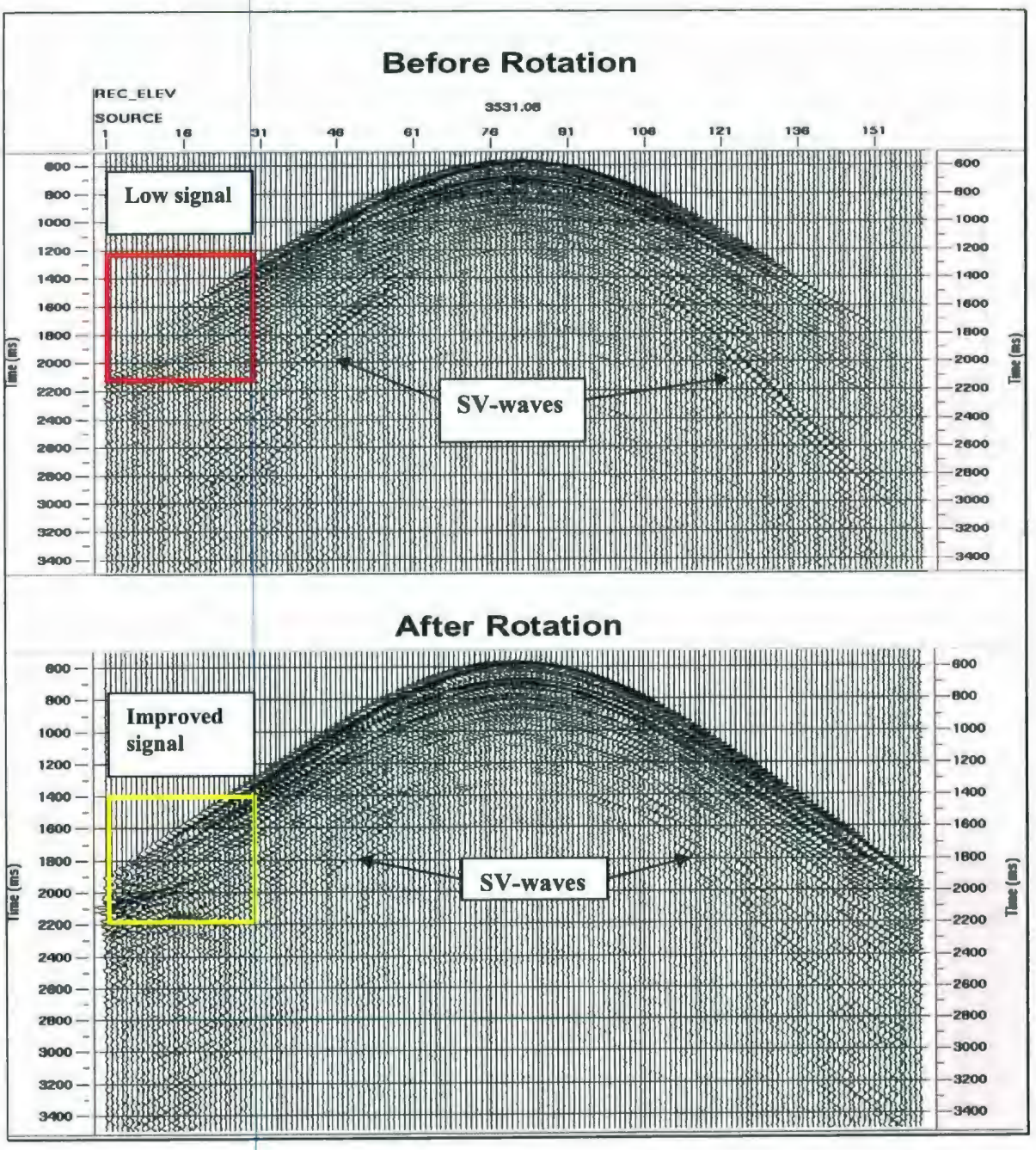

Figure 4.2.6 Trace ensembles of level 5 (TVD 3531.08 meters) vertical component before and after rotational analysis. Note the significant improvement in first break signal at far offsets after rotation. Also, the significant decrease in mode converted SV-shear wave signal.

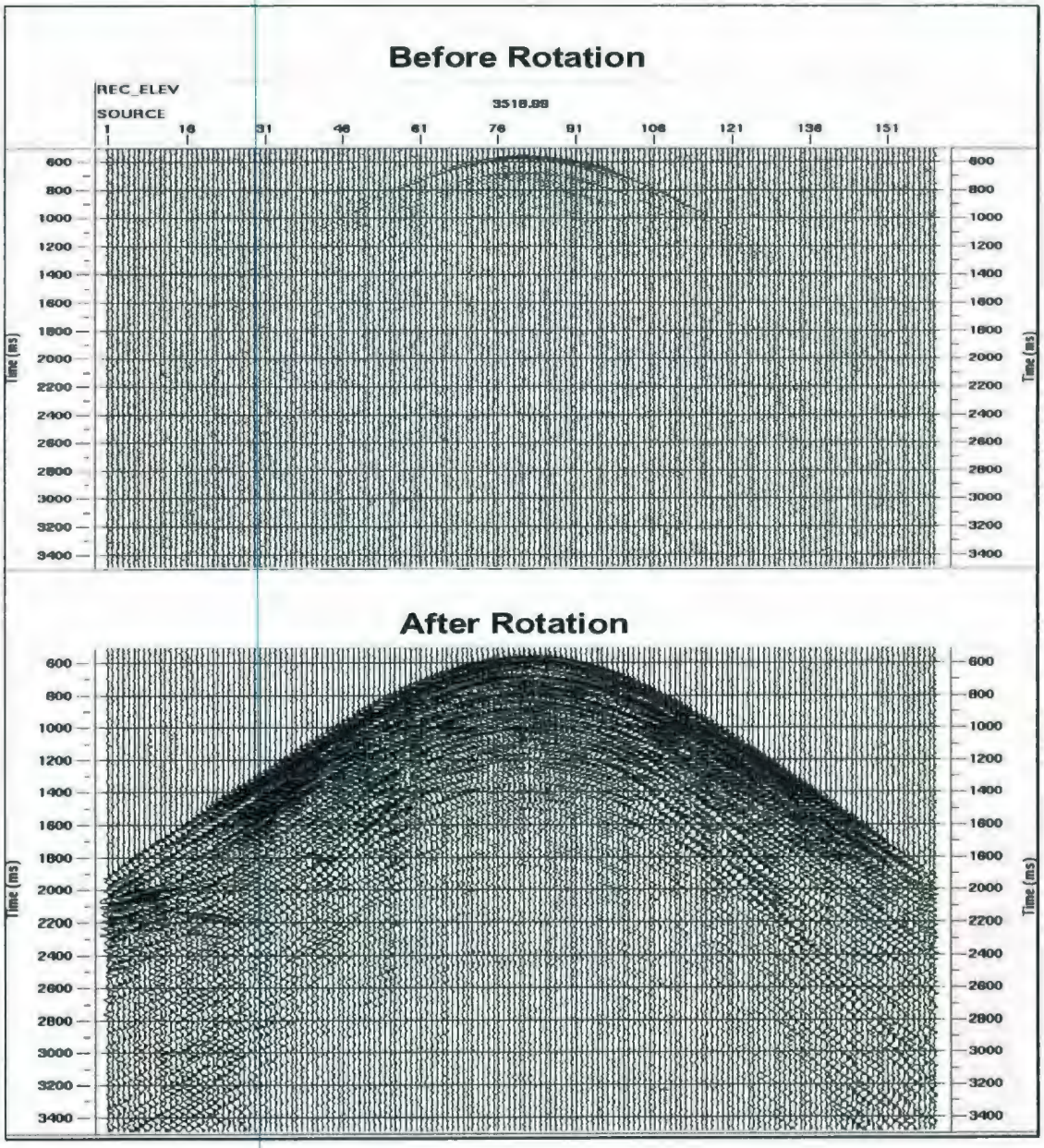

Figure 4.2.7 Trace ensembles of level 4 (TVD 3518.99 meters) vertical component before and after rotational analysis. Note the success of using the horizontal components to transfer a full coherent signal unto the vertical component which contained very little indication of a coherent signal.

4.3 Remarks

Even though the walkaway survey used for this study is conducted in a deviated well, the processing routine is the same for a walkaway done in a vertical well. The only difference between this deviated well situation and a vertical well situation is that there are horizontal displacements of subsequent geophones due to the well deviation. Therefore, for the same source, there will be a slightly different source-receiver plane for each level of the survey. However, this did not prove to be a problem since the rotational analysis rotated each vertical component into the specific source-receiver plane.

The walkaway survey is operationally different than the vertical incidence survey and allows for a measurement of travel times with respect to a change in angle of incidence. This acquisition of angular dependent travel time measurements is needed for the investigation of formation anisotropy. The final chapter of this study will show, using the walkaway and vertical incidence travel times, that with the application of reasonable assumptions, velocity anisotropy measurements can be obtained from VSP's conducted in a deviated well without rigorous computational adjustments.

CHAPTER 5 Application of Travel Times for Velocity Anisotropy Measurements in Deviated Wells

The velocity with which an elastic wave propagates through a rock can depend upon its direction of travel. If, for example, the velocity of an elastic wave is observed to travel faster in the horizontal direction than in the vertical direction then velocity anisotropy is present.

Velocity anisotropy results from directional variations in the mechanical compliance of rocks and has been widely observed in both laboratory and field studies (Jones et al., 1981, Banik, 1984, and Leslie et al., 1999). Velocity anisotropy may be an intrinsic property of a rock related to its mineralogy and grain fabric, or it may be caused by depositional effects such as thin interbedding of different rock types. Even though the cause of velocity anisotropy within a rock may be difficult to determine, there has been much research done on quantifying it.

The reason for quantifying velocity anisotropy is that it occurs in many sedimentary rocks of interest in exploration geophysics. Ignoring the effects of velocity anisotropy in traditional data processing may lead to positional errors in seismic images that increase the risk of dry holes (Isaac et al., 1999, Vestrum et al., 1999).

Vertical seismic profiling has shown great promise as a technique to investigate velocity anisotropy because the measurements are taken within the rock under investigation. Many techniques have been developed to obtain velocity anisotropy measurements using travel times acquired from VSP surveys. However, a literature review on this topic revealed that most techniques were developed using travel times acquired from a VSP survey conducted within a vertical well. Since many wells drilled

today are highly deviated from vertical, most of these techniques need to include a correction for well deviation. A method for acquiring velocity anisotropy measurements, in which the path of the borehole could be ignored, would certainly be well suited for deviated wells.

By using travel times acquired from the vertical incidence and walkaway surveys, I demonstrate that the travel time-inversion method (Slawinski et al., 2003) is well suited for acquiring velocity anisotropy measurements in deviated wells. This method assumes that a buried layer of interest is elliptically anisotropic and that the velocity anisotropy can be described by a single parameter (χ). I will calculate this parameter for a marine shale within the Upper Zone of the Hibernia Reservoir and then give a percent velocity anisotropy estimate.

To demonstrate that this technique produced an appropriate velocity anisotropy estimate for the shale layer, I continue to use the assumption that a buried layer of interest is elliptically anisotropic to modify the widely accepted phase-slowness method (Gaiser, 1990, Miller et al., 1994, Miller and Spencer, 1994). Using the walkaway survey travel times, this assumption will allow for an independent percent velocity anisotropy estimate to be determined under the same conditions.

5.1 Travel Time Inversion Method

5.1.1 Elliptical Anisotropy Assumption

Before applying the travel time inversion method, I will discuss the assumption which this method is based on: a buried layer of interest being elliptically anisotropic. This discussion will also define the terminology and the anisotropy parameter (χ) used throughout this chapter.

In an ideal world, it would be appropriate to use the full elastic wave equation with a complete set of elastic parameters for seismic processing. However, in practice an experiment to measure those parameters is almost impossible to carry out. A useful approach to simplifying the experiment is to assume some form of symmetry that decreases the number of independent elastic parameters.

When velocity anisotropy is present in a rock, the velocity of wave propagation depends on the direction of the propagating wave. Also, the direction of the velocity of a wavefront is different when measured normal to its surface (**phase velocity**) as compared to measured in the direction of energy propagation (**ray velocity**). Due to the number of elastic parameters required to describe a specific medium fully, convenient equations describing phase and ray velocities and their direction are not easily accessible. However, assuming elliptical anisotropy simplifies this situation considerably.

The assumption of elliptical anisotropy is derived from the simplification that a propagating wavefront can be described as an ellipse. Along the symmetry axis of an ellipse, the direction of energy propagation coincides with the wavefront normals.

Therefore, it can be demonstrated that corresponding phase and ray velocities are equal in magnitude (Slawinski et al., 2003). Hence, there are only two velocities within a buried layer of interest to consider, the vertical (V_z) and the horizontal (V_x) ray velocities. However, one has to acknowledge that there is no way of knowing beforehand if the elliptical anisotropy assumption is appropriate for describing the anisotropy of a buried layer.

With that being said, using the simplifications of elliptical anisotropy, Slawinski et al. (2003) describe the anisotropy within a layer of interest by a single parameter (χ). This parameter is defined by:

$$\chi = \frac{V_x^2 - V_z^2}{2V_z^2}, \qquad (A)$$

where V_x = horizontal ray velocity
V_z = vertical ray velocity

and χ is assumed to be constant over a finite depth range. If the magnitudes of a set of χ values determined for a medium are not constant, then the assumption of elliptical anisotropy is not appropriate.

It is not intuitive to try to conceptualize the anisotropy parameter (χ) with respect to the velocity anisotropy present in a rock. However, χ can be used to calculate the percent difference between the horizontal and vertical ray velocities. If the percent difference between the vertical and horizontal ray velocities can be expressed as:

$$\Phi = \frac{V_x - V_z}{V_z} \times 100.$$

Using equation (**A**), V_x can be expressed in terms of χ, as follows:

$$V_x = V_z \sqrt{2\chi + 1}$$

Substituting V_x in terms of χ into the percent difference expression, Φ, one obtains:

$$\Phi = (\sqrt{2\chi + 1} - 1) \times 100 .$$

Using a numerical example to illustrate this, if χ is given a value of 0.20 this implies that the difference between vertical and horizontal ray velocities (Φ) is 18.3 %. Hence, determining χ can be used to give an estimate of the percent velocity anisotropy present in a rock.

5.1.2 Theory

For the travel time inversion method a two-dimensional Cartesian coordinate system (x,z) where x and z correspond to the horizontal and vertical axes of the Cartesian plane is considered (**Figure 5.1.1**). The source position is the origin which is at an offset to a receiver located at some point (x_2 , z_2) in the layer of interest. The interface defined by the transition from the upper medium to the layer of interest is assumed to be horizontal. Also, depth to the interface (H) is assumed to be known from other studies.

This method considers that the medium above the layer of interest is anisotropic and linearly inhomogeneous along the vertical axis. This means that the instantaneous

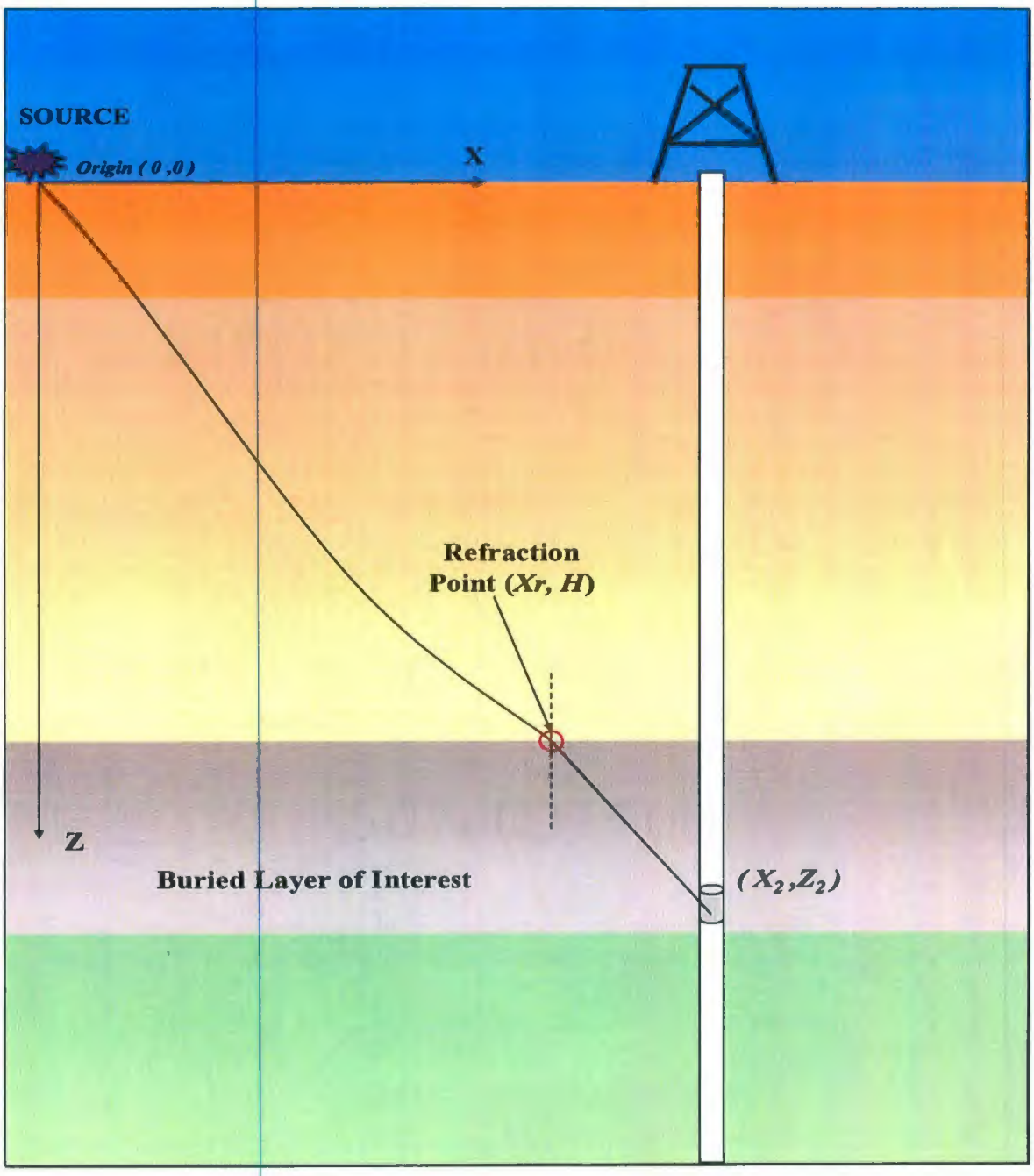

Figure 5.1.1 A two-dimensional model of an elliptically anisotropic homogeneous layer of interest buried below an anisotropic linearly inhomogeneous medium. The layer of interest is separated from the upper medium at a depth H by a horizontal interface. The ray path between the source, (0,0), and the receiver, (X_2,Z_2), refracts at the interface at the point (Xr, H).

velocity (V) of an elastic wave through the medium increases with depth(z)and can be described by the linear function:

$$V(z) = a + bz\,,$$

where **a** is the speed in the medium which contains the source, and **b** is a constant velocity gradient for the medium. This instantaneous linear velocity trend is a valid model within some sedimentary basins (Slotnick, 1959, Acheson, 1981). Hence, the travel time in the upper medium from the source to a refraction point (x_r) on the interface from the upper medium into the layer of interest is defined by the travel time function:

$$t_1(x_r) = \frac{1}{b}\ln\left(\frac{a+bH}{a}\left[\frac{1-\sqrt{1-(pa)^2}}{1-\sqrt{1-[p(a+bH)]^2}}\right]\right)$$

where

$$p = \frac{2bx_r}{\sqrt{\left[(bx_r)^2 + a^2 + (a+bH)^2\right]^2 - \left[2a(a+bH)\right]^2}}$$

is the ray parameter defined and described by Slawinski and Slawinski (1999).

Using the assumption that the layer of interest is elliptically anisotropic and that the anisotropy can describe the parameter χ, an explicit expression is developed by Slawinski et al. (2003) in terms of a single refraction point x_r:

$$\chi(x_r) = \frac{1}{2}\left(\frac{(x_2 - x_r)^2}{[T - t_1(x_r)]^2 V_l^2 - (z_2 - H)^2} - 1\right).$$

This expression incorporates the calculated $t_1(x_r)$ and the travel time measurements (T) acquired from a VSP survey. Also, the expression incorporates the vertical interval velocity (V_1) of the layer of interest which is obtained through previous studies.

It is shown that the refraction point x_r can be determined through the condition

$$\frac{\partial \chi(x_r)}{\partial x_r} = 0 \text{ (Slawinski et al, 2003).}$$

Therefore, this condition states that differentiating the equation $\chi(x_r)$, equating it to zero and solving for x_r, will allow one to obtain the x-ordinate of the refraction point at the interface with a depth expressed as H for a specific source receiver pair. Inserting the refraction coordinate back into the equation for $\chi(x_r)$, can now give a value for the anisotropy parameter. Since χ is assumed to be constant for a given depth, repeating this procedure for multiple shots paired with same receiver should give the same value for χ. If the χ values are not constant for a given depth, then the assumption of elliptical anisotropy may not be valid. The walkaway survey configuration is ideal for verifying this assumption because multiple travel times are acquired at a given depth as the source-receiver offset changes. To conclude this section, I will use the travel times acquired from vertical incident and walkaway surveys to determine an anisotropy parameter for a marine shale, and thus, give an estimate of the percent velocity anisotropy present.

5.1.3 Method and Results

The shale layer under investigation is part of the Cape Island member formation located in the Upper Zone of the Hibernia Reservoir, and is characterized as consisting of silty-shale sequences (Flint and Sinclair, 2001). As outlined in the previous section, there are a number of unknowns that need to be acquired before the anisotropy parameter (χ) for this shale layer can be determined.

Correlating the TVD depths of the vertical incidence survey with lithostratigraphy charts for the B-16_2 well (Bidgood, 2003), reveals that survey level 184 (TVD 3413.6 meters) is just above the shale layer. Because the vertical incidence survey thoroughly sampled the medium above the shale, the vertical incident travel times are used for determining the required instantaneous linear velocity function $V(z)$. Since it was determined in **Chapter 3** that there are no notable differences between the raw and rotated vertical component travel times, I use the raw travel times for determining $V(z)$. Using these travel times, a graph of true vertical depth versus travel times is plotted (**Figure 5.1.2**). The graph displays a non-linear trend, thus, using least squares regression, a second order polynomial curve provides a very close fit. Taking the derivative $\left(\frac{dt}{dz}\right)$ produces a linear instantaneous velocity function with respect to time. Substituting the travel times back into this velocity function gives a set of instantaneous velocities.

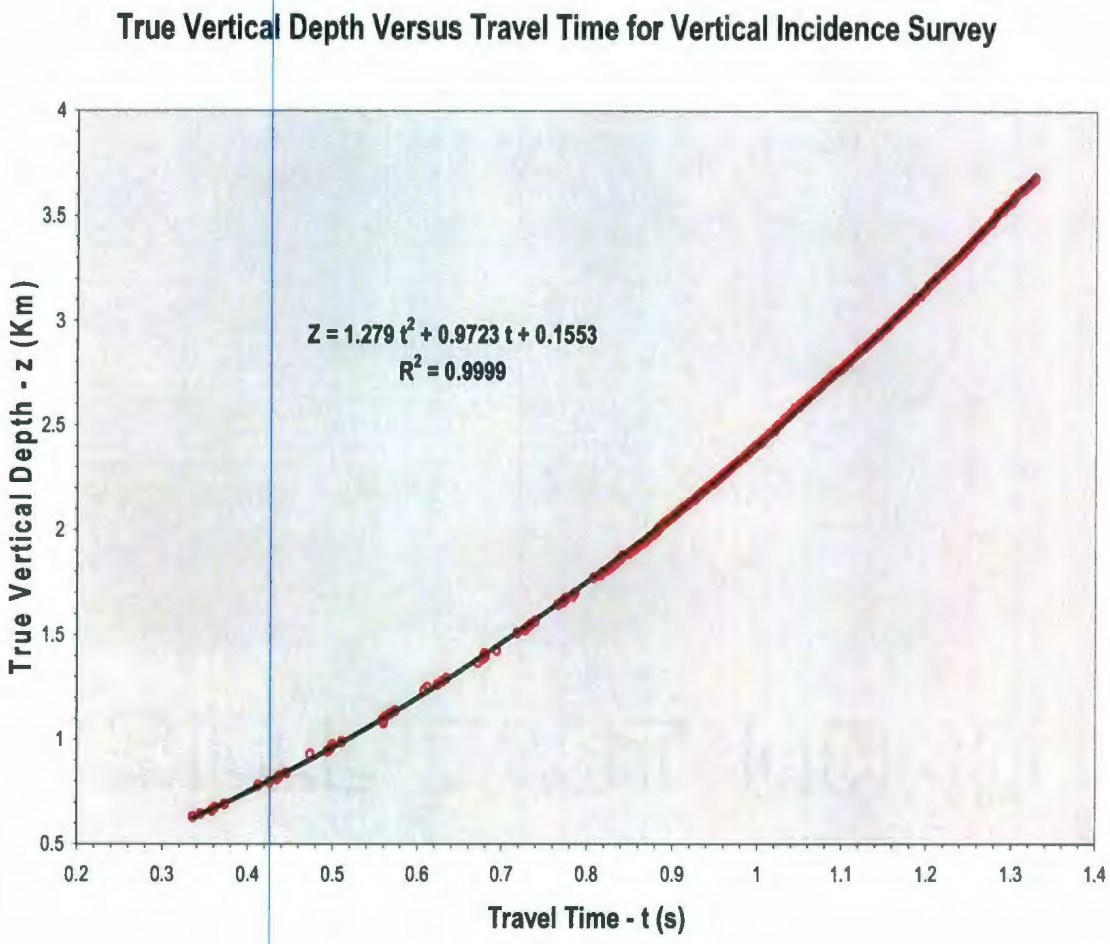

Figure 5.1.2 A true vertical depth vs. travel time graph for the vertical incident survey. Added is a second order polynomial best-fit curve obtained from a least squares regression.

After plotting a graph of instantaneous velocity versus true vertical depth, a near linear trend is visible for depths above the shale layer (**Figure 5.1.3**). Through a linear least squares regression fit the instantaneous velocity function with respect to depth $V(z)$ is found to be:

$$V(z) = 1.553 + 0.803z\ .$$

As outlined in the previous section, **a** = 1.553 Kms^{-1} represents the velocity of the medium which contains the source. Since this study is in a marine environment this value gives the velocity of the propagating source wave in water. The value given in the above equation (1553 ms^{-1}) gives a highly appropriate value for this environment. The velocity gradient of **b** = 0.803 s^{-1} is also a highly appropriate value for this sedimentary environment within the Hibernia Reservoir (Wright, pers. comm., 2002). Even though the graph of instantaneous velocity versus depth displays a near linear trend, the results are acceptable for this environment and will be used for determining the anisotropy parameter.

The vertical incidence survey is also useful for determining the vertical interval velocity (V_I) of the buried layer. By correlating the TVD depths of the vertical incidence survey with lithostratigraphy charts for the B16_2 well (Bidgood, 2003), it is determined that the interval velocity (V_I = 4319 ms^{-1}) calculated from raw travel times for survey levels 188 (TVD 3455.5 meters) and 189 (TVD 3466.0 meters) are within the shale layer.

Now that the velocity function of the medium above the shale and the interval velocity within the shale has been determined, the assumption that the interface between

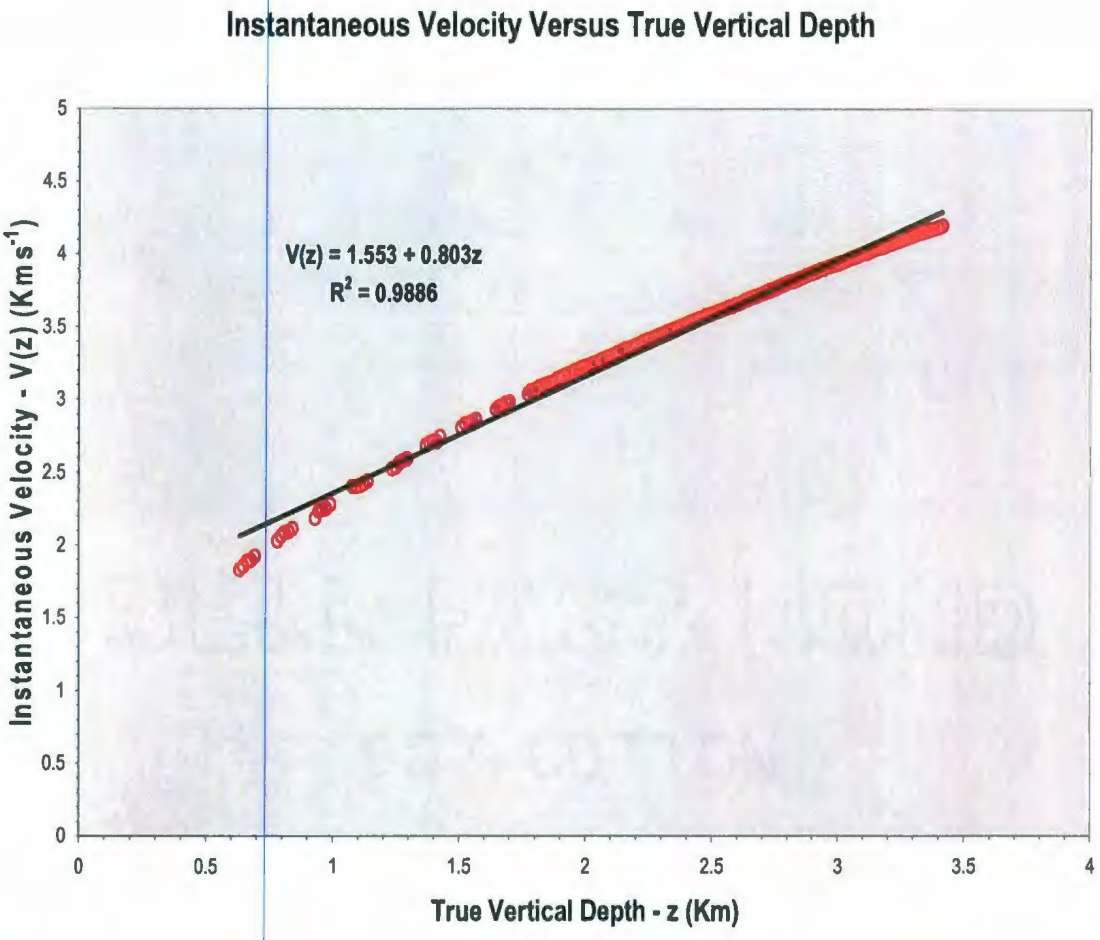

Figure 5.1.3 An instantaneous velocity vs. true vertical depth graph for the vertical incident survey. Added is a linear best-fit line obtained from a least squares regression fit. The vertical axis intercept indicates the velocity of the source wave within water. The gradient indicates the constant velocity gradient for the medium above the shale formation.

the upper medium and the shale layer is horizontal can be verified using the walkaway travel times. If the walkaway travel time curves show a high degree of symmetry about zero offset, then this can indicate the medium is horizontally layered (Miller et al., 1994). By correlating lithostratigraphy charts for the B-16_4z well (Bidgood, 2003) with the TVD depths of the walkaway survey, it is determined that levels 1, 2 and3 are above the shale layer and levels 4 and 5 are within the shale layer. Displaying these travel times with respect to offset for each level indicates a high degree of symmetry, and therefore suggests horizontal layering (**Figure 5.1.4**). Again, using the lithostratigraphy charts for the B-16_4z well (Bidgood, 2003) the depth to the interface (H) is found to be 3509.4 meters (TVD).

Knowing that levels 4 and 5 of the walkaway survey are in the shale layer, I chose level 5 (TVD 3531.08 meters) to be assigned the ordinate z_2 which represents a receiver within the shale at a specific depth. Finally, the travel time (T) for a range of offset positions (x_2) from approximately 8000 meters to 1000 meters on both sides of receiver 5 are used. Now that all the unknown values have been determined, the anisotropy parameter χ can be calculated.

Using the mathematical software package Derive®, the condition $\frac{\partial \chi(x_r)}{\partial x_r} = 0$ is performed on the function $\chi\ (x_r)$. This determines the refraction point (x_r) for each offset. However, the software package could not calculate refraction points for offsets ranging from approximately 1900 meters to 1000 meters. Since it is still possible to

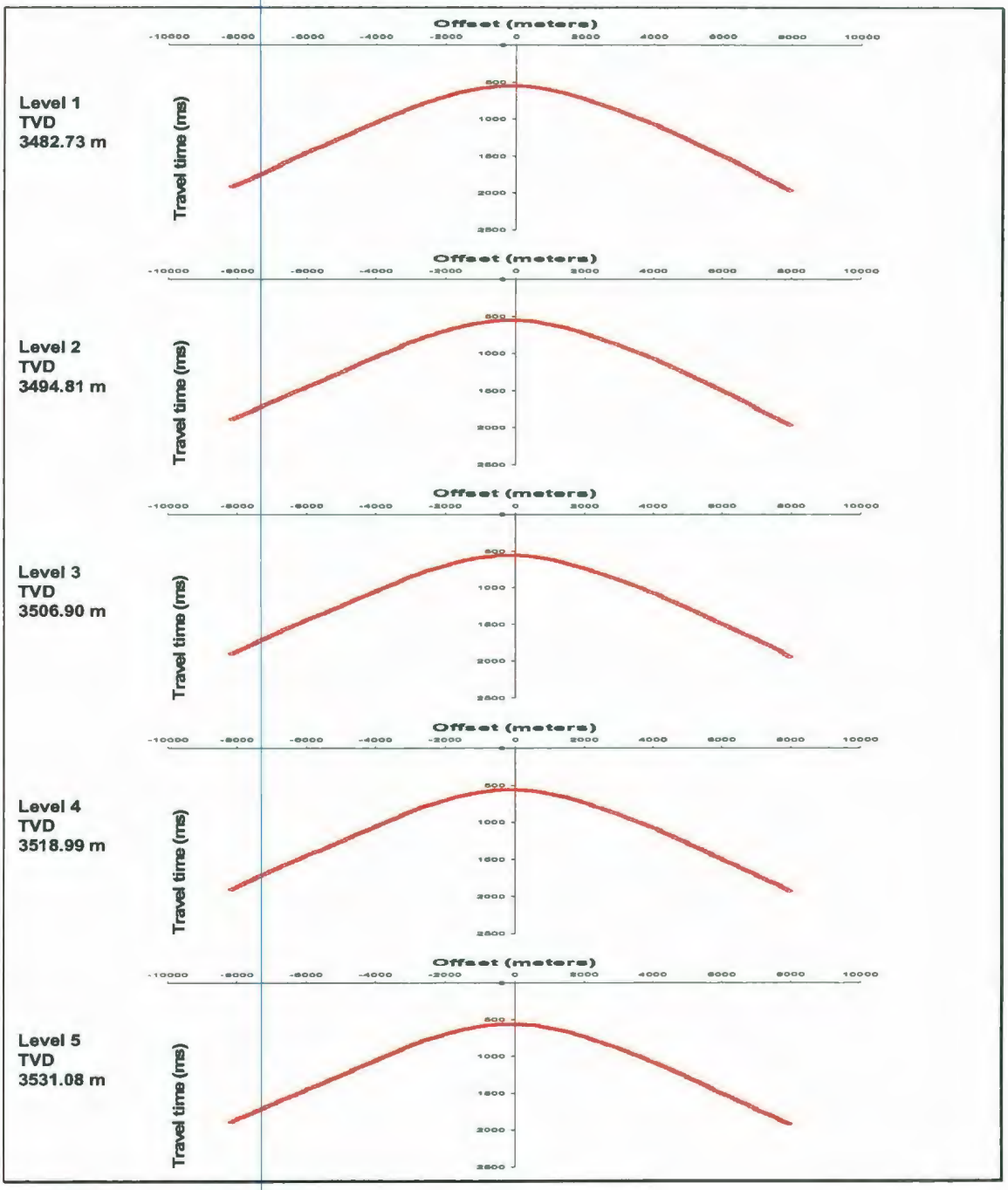

Figure 5.1.4 First break travel time picks of each level of the walkaway survey. Horizontal axes represent East (positive) and West (negative) offsets from a specific geophone and vertical axes represent travel times. Note travel times display a high degree of symmetry which can be an indication of non-dipping subsurface strata and insignificant lateral velocity variations.

determine a large number of independent χ values, I will not continue with an investigation of this outcome.

Substituting each calculated refraction point back into $\chi(x_r)$ yields independent χ values. **Table 5.3.1** gives a sample of refraction point values and specific χ values for offsets ranging from approximately 8000 meters to 2000 meters North-West of the receiver.

Table 5.3.1 Offset Values (x_2) at One Thousand Meter Intervals With Corresponding Travel Times (T), the Calculated Refractions Points (x_r) and the Calculated Anisotropic Parameter Values (χ) for a Shale Layer Within the Cape Island Member Formation, Hibernia Reservoir.

Offset Ordinate (x_2) (m)	Travel Time (T) (s)	Refraction Ordinate (x_r) (m)	Anisotropic Parameter χ (Dimensionless)
8027.3	1.860	7462.3	0.183
7028.1	1.656	4923.1	0.184
6026.9	1.459	3991.9	0.184
5029.7	1.265	3044.7	0.184
4026.4	1.059	1986.4	0.186
3026.4	0.860	731.4	0.185
2026.8	0.704	643.5	0.189

The consistency of the anisotropy parameter for the range of offsets demonstrates that the elliptical anisotropy assumption is valid for this case. Slawinski et al. (2003), shows the stability of this method by demonstrating that a one millisecond travel time error results in an error of about 20% in χ, and that this result is almost one order of magnitude less than the error inherent in the phase-slowness method. The consistency

among the set of the independent χ values given in the table above, not only demonstrates that the elliptical anisotropy assumption is valid for this case, but also provides an indication of the reliability of the method. To determine a single anisotropy parameter value, the average χ value was found to be 0.185. Thus, the average percent velocity anisotropy estimate for the shale layer is 17.1%. This value indicates that weak elastic anisotropy is present (Thomsen, 1986) and correlates well with P-wave velocity anisotropy values obtained from shale samples at corresponding depths (Thomsen, 1986).

To demonstrate that the travel time-inversion method produced an appropriate velocity anisotropy estimate for the shale layer, I continue using the elliptical anisotropy assumption to modify the widely accepted phase-slowness method (Gaiser, 1990, Miller et al., 1994, Miller and Spencer, 1994) so that an anisotropy parameter (χ) can be determined under the same conditions. Finally, using the travel times acquired from the walkaway survey, I calculate an anisotropy parameter (χ) for the shale layer, and thus determine an additional percent velocity anisotropy estimate.

5.2 The Phase Slowness Method

5.2.1 Theory

The phase-slowness method is based on determining horizontal and vertical slowness measurements (S_x and S_z). Slowness is defined as the inverse of the phase velocity ($\hat{v}$), or the inverse of the velocity of a propagating wavefront in a direction normal to its surface. Horizontal and vertical slowness can be represented by the equations:

$$S_x = \left.\frac{\partial t}{\partial x}\right|_z \qquad S_z = \left.\frac{\partial t}{\partial z}\right|_x .$$

Gaiser (1990), demonstrates that if one assumes the layer of interest is homogeneous in the immediate area of sources and receivers, then slowness estimates can be determined from VSP data by first simplifying the above equations to:

$$S_x = \left.\frac{\Delta t}{\Delta x}\right|_z \qquad S_z = \left.\frac{\Delta t}{\Delta z}\right|_x .$$

The horizontal slowness can now be obtained within a layer of interest by the difference in travel times (**Δt**) between two source positions (**Δx**) for a specific receiver depth, and the vertical slowness can be obtained within a layer of interest by the difference in travel times (**Δt**) between two receiver depths (**Δz**) for a specific source position (**Figure 5.2.1**). He then demonstrates that the horizontal slowness estimates can be calculated locally by fitting straight line segments in a squared coordinate space (t^2–x^2), and vertical slowness estimates can be calculated by a linear least squares fit to the direct

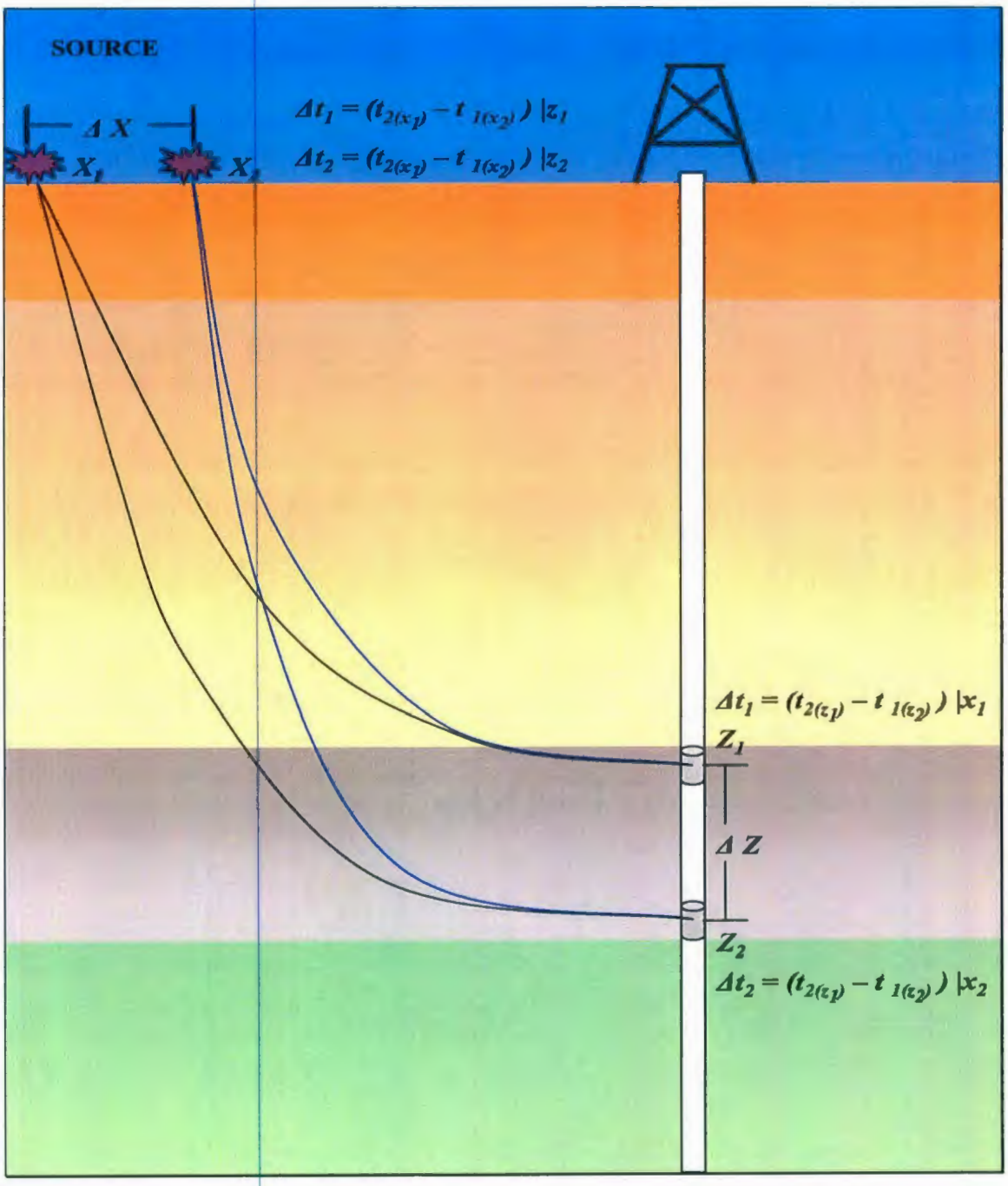

Figure 5.2.1 Illustration showing the phase slowness method (Gaiser, 1990). Note that the average slowness estimates between Z_1 and Z_2 will yield a sample point within the buried layer of interest mid-way between Z_1 and Z_1.

arrival times over a corresponding interval Δt. Even though homogeneity within the layer of interest simplifies the slowness calculations, these fitting procedures can be avoided if we also assume elliptical anisotropy.

As discussed in **Section 5.1**, by assuming elliptical anisotropy, the direction of energy propagation coincides with the wavefront normals along the axis of the ellipse. Hence, the horizontal and vertical ray velocities (V_x and V_z) along the axis of the ellipse are equal in magnitude to the corresponding phase velocities ($\hat{v}_x$ and $\hat{v}_z$). Therefore, determining S_x and S_z along the axis of an elliptical wavefront is now the inverse of the corresponding ray velocities. These ray velocities have to be equal in magnitude along each axis because the same point on the wavefield is sampled for different shot positions. Therefore, magnitudes of the slowness values with respect to each axis are also equal. Hence, using regression techniques to determine a function that will give S_x or S_z values are not needed. However, if it is found that the S_x's are not consistent or the S_z's are not consistent, then the elliptical anisotropy assumption may not be valid. Also, care has to taken to ensure that a range of shot positions will provide slowness estimates along the horizontal and vertical axis of an elliptical wave front. If random shot positions are chosen, one could be sampling the vertical axis instead of the horizontal and vise-versa.

The walkaway survey is ideal for determining slowness estimates, because closely spaced receivers can be fixed within a layer of interest and many specific shots/samples can be taken over a wide range of angles to ensure the wavefront is sampled along each symmetry axis.

To determine shot positions from a walkaway survey that will provide slowness values along the horizontal axis of an elliptical wavefront, I use a classical wavefront chart (Miller et al., 1994). This chart (**Figure 5.2.2**) is a contour plot of first break travel time picks as a function of source-receiver offset and receiver depth. Referring to **Figure 5.2.2**, a choice of near planar wavefront contours over a range of offsets (red box) will ensure that the wavefront normal coincides with the horizontal axis of the ellipical wavefront, and thus axial horizontal slowness estimates can be obtained. To determine shot positions from a walkaway survey that provide samples along the vertical axis of the ellipse, and thus obtain axial vertical slowness estimates, a range of near normal incident shot positions can be used. However, the walkaway survey data used for this study was acquired in a highly deviated well. Referring back to **Figure 5.2.1**, the phase-slowness method was developed using measurements acquire from VSP surveys conducted in vertical wells. When a well is deviated, the vertical slowness estimate will be affected because it is assumed the two receivers are in the same plane of incidence for a specific shot position. For two receivers in a deviated well, there is a horizontal displacement over a)**z**. Therefore, the horizontal coordinate cannot be held constant when determining S_z. Hence, the vertical slowness estimate corresponds to an "apparent" vertical slowness (S_z') and a correction must be made (Gaiser, 1990). The correction that gives the "true" vertical slowness estimate (S_z) along a pair of receivers within a

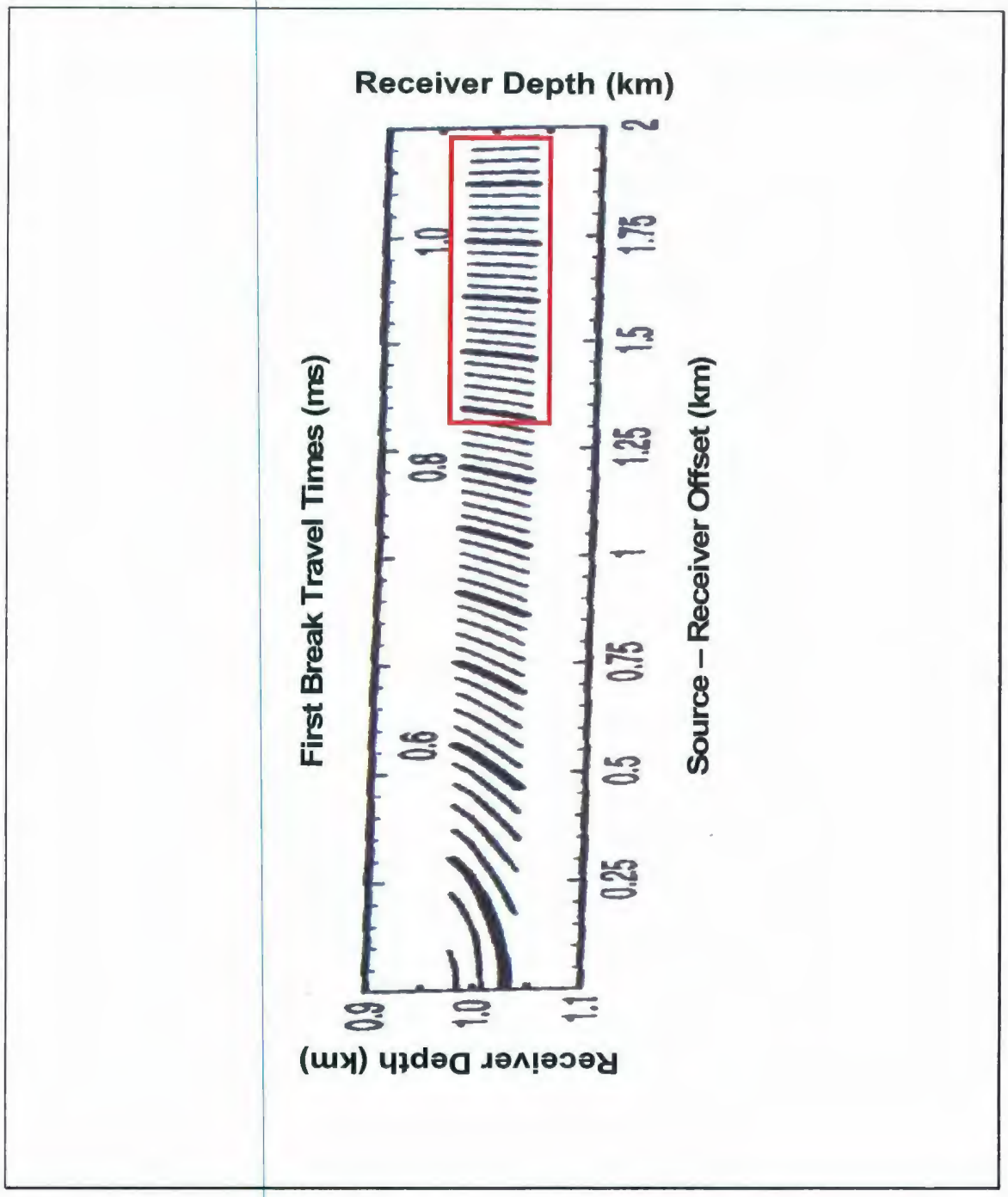

Figure 5.2.2 Wavefront chart made from first break travel times acquired from a walkaway survey (Miller et al., 1994). Red box indicates offset range and travel times that correspond to near planar wavefront contours.

deviated well, is determined by the product of the total slowness vector ($\vec{S}$) and the receiver array orientation ($\vec{a}$). This can be expressed as:

$$S_z = \vec{S} \times \vec{a} = -S_x \sin\theta \cos\psi + S_z' \cos\theta$$

(Ohlsen et al., 1998)

where θ is the inclination of the borehole and ψ is the azimuth with respect to the particular source position line and the array consisting of two receivers. The horizontal slowness values (S_x) were calculated from offsets used to calculate the apparent vertical slowness estimates.

Once confidence in the horizontal and vertical slowness estimates is established, the anisotropy parameter (χ) can now be expressed in terms of horizontal and vertical slowness by first substituting V_x and V_z in:

$$\chi = \frac{V_x^2 - V_z^2}{2V_z^2},$$

with the equivalent horizontal and vertical phase velocities (ϑ_x and ϑ_z) to yield:

$$\chi = \frac{\vartheta_x^2 - \vartheta_z^2}{2\,\vartheta_z^2}.$$

Knowing that slowness is defined as the inverse of the phase velocity, ϑ_x and ϑ_z can be replaced with the inverse of slowness to express χ as:

$$\chi = \frac{1}{2}\left(\left(\frac{S_z}{S_x}\right)^2 - 1\right).$$

Determining χ will now allow for the calculation of a percent velocity anisotropy estimate within a layer of interest.

To conclude this section, the travel times acquired from the walkaway survey are used to determine slowness estimates. These estimates are then used to calculate an anisotropy parameter for the same marine shale and thus a percent velocity anisotropy estimate. This will give further evidence that the percent velocity anisotropy estimate calculated using the travel time inversion method is appropriate.

5.2.2 Method and Results

To acquire a velocity anisotropy estimate of the shale layer using the phase-slowness method two levels of the walkaway survey are needed. It has been established that levels 4 (TVD 3519 meters) and 5 (TVD 3531.08 meters) are within the shale layer (**Section 5.1.3**). Thus, appropriate travel times are utilized to calculate the slowness estimates used to determine an additional anisotropy parameter (χ).

As outlined in the previous section, to determine horizontal slowness estimates, a choice of consistent planar wavefronts over a range of offsets has to be determined so that the direction of the normal to these wavefronts is in line with the horizontal axis of the ellipse. Wavefront charts are created using the travel times, receiver depths and source-receiver offsets for levels 4 and 5. **Figure 5.2.3** illustrates this contour plot of travel times as a function of source-receiver offset and receiver depth for all offsets.

Examining the chart reveals that planar wave fronts become consistent between offsets of approximately 3000 meters to 7000 meters. Hence, using the travel times that

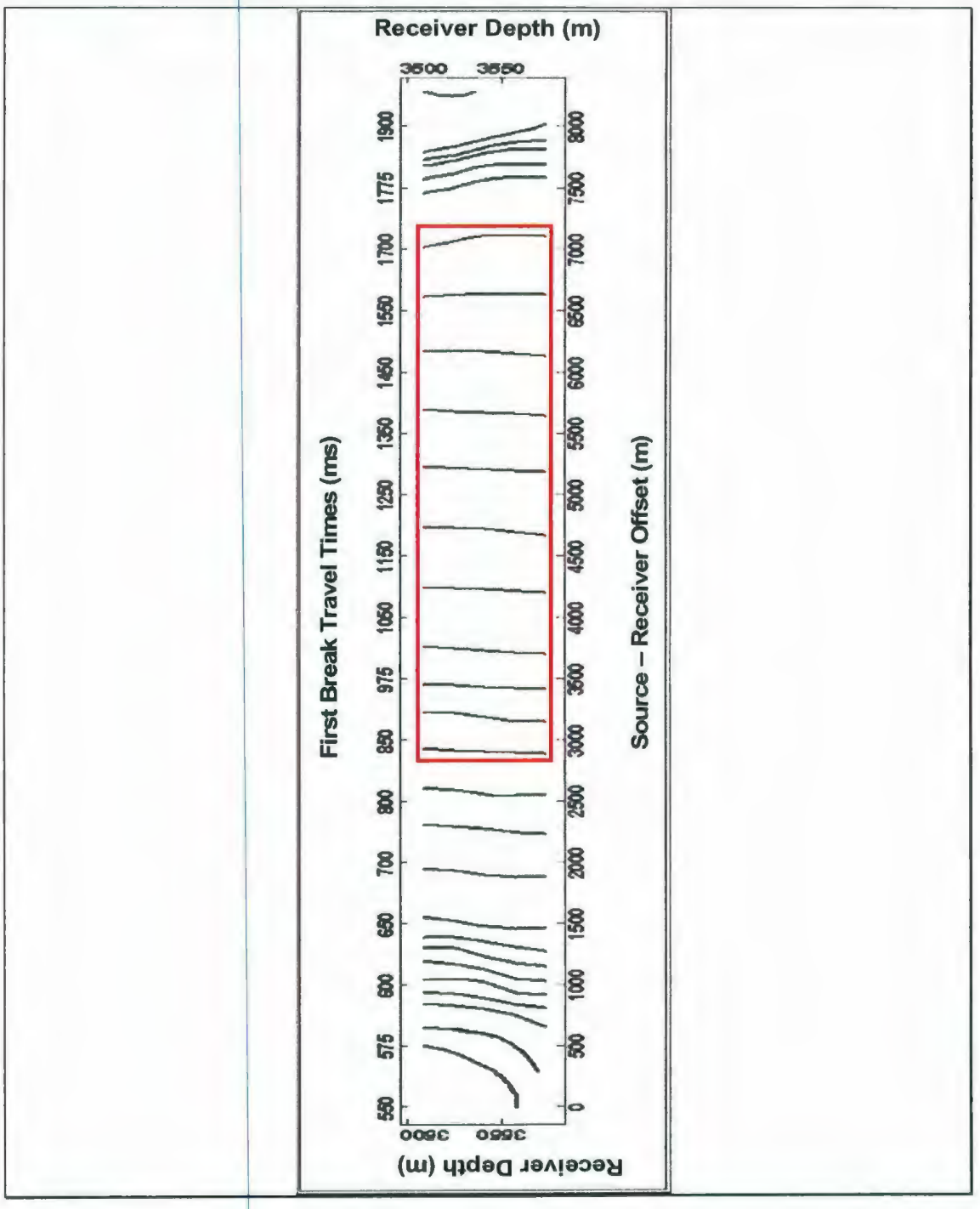

Figure 5.2.3 Wavefront chart made from recorded first break travel times. Red box indicates offset range and travel times used for the calculation of horizontal slowness estimates.

correspond to the offsets within this range, the horizontal slowness estimates are calculated for levels 4 and 5.

To obtain vertical slowness estimates that are along the vertical axis of the assumed elliptical wavefront, travel times acquired from sources at normal incidence with respect to levels 4 and 5 of the walkaway survey are needed. To avoid using travel times that are from offsets beyond normal incidence - which would equate into slowness estimates that are more horizontal than vertical - straight- ray source-to-receiver angles of incidence are calculated. It is found using simple trigonometry that offsets greater than 2000 meters will give angles of incidence greater than 30 degrees. To maintain normal incidence, I use travel times from offsets less than 2000 meters. Once the vertical slowness estimates are obtained, horizontal slowness values corresponding to offsets less than 2000 meters are also determined so a correction for well deviation can be performed. This correction will now allow for "true" vertical slowness estimates to be determined.

Graphing horizontal and vertical slowness versus source-receiver offset (**Figure 5.2.4**), shows the individual slowness estimates are self consistent for both the horizontal and vertical cases. These results are consistent with the assumption of lateral homogeneity and elliptical anisotropy. Using the mean of the horizontal and vertical slowness estimates, a value for χ is calculated (**Table 5.2.1**).

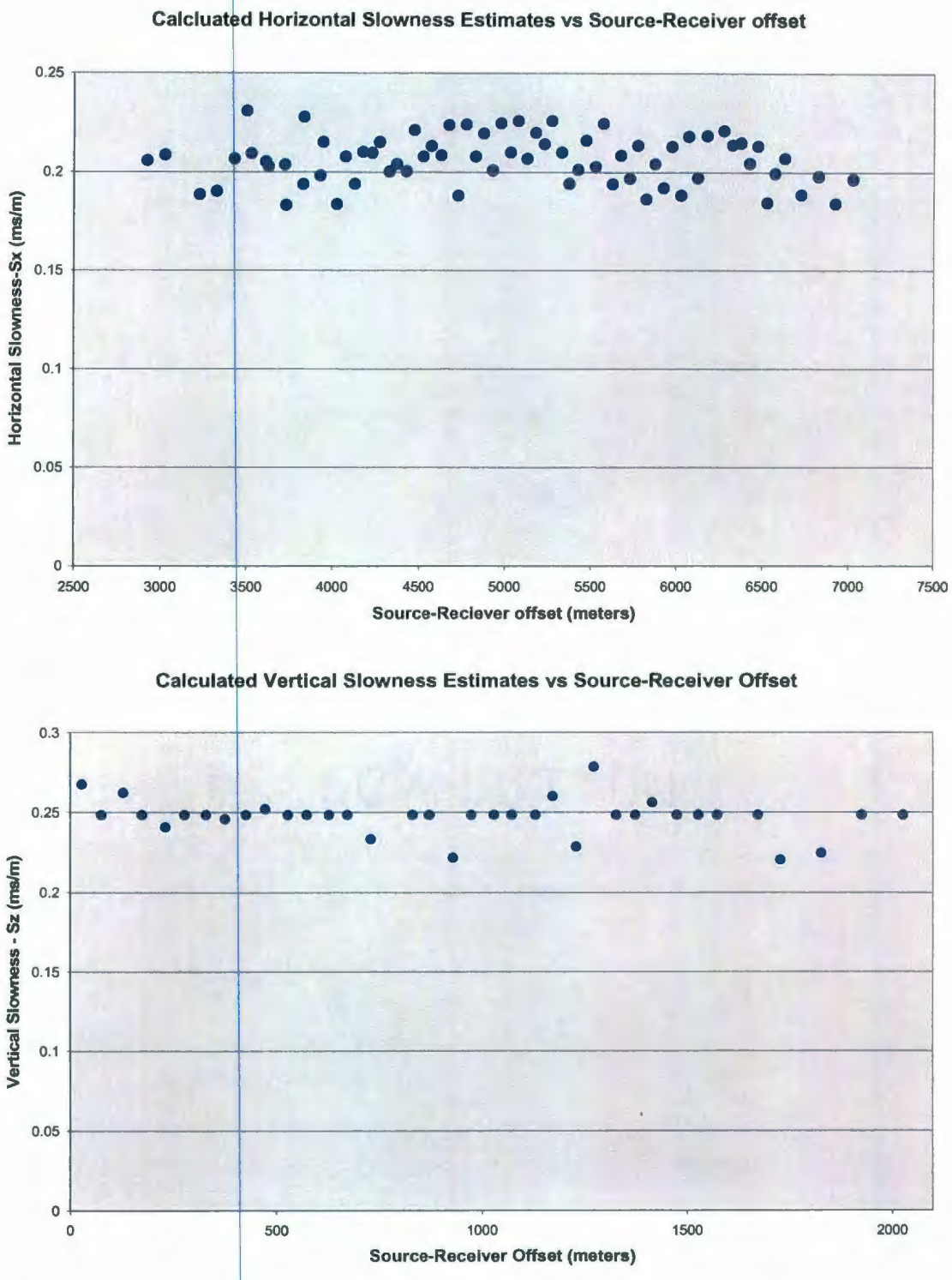

Figure 5.2.4 Scatter diagrams showing calculated horizontal and vertical slowness estimates versus corresponding source-receiver offset ranges.

Table 5.2.1 The Average Horizontal and Vertical Slowness Estimates in Addition to the Corresponding Calculated Anisotropic Parameter χ for a Shale layer Within the Cape Island Member Formation, Hibernia Reservoir.

Average Horizontal Slowness Estimate (ms/m)	Average Vertical Slowness Estimate (ms/m)	Calculated Anisotropic Parameter χ (Dimensionless)
0.2050	0.2418	0.1955

The calculated value of χ gives an additional percent velocity anisotropy estimate of 17.9% for the shale layer. This value indicates weak elastic anisotropy in the shale layer (Thomsen, 1986), and correlates well with P-wave velocity anisotropy values obtained from shale samples at corresponding depths (Thomsen, 1986).

5.3 Summary of Results

By assuming a linear vertical velocity gradient for the medium above an elliptically anisotropic layer of interest, in which the anisotropy can be described by a single parameter χ, Slawinski et al. (2003), developed a travel time inversion method around a point-to-point problem based on a single source-receiver pair within a Cartesian coordinate plane. Because the path of the borehole can be ignored, the travel time inversion method is well suited for acquiring velocity anisotropy estimates within a deviated borehole.

Using the travel times acquired from the vertical incidence and walkaway surveys, the anisotropy parameter (χ) was calculated to be 0.186 for a shale layer located within the Cape Island Member formation of the Hibernia reservoir. This value equates to a percent velocity anisotropy estimate of 17.1%. This suggests that weak anisotropy is present within the shale layer and compares well with published values (Thomsen, 1986).

To verify that this velocity anisotropy estimate is reasonable, the widely accepted phase-slowness method was modified using the same assumption of elliptical anisotropy within the shale layer. Not only did modifying the phase-slowness method allow for an additional χ value to be calculated, it also made this method operationally less intense in comparison to what is outlined by Gaiser, (1990) and Miller et al., (1994). However, a correction for borehole deviation still had to be implemented. The value for χ using this method was found to be 0.196, which equates to a percent anisotropy estimate of 17.9%. Again, this suggests that weak anisotropy is present within this shale and compares well with published values (Thomsen, 1986). Calculating the anisotropy parameter (χ) not only demonstrated that the travel time inversion method is well suited for acquiring velocity anisotropy measurements in deviated wells, but also gave a preliminary understanding of the anisotropic characteristics of a marine shale layer within the Hibernia Reservoir.

CHAPTER 6 Conclusions

This study investigates the processing considerations associated with acquiring precise travel times from three component vertical incidence and walkaway surveys conducted in deviated wells. After compensating for well deviation by rotating the vertical component of the vertical incidence survey into the first arrival P-wave particle motion, the raw and rotated vertical component travel times were differenced. Random differences in travel times were observed. These travel time differences were more apparent in the shallow section of the vertical incidence survey. This was most likely due to the noise associated with these traces making the onset of specific first arrivals harder to determine. The travel time picks acquired from the rotated vertical component displayed a bias towards being greater than the raw travel times. No reason could be found to explain this bias.

These random differences between the raw and rotated vertical component travel times had very little affect on calculated average velocities. However, calculated interval velocities were somewhat sensitive to these variations. Nevertheless, differences in interval velocities were randomly clustered. Comparing calculated interval velocities to sonic log interval velocities could have given more insight on this issue. Unfortunately, sonic log interval velocities were not available. Hence, determining if processing of this vertical incidence survey, to compensate for well deviation, produced travel times with a higher degree of precision was inconclusive. However, I would caution totally dismissing the credence of the rotational process when acquiring travel times from a vertical incidence survey.

The processing considerations associated with acquiring precise travel times from the three component walkaway survey proved to follow conventional practice. Because rotating the vertical component into the source-receiver plane is common practice when processing a walkway survey, deviation of the well was not an issue. However, Level four of the walkaway survey had a vertical component signal that consisted of a high degree of noise. No reason was found for this; however, the rotational process allowed for the P-wave signal to be recovered. The high degree a symmetry displayed by the travel time versus offset graphs proved to be useful in the final chapter. These graphs provided evidence that the assumption of horizontal layering of the rocks directly above the layer of interest was valid for this study.

Using the travel times acquired from the vertical incidence and walkaway survey, it was demonstrated that the travel time inversion method, developed by Slawinski et al. (2001) is well suited for acquiring velocity anisotropy measurements in deviated wells. The assumption that the buried layer of interest is elliptically anisotropic and described by a single anisotropy parameter provided the means for a percent velocity anisotropy estimate of 17.1% to be calculated for a marine shale. The percent velocity anisotropy estimate indicated that weak anisotropy is present and compared well with P-wave velocity anisotropy values for shales at corresponding depths (Thomsen, 1986).

To further verify that the travel time inversion method produced an appropriate velocity anisotropy estimate, the widely accepted phase-slowness method (Gaiser, 1990) was modified using the same assumptions that govern the travel time-inversion method. This allowed for an independent percent velocity anisotropy estimate of 17.9% to be

calculated. Again, this suggests that weak anisotropy is present within the marine shale and compares well with published values (Thomsen, 1986). Even though, correction for well deviation had to be implemented, the assumptions used to modify the phase-slowness method made it operationally less intense in comparison to what is outlined by Gaiser, (1990) and Miller et al., (1994). In general, using these travel times demonstrated that with the application of reasonable assumptions, velocity anisotropy measurements can be obtained within a deviated well without rigorous computational adjustments.

References

Acheson, C. H., 1981, Time-depth and velocity-depth relations in sedimentary basins – A study based on current investigation in the Arctic Islands and an interpretation of experience elsewhere: Geophysics, v. 46, 707-716.

Ahmed, H., Dillon, P. B., Johnstad, S. E. and Johnston, C. D., 1986, Northern Viking Graben Multilevel three-component walkaway VSP's - a case history: First Break, October, 9-26.

Balch, A.H. and Lee, M.W., (editors), 1984, Vertical seismic profiling - technique, applications, and case histories: International Human Resources Development Corporation, Boston, 488 pages.

Banik, N. C., 1984, Velocity anisotropy of shales and depth estimation in the North Sea basin: Geophysics, v. 49, 1411-1419.

Bidgood, M. J., 2003, Hibernia formation sequences and Breathitt Group (Kentucky) analogue: Unpublished Masters Thesis, Memorial University of Newfoundland, 240 pages.

Cassell, B.R., 1984, Vertical seismic profiles - an introduction: First Break, v. 2, No. 11, p. 9-19.

Coulombe, C. A., 1993, Amplitude-versus-offset analysis using Vertical seismic profiling and well-log data: Unpublished Masters Thesis, University of Calgary.

DiSiena, J.P., Gaiser, J.E., and Corrigan, D., 1981, Three-component vertical seismic profiles - orientation of horizontal components for shear wave analysis: Tech. Paper S5.4, p. 1990-2011. 51st Annual International Meeting of SEG.

Dix, C.H., 1939, The interpretation of well-shot data (Part I): Geophysics, v. 4, p. 24-32.

Flint, S., and Sinclair, I., 2001, Sedimentology and sequence stratigraphy of upper Breathitt Group, Eastern Kentucky, analogue to the Hibernia reservoir. A field reservoir modeling workshop for HMDC and partners.

Gaiser, J. E., 1990, Transversely isotropic phase velocity analysis from slowness estimates: J. Geophy. Res, v. 95, No. B7, p. 11,241-11,254.

Gal'perin, E.I., 1974, Vertical seismic profiling: Society of Exploration Geophysicists Special Publication No. 12, Tulsa, 270 pages.

Gal'perin, E.I., 1985, VSP potential in exploration geophysics: D. Reidel Publishing Company, Dordrecht, Holland, 300 pages.

Gretener, P. E. F., 1961, An analysis of the observed time discrepancies between continuous and conventional well velocities surveys: Geophysics, v. 26, p. 1-11.

Hardage, B. A., 1985, Vertical seismic profiling (Part A): Geophysical Press, London and Amsterdam.

Hardage, B. A., 2000, Vertical seismic profiling (Part A): Geophysical Press, London and Amsterdam.

Issac et. al, 1999, Image mispositioning due to dipping TI media: A physical seismic modeling study: Geophysics, v. 64, p. 1230-1238.

Jolly, R.N., 1953, Deep-hole geophone study in Garvin County, Oklahoma: Geophysics, v. 18, P. 662-670.

Jones et. al 1981, Ultrasonic velocities in Cretaceous shales from the Williston basin: Geophysics, v. 46, p. 288-297.

Kawahara, H., Saito, Y., Sugiyama, H., Fukuhara, M., Fujinawa, T., Shirota, A., and kamata, M., 1990, Enginerring design and field performance of an array type downhole seismic tool for cased hole VSP surveys: Paper BG6.7, 60th Ann. Internat. Mtg., Soc. Expl. Geophys., Expanded Abstracts, 144-147.

Kennett, P. and Ireson, R.L., 1971, Recent developments in well velocity surveys and the use of calibrated acoustic logs: Geophys. Prosp., v. 19, p. 395-411.

Leslie et. al. 1999, Determination of anisotropic parameters, *in situ*, using a multi-offset vertical seismic profile: SEG Technical Program Expanded Abstracts, p. 1267 -1270.

Levin, F.K. and Lynn, R.D., 1958, Deep hole geophone studies: Geophysics, v. 23, p. 639-664.

McCollum, B. and LaRue, W.W., 1931, Utilization of existing wells in seismograph work: Early Geophysical Papers, v. 1, p. 119-127. (Also Bull. AMER. Ass. Pet. Geol., v. 15, p. 1409-1417.)

Miller, D. E., Leaney, S., and Borland, W. H., 1994, An in situ estimation of anisotropic elastic moduli for a submarine shale: J. Geophy. Res, v.99, No. B11, p. 21,659-21,665.

Miller, D. E.,and Spencer, C., 1994, An exact inversion for anisotropic moduli from phase slowness data: J. Geophy. Res, v. 99, No. B11, p. 21,651-21,657.

Ohlsen, F., MacBeth, C., Magnus, I., and Vestby, J., 1998, Anistropy estimates from a North Sea VSP: SEG Extended Abstract.

Pearcy, R., 2000, Borehole Seismic School: Schlumberger Education Services.

Riggs, E.D., 1955, Seismic wave types in a borehole: Geophysics, v. 20, p. 53-67.

Slawinski, R. A., and Salwinski, M. A., 2001, On raytracing in constant velocity-gradient media: Calculus approach: Canadian Journal of Exploration Geophysics, v. 35, No. 1, p. 24-27.

Slawinski, M. A., Lamoureux, M. P., Slawinski, R. A., and Brown, R. J., 2003, VSP traveltime inversion for anisotropy in a buried layer: Geophysical Prospecting, v. 51, No. 2, p. 131-139.

Slotnick, M. M., 1959, Lessons in seismic computing: A memorial to the author: Society of Exploration Geophysics.

Stewart, R. R., Huddleston, P.D., and Kan, T. K., 1984, Seismic versus sonic velocities: A vertical seismic profiling study: Geophysics, v. 49, p. 1153-1169.

Strick, E., 1971, An explanation of observed time discrepancies between continuous and conventional well surveys: Geophysics, v. 36, p. 285-295.

Sydora, L. J., 1999, The Hibernia Oil Field: Integration of geophysics, geological, and production data into reservoir characterization and monitoring: Paper OTC 10741, Offshore Technology Conference, p. 115-119.

Tatham, R. H., and McCormack, M. D., 1991, Multicomponent seismology in petroleum exploration: Society of Exploration Geophysicists, v. 6, 248 pages.

Thomsen, L., 1986, Weak elastic anisotropy: Geophysics, v. 51, No. 10, p. 1954-1966.

Toksöz, M.n., and Stewart, R.R., (editors), 1984, Vertical seismic profiling - part B advanced concepts: Geophysical Press, Amsterdam, 419 pages.

Vestrum, R. W., Lawton, D. C., and Schmid, R., 1990, Imaging structures below dipping TI media: Geophysics, v. 64, p. 1239-1246.

Wyatt, K.D., 1981a, Synthetic vertical seismic profile: Geophysics, v. 46, p. 880-891.

Wyatt, K.D. and Wyatt, S. B., 1981b, The determination of subsurface structural information using the vertical seismic profile: Tech. Paper S5.2, p. 1915-1949, 51st Annual International Meeting of SEG.

APPENDIX A

Vertical Component Rotation Angle (Phi) for Vertical Incidence Survey Conducted in the B-16_2 Cased Production Well, Hibernia Oil Field.

APPENDIX A

Component Rotation Angles (Theta and Phi) for Vertical Incident Survey conducted in the B-16_2 Cased Production Well, Hibernia Oil Field.

Table A1: Vertical Component Rotation through the Angle Phi for Each Receiver Depth.

True Vertical Depth From (SRD). (meters)	Original Azimuth of Vertical Component. (degrees)	Original Inclination of Vertical Component. (degrees)	The Angle Phi for Which the Vertical Component is Rotated Through.(degrees)
3682.4	334.1	47.7	50
3672.3	334.1	47.7	47.01
3662.2	334.3	48	43
3652.1	334.3	48	47
3642	333.6	47.4	46.71
3631.8	334	47.4	42.99
3621.5	334	46.8	44
3611.2	334	46.2	42.01
3600.8	334.4	46.2	42
3590.4	334.4	46	42
3580.1	334.3	46.4	46
3569.7	334.7	46.4	45.01
3559.3	334.1	46.3	44.98
3549	334.3	46.3	48.01
3538.6	334.3	46.3	49
3528.3	334.3	46.6	47.01
3517.9	334	46.6	43.5
3507.6	334	46.1	44.99
3497.2	333.4	46.4	46
3486.8	333.4	46.4	47
3476.4	334.4	45.8	46.01
3466	334.4	45.8	45.5
3455.5	334.4	45.7	46.01
3445.1	334.4	45.7	47.01
3434.6	338.1	45.6	45.99
3424.1	338.1	45.6	46.01
3413.6	340.8	45.5	44.99
3403	340.8	45.5	44.5

3392.4	346.8	44.4	45.01
3381.7	347.1	44.4	44.5
3371	348.3	44.1	40.01
3360.2	350	44.1	43
3349.4	351.8	43.6	40.01
3338.4	353.5	43.2	42
3327.5	355.2	43.2	39
3316.6	357.1	43.4	40.01
3305.7	359.1	43.7	37.99
3294.9	0.5	43.5	40
3284	2	43.4	39.01
3273.1	3.8	43	37.96
3262.1	4.5	42.7	35
3251.1	5.1	42.6	43.01
3240	6	42.4	32.99
3228.9	6.7	42.2	43.01
3217.7	7.4	41.7	33.93
3206.4	8	41.2	34.01
3195.1	8.4	40.5	36.01
3183.7	9.2	39.8	25.96
3172.1	9.9	39.6	87.5
3160.5	10	39.5	29.95
3149	10.8	39.7	31.5
3137.5	11.6	39.8	29.94
3126	12.2	40.1	30.5
3114.5	12.5	40.1	37.5
3103	12.7	40.2	34.01
3091.6	13.1	40.1	30.01
3080.1	13.4	40	34.01
3068.6	13.2	40.2	37
3057.2	13.2	40.6	33
3045.8	13.4	40.7	29.5
3034.4	13.3	40.4	38.01
3022.9	13.3	40.6	38.99
3011.5	13.6	40.5	32.01
3000.1	13.7	40.1	33
2988.7	14.4	40.3	35.5
2977.2	14.4	40.3	32.99
2965.8	14.7	40.6	35
2945.4	15.2	40.6	29
2943	15.5	40.9	38.01
2931.7	15.9	41	31.5

2920.4	15.7	40.9	32
2909.1	15.9	41.1	32.01
2897.8	16.2	41.1	29
2886.5	16.2	41.1	38.01
2875.1	16.5	41.2	28
2863.9	16.7	41	30.01
2852.6	16.6	41.3	34
2841.3	16.7	41.2	32.5
2830	16.8	41.2	33.99
2818.7	16.9	41.3	37
2807.5	16.8	41.6	29.5
2796.3	17.1	41.7	33.96
2785.1	17.2	41.6	31.99
2773.9	17.4	41.8	41.5
2762.7	17.4	41.8	31
2751.5	17.5	41.9	37
2740.3	17.5	41.9	33.99
2729.2	17.7	41.8	31
2718	17.4	41.8	33.5
2706.8	17.4	41.5	46.01
2695.6	17.4	41.5	39.01
2684.4	17.7	41.3	30.99
2673.1	17.4	41.4	40.01
2661.8	17.5	40.9	35.95
2650.4	17.5	40.6	36.98
2639	17.9	40.4	27.99
2627.5	18.2	40.1	34.5
2616.1	18.3	40	36
2604.6	18.1	40.4	33.01
2593.1	18.2	39.5	37.01
2581.6	18.3	39.3	33.5
2570	18.4	39.5	34.5
2558.4	18.3	39.7	33.01
2546.9	18.2	40.1	39.99
2535.4	18.3	40	30.99
2523.9	18.6	39.3	32.97
2512.3	18.9	39.2	35
2500.7	19.1	39.4	33
2489.1	19.1	39.3	36
2477.4	19.4	38.5	37.01
2465.6	19.5	38.4	32
2453.9	19.4	38.7	31.98

2442.2	19.2	39	32.99
2430.6	19.1	39.3	40.01
2419	19	39.4	36.94
2407.4	18.9	39.7	30.01
2395.8	18.9	39.3	35.01
2384.1	19.6	38.4	32.01
2372.4	19.5	38.4	30.01
2360.7	19.4	38.8	32.98
2349	19.3	38.8	34
2337.3	19.2	39.1	29.98
2325.7	19	39.1	33.01
2314	18.9	39.4	32
2302.4	19	39.3	35.01
2290.8	18.6	39.8	25.99
2279.3	18.8	39.5	35.01
2267.7	18.8	39.5	35
2256.1	19	39.3	35
2244.5	19.4	39.4	39
2232.9	19.2	39.5	31.99
2221.4	19.3	39.5	35.98
2209.7	19.4	38.5	40.01
2197.9	19.2	37.6	33.01
2186	19	36.7	34
2173.9	18.8	36.5	30.5
2161.8	18.6	36.6	32
2149.8	18.7	36.5	47.5
2137.8	18.5	36.6	27.5
2125.7	18.4	36.3	38.95
2113.6	18.5	35.9	28
2101.5	18.8	36.7	33.01
2089.5	18.7	37	33.01
2077.5	18.7	37.5	33.01
2065.7	18.6	37.9	39
2053.9	18.4	37.9	30.5
2042.1	18.3	38.1	31.01
2030.3	18.2	38.1	32.01
2018.5	18.3	38.6	33
2006.8	18.3	38.8	33.99
1995.2	18.2	39.1	29.5
1983.5	18	39.3	35.5
1971.9	17.9	39.4	34
1960.3	17.6	39.2	31.96

1948.7	17.4	39.2	36.01
1937.1	17.1	39.5	35
1925.6	17	40	34.5
1914.1	17	40.1	38.97
1902.6	16.9	39.7	39.01
1891	16.9	39.8	40
1879.4	16.9	39.9	36.97
1867.9	17.2	39.3	43.5
1856.2	17.6	38.4	53.97
1844.4	17.7	37.7	38.01
1832.6	17.8	38.1	31.98
1820.8	17.8	37.9	33.5
1809	17.6	37.7	36.98
1797.1	17.5	37.5	27
1785.2	17.1	37.6	40
1773.3	17.1	37.7	35.99
1700.2	18.5	32.7	30
1687.4	18.4	31.4	32
1674.5	18.5	30.3	31.96
1661.5	18.7	29.1	30
1648.4	19	28.2	33
1567.6	19.3	23.9	23.99
1553.8	19.2	22.9	25
1540	18.8	21.9	22.01
1526	18.5	20.9	29.5
1512	18.5	20.2	36
1427.3	17.8	19.1	17.5
1413.1	17.6	18.6	351.98
1398.9	17.3	18.4	11
1384.7	17.2	18.3	12
1370.4	17.2	18.6	19.5
1294.5	16.5	17	19
1280.1	16.1	16.3	36.98
1265.7	15.8	15.7	20.01
1251.3	15.6	15.4	4.01
1236.8	15.7	15.4	18.96
1139.6	20.2	10.2	11.99
1124.8	20.2	9.1	1.01
1110	20	7.7	14
1095.1	19.9	6.7	0.99
1080.2	20.5	6.7	8.75
990.8	21.1	6.7	1.79

975.9	20.2	6.6	8.99
961	21.1	6.6	7.99
946.1	21.1	6.5	5.6
931.2	21.6	6.4	3.55
841.7	22.4	6.1	13.01
826.8	22.1	6.2	3.59
811.9	21.9	6.2	5.00
796.9	21.6	6.2	1.62
782	20.6	6.3	3.51
692.6	19.2	6.3	7.60
677.7	16.2	6.2	17.01
662.8	14.9	6.1	17.2
647.9	14.7	6.1	5.75
632.9	14.5	6.1	3.51

APPENDIX B

Raw and Rotated Vertical Component Travel Times Acquired from the Vertical Incidence Survey conducted in the B-16_2 Cased Production Well, Hibernia Oil Field.

APPENDIX B

Table B1 Raw and Rotated Vertical Component Travel Times Acquired from the Vertical Incidence Survey conducted in the B-16_2 Cased Production Well, Hibernia Oil Field.

True Vertical Depth From SRD (meters).	Raw First Break Travel Times Form Vertical Component (ms).	First Break Travel Times After Rotation of Vertical Component (ms).
3682.4	1327	1326
3672.3	1324	1323
3662.2	1322	1321
3652.1	1319	1318
3642	1316	1316
3631.8	1313	1314
3621.5	1310	1310
3611.2	1306	1307
3600.8	1304	1304
3590.4	1301	1302
3580.1	1301	1301
3569.7	1299	1298
3559.3	1295	1295
3549	1292	1291
3538.6	1290	1290
3528.3	1287	1287
3517.9	1282	1283
3507.6	1281	1281
3497.2	1279	1278
3486.8	1277	1276
3476.4	1276	1275
3466	1273	1272
3455.5	1270	1270
3445.1	1268	1267
3434.6	1265	1265
3424.1	1263	1263
3413.6	1261	1260
3403	1258	1258
3392.4	1255	1255
3381.7	1253	1252
3371	1251	1251
3360.2	1249	1249

	3349.4	1246	1246
	3338.4	1243	1243
	3327.5	1242	1242
	3316.6	1239	1239
	3305.7	1236	1236
	3294.9	1233	1233
	3284	1230	1231
	3273.1	1228	1228
	3262.1	1225	1225
	3251.1	1222	1222
	3240	1219	1220
	3228.9	1217	1216
	3217.7	1213	1213
	3206.4	1211	1210
	3195.1	1208	1208
	3183.7	1205	1205
	3172.1	1202	1204
	3160.5	1200	1200
	3149	1198	1198
	3137.5	1195	1194
	3126	1193	1193
	3114.5	1187	1190
	3103	1186	1185
	3091.6	1182	1181
	3080.1	1180	1180
	3068.6	1177	1178
	3057.2	1174	1174
	3045.8	1171	1172
	3034.4	1168	1169
	3022.9	1165	1166
	3011.5	1162	1162
	3000.1	1159	1160
	2988.7	1157	1157
	2977.2	1154	1154
	2965.8	1151	1151
	2945.4	1145	1147
	2943	1145	1144
	2931.7	1142	1142
	2920.4	1139	1139
	2909.1	1136	1136
	2897.8	1133	1132
	2886.5	1130	1129
	2875.1	1127	1127
	2863.9	1123	1123
	2852.6	1120	1120

	2841.3	1117	1118
	2830	1114	1115
	2818.7	1111	1111
	2807.5	1109	1109
	2796.3	1105	1106
	2785.1	1103	1102
	2773.9	1100	1099
	2762.7	1096	1096
	2751.5	1092	1092
	2740.3	1089	1090
	2729.2	1086	1086
	2718	1083	1083
	2706.8	1080	1080
	2695.6	1077	1077
	2684.4	1074	1074
	2673.1	1071	1071
	2661.8	1068	1068
	2650.4	1065	1065
	2639	1061	1060
	2627.5	1059	1058
	2616.1	1055	1055
	2604.6	1051	1051
	2593.1	1049	1048
	2581.6	1044	1045
	2570	1042	1043
	2558.4	1039	1039
	2546.9	1036	1036
	2535.4	1032	1034
	2523.9	1030	1030
	2512.3	1027	1027
	2500.7	1024	1024
	2489.1	1021	1021
	2477.4	1020	1019
	2465.6	1015	1015
	2453.9	1012	1012
	2442.2	1009	1009
	2430.6	1006	1006
	2419	1003	1005
	2407.4	999	999
	2395.8	996	996
	2384.1	992	993
	2372.4	990	989
	2360.7	986	986
	2349	983	982
	2337.3	979	979

	2325.7	976	976
	2314	972	972
	2302.4	969	969
	2290.8	966	965
	2279.3	963	962
	2267.7	959	960
	2256.1	956	956
	2244.5	953	953
	2232.9	950	949
	2221.4	946	946
	2209.7	942	943
	2197.9	939	940
	2186	935	936
	2173.9	932	932
	2161.8	929	929
	2149.8	926	925
	2137.8	921	922
	2125.7	918	918
	2113.6	913	913
	2101.5	910	910
	2089.5	907	907
	2077.5	903	903
	2065.7	900	900
	2053.9	896	896
	2042.1	892	892
	2030.3	889	889
	2018.5	886	886
	2006.8	883	883
	1995.2	881	881
	1983.5	878	878
	1971.9	874	875
	1960.3	871	871
	1948.7	868	868
	1937.1	864	864
	1925.6	860	861
	1914.1	857	856
	1902.6	853	853
	1891	849	850
	1879.4	842	843
	1867.9	840	839
	1856.2	837	840
	1844.4	834	834
	1832.6	830	831
	1820.8	827	827
	1809	823	823

	1797.1	818	820
	1785.2	816	816
	1773.3	808	808
	1700.2	786	787
	1687.4	783	783
	1674.5	775	776
	1661.5	772	773
	1648.4	766	768
	1567.6	739	739
	1553.8	734	733
	1540	730	730
	1526	727	727
	1512	718	718
	1427.3	694	694
	1413.1	679	684
	1398.9	680	680
	1384.7	676	676
	1370.4	671	671
	1294.5	634	634
	1280.1	629	629
	1265.7	624	624
	1251.3	612	612
	1236.8	608	608
	1139.6	574	574
	1124.8	568	568
	1110	562	562
	1095.1	559	559
	1080.2	560	560
	990.8	511	511
	975.9	500	500
	961	498	498
	946.1	494	494
	931.2	474	474
	841.7	446	447
	826.8	438	438
	811.9	435	435
	796.9	426	424
	782	413	413
	692.6	373	373
	677.7	362	361
	662.8	358	358
	647.9	345	345
	632.9	336	336

APPENDIX C

Rotated Vertical Component Travel Times Acquired from the Walkaway Survey conducted in the B-16_4 Cased Production Well, Hibernia Oil Field.

Table C1 Rotated Vertical Component Travel Times Acquired from the Walkaway Survey conducted in the B-16_4 Cased Production Well, Hibernia Oil Field.

Source Offset (meters).	Receiver 1 (3482.73 meters TVD) Travel Times (ms).	Receiver 2 (3494.81 meters TVD) Travel Times (ms).	Receiver 3 (3506.90 meters TVD) Travel Times (ms).	Receiver 4 (3518.99 meters TVD) Travel Times (ms).	Receiver 5 (3531.08 meters TVD) Travel Times (ms).
8128.39	1912	1888	1899	1901	1884
8027.22	1892	1867	1875	1878	1860
7925.25	1872	1846	1851	1854	1834
7828.03	1852	1825	1831	1831	1816
7726.85	1831	1807	1810	1808	1796
7626.92	1809	1786	1788	1788	1776
7528.88	1787	1766	1765	1767	1758
7426.11	1766	1742	1746	1742	1737
7326.5	1745	1720	1722	1722	1718
7226.65	1723	1696	1700	1701	1698
7125.98	1701	1675	1679	1678	1676
7027.95	1678	1653	1654	1655	1656
6925.19	1655	1633	1633	1634	1637
6827.84	1633	1612	1612	1615	1614
6728.16	1607	1594	1591	1593	1595
6628.86	1583	1573	1570	1572	1577
6528.3	1559	1552	1550	1553	1559
6424.68	1536	1531	1531	1534	1537
6326.57	1514	1510	1511	1515	1519
6227.61	1493	1491	1491	1495	1498
6124.6	1472	1472	1470	1475	1480
6026.75	1451	1453	1449	1456	1459
5926.19	1432	1435	1429	1434	1438
5825.65	1412	1416	1410	1416	1421
5726.67	1392	1396	1391	1396	1402
5625.77	1373	1376	1372	1379	1381
5526.78	1353	1357	1353	1360	1362
5424.8	1334	1336	1334	1341	1343
5328.17	1314	1316	1316	1322	1324
5227.61	1294	1295	1295	1302	1305
5126.44	1273	1274	1274	1282	1284
5029.51	1252	1255	1254	1262	1265
4927.07	1232	1234	1233	1241	1243

4826.66		1211	1213	1212	1220	1221
4727.45		1189	1193	1190	1199	1201
4627.43		1168	1172	1169	1178	1180
4525.3		1147	1150	1150	1157	1160
4426.63		1127	1127	1132	1137	1139
4328.12		1105	1107	1110	1118	1121
4227.38		1086	1087	1088	1098	1099
4128.56		1066	1066	1070	1077	1079
4026.25		1047	1047	1050	1056	1059
3928.78		1027	1028	1031	1037	1039
3828.6		1007	1008	1011	1016	1018
3728.04		987	989	991	996	999
3627.17		967	972	972	978	980
3526.08		948	952	952	958	960
3427.95		928	931	930	939	941
3324.23		910	911	911	920	922
3225.56		890	889	891	900	902
3127.62		870	869	873	879	882
3025.95		851	849	853	859	860
2923.25		832	832	836	840	840
2829.34		814	815	818	820	821
2727.35		797	798	800	802	805
2629.15		782	780	784	788	789
2529.63		767	765	768	774	775
2425.28		752	755	754	760	761
2323.14		738	740	740	745	748
2223.43		723	723	727	731	734
2124.29		709	708	713	717	719
2026.43		695	696	699	702	704
1924.76		681	683	685	689	690
1826.56		668	669	671	675	678
1726.1		655	657	659	662	665
1626.71		643	645	647	651	654
1527.1		631	634	636	640	642
1414.38		620	621	624	628	631
1327.03		609	613	615	619	622
1229.18		601	603	606	611	613
1129.43		593	597	598	602	605
1028.55		585	588	591	595	597
928.54		578	581	584	587	590
829.86		573	578	578	582	585
728.62		567	570	573	575	578

627.78	562	565	567	571	574
527.99	557	560	562	565	568
425.55	553	556	558	561	565
328.29	549	552	556	558	562
229.31	546	551	554	557	560
127.33	546	549	553	557	560
28.44	547	550	553	556	559
75.77	549	551	555	557	560
172.42	552	554	557	560	563
274.49	554	557	560	563	566
374.07	556	560	563	566	569
473.02	561	564	567	570	573
573.86	566	570	573	575	578
672.95	573	576	580	582	585
770	581	584	587	589	592
871.74	589	592	596	597	601
973.56	598	601	604	606	610
1071.59	606	610	613	616	619
1171.45	616	619	624	625	628
1272.03	626	630	635	636	639
1373.56	636	639	647	646	649
1475.09	647	649	660	658	659
1573.86	660	662	674	671	671
1671.6	673	674	687	683	684
1770.86	686	689	700	696	698
1872.63	701	703	713	710	712
1972.11	716	718	727	725	726
2073.08	731	733	741	741	743
2173.08	747	750	757	757	759
2272.38	764	766	772	774	776
2373.56	780	783	788	791	793
2501.79	798	799	805	808	807
2613.23	817	817	823	824	825
2723.72	835	837	841	842	844
2835.16	854	856	859	861	863
2945.65	873	875	878	880	882
3057.09	892	895	897	900	902
3167.57	912	914	916	920	921
3279.01	931	933	935	939	939
3389.5	950	953	955	958	958
3500.94	970	971	975	977	978
3611.46	991	991	995	997	999

3722.9		1012	1010	1015	1018	1020
3833.39		1032	1032	1036	1039	1041
3944.83		1051	1054	1057	1060	1062
4074.57		1072	1074	1077	1081	1082
4175.26		1093	1095	1097	1101	1104
4272.49		1115	1116	1118	1122	1123
4372.11		1136	1137	1142	1145	1146
4472.08		1157	1159	1163	1165	1167
4572.85		1179	1181	1184	1186	1187
4673.88		1202	1201	1204	1209	1210
4773.85		1222	1225	1227	1230	1232
4874.99		1245	1248	1247	1251	1253
4974.88		1267	1269	1270	1273	1273
5077.17		1289	1291	1292	1294	1296
5175.27		1311	1312	1311	1315	1315
5272.49		1333	1334	1332	1336	1337
5371.03		1354	1355	1354	1357	1358
5471.67		1377	1378	1376	1378	1382
5574.39		1400	1403	1399	1401	1405
5674.65		1422	1421	1422	1423	1427
5774.77		1444	1445	1445	1446	1449
5874.33		1466	1468	1467	1468	1472
5974.51		1488	1491	1489	1490	1494
6071.92		1510	1513	1510	1512	1516
6177.62		1531	1534	1531	1533	1536
6274.88		1554	1556	1553	1555	1556
6375.18		1576	1579	1574	1577	1579
6473.51		1600	1602	1595	1597	1600
6571.87		1623	1626	1617	1618	1621
6674.78		1646	1650	1637	1639	1642
6775.72		1671	1676	1660	1661	1663
6874.33		1697	1703	1679	1681	1686
6972.79		1722	1730	1700	1702	1708
7072.35		1748	1756	1722	1724	1730
7172.43		1773	1781	1744	1745	1752
7271.01		1797	1806	1765	1768	1771
7373.92		1820	1828	1788	1790	1790
7473.82		1842	1851	1811	1812	1812
7573.71		1864	1873	1836	1833	1834
7674.36		1890	1896	1861	1855	1856
7774.16		1916	1918	1888	1877	1879
7872.33		1941	1941	1917	1899	1899
7977.12		1966	1966	1945	1922	1920